Spring 5-4-2024

The Interactions of Centromeric Nucleosomes Elucidated by Atomic Force Microscopy

Shaun Filliaux
University of Nebraska Medical Center

The Interactions of Centromeric Nucleosomes Elucidated by Atomic Force Microscopy

By: **Shaun Filliaux**

A DISSERTATION

Presented to the Faculty of the University of Nebraska Graduate college in Partial Fulfillment of the Requirements for the degree of Doctor of Philosophy

Pharmaceutical Sciences Graduate Program

Under the Supervision of Professor Yuri L. Lyubchenko

University of Nebraska Medical Center

Omaha, Nebraska

April 2nd 2024

Supervisory Committee:

Gloria Borgstahl, PhD

Don Ronning, PhD

Joe Vetro, PhD

Dedicated to my supportive parents, wife, kid(s), and dogs, who were always there for me.

Acknowledgments

First and foremost, I would like to express my sincere gratitude to my advisor, Professor Yuri Lyubchenko, for the continuous support of my Ph.D. study and research and for his patience, motivation, enthusiasm, and immense knowledge. His guidance helped me in all the research and writing this thesis. I could not have imagined having a better advisor and mentor for my Ph.D. study.

Besides my advisor, I would like to thank the rest of my thesis committee, Drs. Gloria Borgstahl, Don Ronning, and Joe Vetro, for their insightful comments and encouragement and the hard questions that encouraged me to widen my research from various perspectives.

I also sincerely thank the Pharmaceutical Science Graduate Program at the University of Nebraska Medical Center for providing the necessary resources and support to complete my research.

I thank my fellow lab mates in the Lyubchenko Lab: Yaqing Wang, my first mentor in the lab, who taught me everything I know about Atomic Force Microscopy and who had the patience to put up with my questions. Karen Zagorski, easily one of the most brilliant people I have ever met, would have me join his projects because he enjoyed our conversations. He was someone that I am happy to have called a friend and could ask any question, and he would have a scientifically backed answer; even for the most abstract topics, you will forever be missed. Tommy Stormberg, who helped motivate me to get my work done. Mohtadin Hashemi, another great mentor and friend, would go out of his way to help you with your project, especially when it was an equipment problem, even if it was most likely a user-caused error. Sridhar Vermulapalli, for the stimulating discussions, all the fun we have had in the last few years, and the friendship we have forged from our journey together.

I am grateful to my parents, Norm Filliaux and Cathy Filliaux, for giving me endless support and encouragement throughout my journey of higher education and instilling in me a love for learning.

To my beloved wife, Shea, words cannot express how grateful I am to have you by my side. Your unwavering love, understanding, and unwavering support have been my pillar of strength throughout this

journey. Your patience, sacrifices, and constant belief in me have fueled my determination and helped me overcome every obstacle. Your unwavering belief in my abilities has given me the confidence to pursue my dreams fearlessly. Thank you for always being there, cheering me on, and celebrating every milestone. I am truly blessed to have you as my partner in life.

The Interactions of Centromeric Nucleosomes Elucidated by Atomic Force Microscopy

Abstract

Shaun Filliaux, Ph.D.

University of Nebraska Medical Center, 2024

Supervisor: Yuri Lyubchenko, Ph.D., D.Sc.

Nucleosomes are the fundamental unit of compaction for DNA in the genome. These positively charged proteins have two main types of nucleosomes: canonical (H3 containing) and centromere (CENP-A containing). The compacting of DNA allows for DNA to fit into the nucleus of cells, but creates a barrier for DNA accessibility for operations such as replication or transcription. Centromeric chromatin is a subset of chromatin structure and governs chromosome segregation. Compared to the bulk chromosome, centromeres are composed of H3 and CENP-A nucleosomes in which H3 histones is replaced by its homolog CENP-A histone. This results in nucleosomes with different structures, decreasing the bp of wrapped DNA from 147 bp for H3 nucleosomes to 121 bp for CENP-A nucleosomes. All these factors can contribute to centromere function.

We first studied H3 and CENP-A nucleosomes on dry AFM samples, using a novel three-way junction (3WJ) as a DNA marker, and determined the affinity of mononucleosomes on the 601 sequence, which yielded the result of H3 nucleosomes having a higher binding affinity to the sequence 99% and 92% for H3 and CENP-A nucleosomes, respectively. A similar trend was seen for the dinucleosomes with a lower percentage binding to the 601 for the CENP-A nucleosomes then than H3 nucleosomes. Next, we applied time-lapse, high-speed AFM (HS-AFM) to characterize the dynamics of nucleosomes. For both nucleosomes, spontaneous asymmetric unwrapping of DNA was observed, and this process occurs via a

transient state with ~100 bp DNA wrapped around the core, followed by a rapid dissociation of DNA. Additionally, HS-AFM revealed higher stability of CENP-A nucleosomes compared with H3 ones, in which dissociation of the histone core occurs prior to the nucleosome dissociation. The histone core of CENP-A nucleosomes remains intact even after the dissociation of DNA. All of the nucleosomes dynamics studies, indicated a higher stability in CENP-A nucleosome cores vs H3 nucleosomes, a surprising finding due to the lower DNA wrapping of CENP-A nucleosomes.

Transcription is a crucial biological function, and we studied the interaction of H3 and CENP-A nucleosomes separately with NF-κB, one of the critical transcription factors for regulating the immune response and inflammation. We utilized Atomic Force Microscopy (AFM) to characterize complexes of both types of nucleosomes with NF-κB. We found that this transcription factor unravels H3 nucleosomes removing more than 20 base pairs of DNA, and that NF-κB binds to the nucleosome core. Similar results were obtained for the truncated variant of NF-κB comprised only of the Rel Homology domain and missing the transcription activation domain (TAD). This finding suggests that the RelA TAD is not critical in unraveling H3 nucleosomes by NF-κB. By contrast, NF-κB did not bind to or unravel CENP-A nucleosomes. These findings with different affinities for two types of nucleosomes to NF-κB may have implications for understanding the mechanisms of gene expression which are different for the bulk and centromere chromatin.

Atomic Force Microscopy (AFM) is widely used for topographic imaging of DNA and protein–DNA complexes in ambient conditions with nanometer resolution. In AFM studies of protein–DNA complexes, identifying the protein's location on the DNA substrate is one of the major goals. Such studies require distinguishing between the DNA ends, which can be accomplished by end-specific labeling of the DNA substrate. We selected as labels the three-way DNA junctions (3WJ) assembled from synthetic DNA oligonucleotides with two arms of 39–40 bp each. The third arm has a three-nucleotide overhang, GCT, which is paired with the sticky end of the DNA substrate generated by the SapI enzyme. Ligation of the 3WJ results in the formation of a Y-type structure at the end of the linear DNA molecule, which is

routinely identified in the AFM images. The yield of labeling is 69%. The relative orientation of arms in the Y-end varies, such dynamics were directly visualized with time-lapse AFM studies using high-speed AFM (HS-AFM). This labeling approach was applied to the characterization of the nucleosome arrays assembled on different DNA templates. HS-AFM experiments revealed a high dynamic of nucleosomes resulting in a spontaneous unraveling followed by disassembly of nucleosomes.

Future studies expanding on this body of work would look at the effect of three or more nucleosomes on a single DNA strand and how the addition of more nucleosomes starts the higher-order compaction, including both H3 nucleosomes and CENP-A nucleosomes to better elucidate the effects both in the centromere and throughout the chromosome. Additionally the effect of NF-κB on dinucleosomes or trinucleosomes could better elucidate what happens in vivo when DNA is completely wrapped by nucleosomes and a transcription factor must access a specific DNA sequence.

Table of Contents

List of Figures

List of Tables

Abbreviations	**Definition**
3WJ	3-way junction
AFM	atomic force microscopy
a-sat	alpha-satellite
Bp	base pairs
CENP-A_{nuc}	centromeric nucleosomes containing CENP-A histone
DNA	deoxyribonucleic acid
EDTA	ethylenediaminetetraacetic acid
$H3_{nuc}$	canonical nucleosomes containing H3 histone
HS-AFM	high-speed atomic force microscopy
NF-κB	nuclear factor kappa-light-chain-enhancer of activated B cells
NF-κB_{FL}	NF-κB Full Length
NF-κB_{RHD}	NF-κB Truncated
PTM	post-translational modifications
SEM	standard error of the mean
ssDNA	single-stranded DNA
TAD	transcription activation domain
TFs	transcription factors

Table 1-List of Abbreviations

List of Contributions

Chapter 2 described the methodology from many of our publications listed below.

Chapter 3 is reformatted from publications "Stormberg T, Vemulapalli S, Filliaux S, Lyubchenko YL. Effect of histone H4 tail on nucleosome stability and internucleosomal interactions. *Scientific Reports*. 2021;11(1). doi:10.1038/s41598-021-03561-9" and "Sun Z, Stormberg T, Filliaux S, Lyubchenko YL. Three-Way DNA Junction as an End Label for DNA in Atomic Force Microscopy Studies. *IJMS*. 2022;23(19):11404. doi:10.3390/ijms231911404".

Chapter 4 is reformatted from the publication "Filliaux S, Sun Z, Lyubchenko YL. Nanoscale Structure, Interactions, and Dynamics of Centromere Nucleosomes. *bioRxiv* Biophysics; 2024. doi: 10.1101/2024.02.12.579909".

Chapter 5 is reformatted from the publication NF-κB Paper "Filliaux S, Bertelsen C, Baughman H, Komives E, Lyubchenko YL. The Interaction of NF-κB Transcription Factor with Centromeric Chromatin. *bioRxiv* Biophysics; 2024. doi: 10.1101/2024.02.13.580208".

Chapter 1. INTRODUCTION

1.1 DNA

Deoxyribonucleic acid (DNA) is crucial for numerous bodily functions such as storage of genetic information, transmission of genetic information, protein synthesis, cell function and regulation, and evolution.[1–4]

DNA stores the genetic information and contains the instructions needed for an organism to grow, develop, function, and reproduce. These instructions are encoded in the sequence of its four types of nitrogenous bases: adenine (A), guanine (G), cytosine (C), and thymine (T).[1,5,6]

Transmission of genetic information occurs when DNA is passed from parents to their offspring during reproduction, ensuring that the new organism receives the necessary information to develop and function properly.[7,8]

DNA is the site of protein synthesis because it contains the blueprints for building proteins, which are required for many cellular processes but often overlooked. Proteins are essential for the function of every cell in the body, providing structural support, catalyzing chemical reactions (as enzymes), transporting molecules, and responding to signals.[9,10]

Gene expression is the process by which DNA instructs the cell how to carry out its functions and regulate itself. Transcription of DNA into RNA is followed by translation of mRNA into proteins. Different genes' expression levels are controlled to coordinate the production of specific proteins at specific times.[11–13]

The importance of DNA is unprecedented in the body. However, DNA in a single chromosome is approximately 155 million bp of DNA and approximately two meters long if all the DNA in a cell was uncoiled, and fitting it inside a cell (approximately 10 to 100 micrometers), which is extremely small and a remarkable feat of biological organization.[14–16] The DNA in a cell is packaged and organized in a highly structured manner to ensure that it is both accessible for cellular processes and compact enough to fit

inside the nucleus in eukaryotic cells. A problem arises when the highly compacted DNA is required for biological functions such as transcription and replication.[17,18]

The DNA compacts into eukaryotic cells' nucleus through multiple compaction stages. The fundamental level of compaction is nucleosomes, the middle level of compaction is chromatin, and lastly, chromosomes.[19,20]

1.2 Nucleosomes

DNA is compacted at the cellular level by nucleosomes, which consist of DNA wrapped around an octameric core of histones. These canonical octameric cores are composed of two copies of each of the histone proteins H2A, H2B, H3, and H4, and their predominantly positive charges aid in binding the DNA around the core.[21,22]

While the DNA in a human cell is about 2 meters long, the nucleus is only about 6 micrometers across.[23] Nucleosomes compress DNA so that it can fit into the relatively small nucleus of a cell. In addition to helping compact DNA into higher-order structures like chromatin fibers, loops, and chromosomes, nucleosomes also play a role in the initial folding and organization of chromatin.[24–27]

Nucleosomes regulate access to DNA because DNA is still required even when wrapped around them for processes like transcription, nucleosome dynamics, and replication. Nucleosomes can be altered or repositioned to make specific DNA sequences accessible or inaccessible, allowing for the binding of transcription factors and other proteins that regulate gene expression.[28–31]

1.3 Centromeres

The centromere is a unique part of a chromosome that serves an essential function during cell division. Here, two copies of a chromosome, called sister chromatids, are physically joined until they are separated and pulled to opposite poles of the cell.[32–34] Spindle fibers, structures that aid in separating chromosomes during cell division, attach to the centromere.[35,36] The location of the centromere varies from chromosome to chromosome, which alters the overall morphology of the chromosome.[37,38]

Centromeres play a crucial role in chromosome alignment and movement, ensuring that the correct number of chromosomes is passed on to each daughter cell during mitosis.[39] Improper chromosome segregation, caused by mutations or abnormalities in the centromere, can lead to cells with abnormal chromosome numbers linked to several diseases and cancers.[40–42]

The centromere contains specialized nucleosomes called a CENP-A nucleosome (CENP-A_{nuc}) that help with the unique requirements of the centromere's responsibilities. These CENP-A_{nuc} contain an octameric core, similar to the H3, with two H2A, H2B, CENP-A, and H4, where the H3 histones of the canonical nucleosomes are replaced with CENP-A histones.[43–45] These centromeric CENP-A_{nuc} share 75% of the same histones as the H3 counterparts (H2A, H2B, and H4 histones) but behave differently on the individual nucleosome level. For example, CENP-A_{nuc} have a wrapping efficiency of ~20 bp less than the $H3_{nuc}$ and are responsible for forming the kinetochore foundation.[46–48] A specific ratio for CENP-A_{nuc} to $H3_{nuc}$ in the centromere has been recently found to be between 8:1 and 11:1, which means that the centromere is almost exclusively composed of CENP-A_{nuc}.[49]

CENP-A_{nuc} are vital to the establishment and maintenance of centromere identity. CENP-A_{nuc} play a critical role in maintaining genomic stability by ensuring accurate chromosome segregation. Errors in this process can lead to aneuploidy, a condition where cells have an abnormal number of chromosomes, which is associated with cancer and various genetic disorders.[50,51]

1.4 Chromatin and Higher-Order Structure

Chromosomes, chromatin, and nucleosomes, listed from highest to lowest order of compaction and, are closely related structures that play crucial roles in the organization, packaging, and regulation of genetic material in eukaryotic cells. Chromosomes are the highest-order of compaction of long DNA, thread-like structures located in the nucleus of eukaryotic cells. They ensure DNA is accurately replicated and distributed to new cells during cell division.[52–54]

Chromatin's primary function is the packaging of long DNA molecules wrapped around nucleosomes into more compact, dense structures, preventing the strands from becoming tangled and also playing essential roles in reinforcing the DNA during cell division and regulating gene expression and DNA replication. There are two forms of chromatin: heterochromatin (condensed) and euchromatin (less condensed). Heterochromatin consists mostly of repetitive DNA sequences and non-coding RNA transcripts, mostly commonly found in the centromere and telomeres. Conversely, euchromatin is enriched in genes and is often under active transcription, therefore in the presence of DNA, RNA, and protein.[55–59]

Nucleosomes (Section 1.2) serve as the building blocks of chromatin, wrapping DNA into a compact and manageable structure, which in turn folds and compacts to form chromosomes during cell division. This hierarchical organization ensures that the long DNA molecules are properly maintained, replicated, and divided while also regulating access to genetic information for gene expression.[60,61]

At the most basic level, nucleosomes help to package the DNA into a compact, dense structure. This packaging continues to fold and refold until it forms the chromatin structure, which is then folded more until a chromosome is formed. Both nucleosomes and chromatin structure play a critical role in gene regulation. Certain regions of chromatin can be opened or closed, making them more or less accessible to transcription factors and RNA polymerase, which are crucial for gene expression.[62,63]

During cell division, chromatin condenses to form chromosomes, ensuring proper segregation of the genetic material between daughter cells. Nucleosomes help in this process by allowing the DNA to be compacted and organized in a way that supports chromosome formation.

1.5 Regulation of Transcription of Chromatin: Transcription Factor NF-κB

Transcription factors are proteins that regulate the transcription of genetic information from DNA to RNA by binding to specific DNA sequences.[64] Transcription factors regulate the rate of transcription of particular proteins. For example, NF-κB (Nuclear Factor kappa-light-chain-enhancer of activated B cells)

is a critical signaling pathway in cells, which is vital in regulating the immune response, inflammation, cell growth, and survival. It's one of the most studied pathways due to its relevance in many diseases, including cancer, autoimmune disorders, and inflammatory conditions.[65,66]

NF-κB is a family of transcription factors that includes several proteins, such as NF-κB1 (p50/p105), NF-κB2 (p52/p100), RelA (p65), RelB, and c-Rel. In the studies discussed in this paper, we will focus on the heterodimer of p50/RelA(p65), which is considered the canonical and most abundant form of the protein. In unstimulated cells, NF-κB dimers are typically held in the cytoplasm in an inactive state by inhibitory proteins called IκBs (Inhibitor of kappa B). The most common of these is IκBα. The NF-κB pathway can be activated by various stimuli, including cytokines (like TNF-α and IL-1), growth factors, stress signals, reactive oxygen species, and pathogens (like viruses and bacteria). Upon stimulation, the IκB kinase (IKK) complex, which includes IKKα, IKKβ, and a regulatory subunit NEMO (IKKγ), becomes activated.[67–69]

IKK complex then phosphorylates IκB proteins, marking them for ubiquitination and subsequent degradation by the 26S proteasome. The degradation of IκB releases NF-κB dimers, most commonly p50/RelA heterodimers, allowing them to translocate into the nucleus.[70–72]

Once in the nucleus, NF-κB dimers bind to specific DNA sequences called κB sites in the promoters or enhancers of target genes. This binding results in the transcriptional activation (or sometimes repression) of genes involved in immune and inflammatory responses, cell proliferation, apoptosis, and other vital cellular processes.[73–75]

The pathway is tightly regulated at multiple levels, including the degradation and synthesis of IκB, post-translational modifications of NF-κB subunits, and interactions with other transcription factors and co-regulators. We have recently published a paper in our lab demonstrating that NF-κB is a pioneer transcription factor.[76]

Negative feedback loops, such as the resynthesis of IκB proteins, which can bind to and inactivate NF-κB in the nucleus, help terminate the response. Given its central role in immune and inflammatory responses and cell survival, the NF-κB pathway is implicated in a wide range of diseases. Dysregulation of this pathway can lead to chronic inflammation, autoimmune diseases, cancer, and other pathological conditions.[77,78]

Due to its importance in various diseases, the NF-κB pathway is a target for drug development. Various inhibitors targeting different components of this pathway are being studied to treat cancer, inflammatory diseases, and autoimmune disorders.[79–83]

Understanding the interaction between NF-κB and nucleosomes is crucial in medical research, as it offers insights into the mechanisms underlying many diseases and provides potential targets for therapeutic intervention. The aberrant regulation of NF-κB and its interaction with chromatin has been linked to various diseases, particularly inflammation and immune responses. For example, dysregulation of NF-κB has been implicated in cancer, which can promote cell proliferation and survival.[84–86]

1.6 Significance

The study of nucleosomes, as detailed in this text, holds paramount significance in molecular biology and genetics. Nucleosomes, consisting of DNA wrapped around histone protein cores, are essential for efficiently packaging DNA within the confines of a cell's nucleus.[21,87,88] This packaging is not just a structural necessity; it plays a critical role in regulating gene expression and maintaining genomic stability. The intricate organization of nucleosomes determines how genes are accessed and expressed, impacting everything from cell development to the body's response to environmental stimuli.[89–92] Transcription factors, such as NF-κB, require access to the DNA to function, which ultimately results in the transcription of inflammatory cytokines and chemokines.[65,93] By understanding how nucleosomes work, we will gain insights into the fundamental processes of gene regulation, the basis of various diseases, and the accessibility of DNA to proteins, such as transcription factors. Moreover, the dynamic

nature of nucleosomes, which can be remodeled in response to cellular signals, is central to our understanding of epigenetic changes and their implications in health and disease. For instance, the unique features of CENP-A_{nuc} at the centromeres are crucial for chromosome segregation during cell division, a process integral to maintaining genomic integrity. However, there is a lack of understanding in the differences between H3 and CENP-A nucleosomes. Any malfunction in this process can lead to severe conditions like aneuploidy, often associated with cancers and various genetic disorders. The interplay between different types of nucleosomes and their role in compacting DNA, regulating gene expression, facilitating DNA replication and repair, and regulating DNA accessibility underscores the essentiality of nucleosomes in life's molecular architecture. Although there is a basic understanding of H3 and CENP-A nucleosomes, some knowledge gaps prompt the following questions. (1) What are the differences in DNA specificity, wrapping, and stability between H3 and CENP-A nucleosomes? (2) How does NF-κB interact and impact both H3 and CENP-A nucleosomes? (3) Are there alternatives to bulky protein labeling for AFM imaging?

Answering these questions thereby provides the scientific premise of these projects, which combines the development of a novel DNA marker, the discovery of NF-κB: nucleosome(H3 and CENP-A) interactions, and elucidating nucleosome dynamics.

The project described here is entirely innovative. The interactions of nucleosomes have a crucial biological role, but the understanding of the dynamics and internucleosomal interactions has not yet been clearly elucidated. Therefore, we studied nucleosomes using a novel (3WJ) DNA marker, enabling the quantitative analysis of nucleosomes in both dry imaging and HS-AFM imaging. This importantly looks closely at the CENP-A nucleosomes to uncover new information about how the nucleosome's stability, unwrapping, and dynamics differ from the H3 nucleosome. These differences further explain the differences between the bulk chromosome (H3 nucleosomes) and the centromere (CENP-A nucleosomes), which can be the cause of disease and aneuploidy. Additionally, we add NF-κB to both nucleosome systems, which is an entirely novel experiment and approach that uncovers the mechanisms of the role of

transcription factors in the centromere, which, until recently, the centromere was thought to have no transcriptional activity.[94] These experiments lay the foundation for future studies of both H3 and CENP-A nucleosomes and their impact on interactions with transcription factors and cell viability.

Chapter 2. METHODS

2.1 Introduction

The Methods section of this thesis elucidates the procedures and techniques utilized to conduct the research and gather pertinent data. The integrity of the research findings hinges on the rigorous and systematic implementation of these methods, ensuring the reliability and validity of the results. This chapter provides a comprehensive overview of the research design, sample selection, data collection instruments, and analytical strategies employed in this study.[95,96]

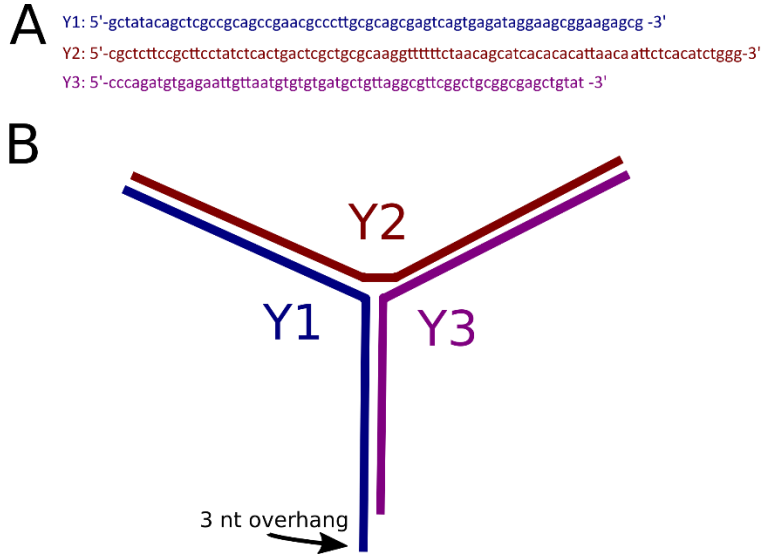

Figure 1- Three-way Junction design.

(A) Oligonucleotides used in 3WJ assembly. (B) Schematic of 3WJ. The arm lengths are 40 bp, 39 bp, and 20 bp between Y1–Y2, Y2–Y3, and Y1–Y3, respectively. The 3nt overhang is GCT. The addition of 6 T's in the center of the Y2 ssDNA and at the 3WJ intersection site was to help the DNA flanks to prefer the T and Y conformations. These 6 T's do not have complementary DNA.

2.2 DNA Substrate Preparations

2.2.1 Preparation of 3WJ End Label

Protein markers, such as streptavidin, have historically been used as DNA markers by binding to biotin on the DNA. Problems arise from these protein-based DNA markers when looking at complex

systems that may include multiple proteins such as nucleosomes and transcription factors. Therefore, a novel approach was designed to eliminate the necessity for extra proteins, which we termed the 3WJ.

The oligonucleotides comprising the 3WJ were designed to have complementarity to one another to form the "Y" shape of the 3WJ, as seen in Figure 1. A six-nucleotide thymine (T) repeat was added to Y2 to facilitate the assembly of the Y structure of the 3WJ end.[95,96] A three-nucleotide (GCT) overhang was added to Y1 to facilitate the complete DNA construct ligation with a complementary sticky end generated with the SapI restriction enzyme. The oligonucleotides used and a schematic of the 3WJ are shown in Figure 1. The three oligonucleotides (Y1, Y2, Y3) were mixed at an equimolar ratio and heated to 95 °C, and as the denatured DNA cooled, they annealed together forming the 3WJ. Assembly was verified by gel electrophoresis. A representative gel can be seen in Figure 2.

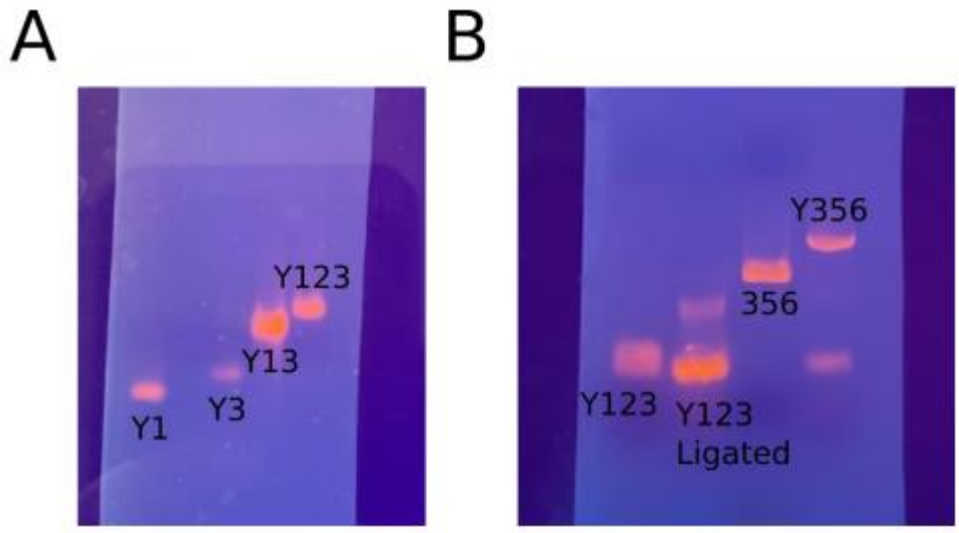

Figure 2- Agarose gels of 3WJ assembly.

Agarose (1%) gels of labeled DNA complex assembly. (A) The gel of 3WJ assembly. The Y1 and Y3 indicated the position of single-strand oligonucleotides (The length of Y2 is similar to Y3 but not shown in the gel.) Lanes Y13 and Y123 are the annealing products of Y1-Y3 and Y1-Y2-Y3. The position of Y13 is higher than Y1 and Y3 but lower than Y123, suggesting that we annealed the Y1-Y2-Y3 together. (B) The gel of label-DNA complex assembly. Y123 and 356 are the two parts of the segment we need to ligate together. Y123 ligated shows control results for self-ligation of Y123. The main band of ligated Y123 is the same as Y123 before ligation. The Y356 is the final ligation product with a higher main band than 356 and Y123. A final test is completed on AFM to ensure the 3WJ are proper lengths.

2.2.2 3WJ DNA Full Construct Preparation

Two DNA substrates were used in the three-way junction (3WJ) experiments. The first is a nonspecific DNA sequence 356 bp in length. The second is a 600 bp sequence capable of binding two nucleosomes. This sequence contains the strong nucleosome positioning 601 motif at the far end of the template, as seen in Figure 3.[97] The duplexes are generated from PCR using a plasmid vector pUC19 with these primers. The primer includes the cutting region for the restriction enzyme SapI (5′-GAAGAGC-3′) (New England Biolabs, Ipswich, MA, USA), which creates a three-nucleotide overhang complementary to our 3WJ after cutting. The DNA substrates were concentrated from the PCR product and purified using

gel electrophoresis. The purified DNA was digested with SapI and ligated with the Y junction overnight at 16 °C. The final product was then purified by gel electrophoresis. A representative gel can be seen in

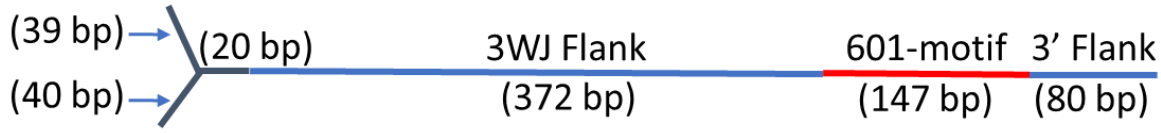

Figure 3- DNA diagram of DNA construct with a terminal 3WJ.

DNA diagram of the 3WJ DNA with a single 601-motif site (red line), 80 bp from the 3' end. The 20 bp in gray is part of the 3WJ assembly. The blue 372 bp sequence is a flank that allows nucleosomes to bind more freely.

Figure 2B. DNA concentration was then determined using a NanoDrop Spectrophotometer (ND-1000, Thermo Fisher, Waltham, MA, USA) and stored at 4 °C before being used for experiments.

2.2.3 Alpha-Satellite DNA Preparation

The DNA construct was prepared the same way as we have done previously.[76,98,99] The alpha satellite-containing construct was made using PCR with a pUC57 plasmid vector from BioBasic (Markham, ON, CA). The DNA total sequence was 410 bp, with the alpha satellite sequence in the middle. The specific sequence used is 5'-GATGTGCTGCAAGGCGATTAAGTTGGGTAACGCCAGGGTTTTCCCAGTCACGACGTTGTAAAACGACGGCCAGTGAATTCGAGCTCGGTACCTCGCGAATGCATCTAGATGACCATTGGATTGAACTAACAGAGCTGAACACTCCTTTAGATGGAGCAGATTCCAAACACACTTTCTGTAGAATCTGCAAGTGGATATTTGGACTTCTCTGAGGATTTCGTTGGAAACGGGATAAAATTCCCAGAACTACACGGAAGCATTCTCAGAAACTTCTTTGTGATGAAGGGCGAATTCGAATCGGATCCCGGGCCCGTCGACTGCAGAGGCCTGCATGCAAGCTTGGCGTAATCATGGTCATAGCTGTTTCCTGTGTGAAATTGTTATCCGCTCACAATTCCACACAACATACG -3'. After the PCR amplification of the DNA substrate, the DNA was concentrated using a vacufuge to evaporate excess water and purified using the Gel Extraction Kit from Qiagen (Hilden, DE). Lastly, the DNA concentrations were calculated using a NanoDrop Spectrophotometer (ND-1000, Thermo Fischer).

2.3 Nucleosome Assembly

The nucleosome assemblies of both H3 and CENPA are completed through 24-hour dialysis, starting at 2 M NaCl and ending at 2.5 mM NaCl, the same as we have published previously.[76,100,101] This process occurs at 4 °C and utilizes a peristaltic pump that continuously pumps the low salt buffer into the reaction beaker at the same rate that it pumps the high salt buffer out. The $H3_{nuc}$ are purchased from The Histone Source (Fort Collins, CO) and are already in an octameric form. It requires mixing the nucleosomes and DNA and a predialysis to remove the glycerol from the stock. The CENP-A_{nuc} are purchased from EpiCypher (Durham, NC) and come in two stocks, one containing the H2A/H2B dimers and one containing the CENP-A/H4 tetramer. The CENP-A_{nuc} requires an extra step of mixing the two histone stocks in equimolar concentration to obtain an octameric core with two dimers and a single tetramer.

2.4 Protein Procedures

2.4.1 NF-κB Preparation (Prepared by Collaborator)

The Elizabeth Komives group at UC San Diego conducted the NF-κB preparation and provided expertise on the protein. N-terminal hexahistidine murine $p50_{39–350}$/$RelA_{19–321}$ (hereafter referred to as NF-$κB_{RHD}$) was expressed using a modified pET22b vector containing the genes for both polypeptides as described previously [102]. The DNA for murine RelA residues 19-549 was synthesized and subcloned into a modified pET22b vector, which already contained the gene for N-terminal hexahistidine-$p50_{39-350}$ (hereafter referred to as NF-$κBA_{FL}$). The DNA sequence of the $RelA_{TAD}$ (RelA residues 340-549) was subcloned into a pET28a vector with a C-terminal hexahistidine tag.

All vectors were introduced into E. coli BL-21 (DE3) cells using a transformation process, and these cells were then cultured in M9 minimal media containing antibiotics at 37 °C until they reached an optical density (O.D. 600 nm) of 0.5-0.7. Cultures were cooled on ice for 20 minutes, and then protein expression was initiated by adding 0.2 mM IPTG. Cultures were incubated at 18 °C for 16 hours, then harvested by centrifugation. Pellets were stored at -80 °C.

The NF-κB$_{RHD}$, NF-κB$_{FL}$, and RelA$_{TAD}$ constructs were lysed by sonication and purified by Ni^{2+}-NTA chromatography as described previously for NF-κB$_{RHD}$.[76] Following overnight dialysis, the protein was aliquoted and stored at -80 °C. Prior to experiments, aliquots were thawed and further purified. As described previously, NF-κB$_{RHD}$ and NF-κB$_{FL}$ were purified by cation exchange chromatography (MonoS; GE healthcare) to remove bound nucleic acids.[76] The protein was further purified by size-exclusion chromatography using a Superdex 200 column (GE healthcare) in SEC buffer (25 mM Tris, 150 mM NaCl, 0.5 mM EDTA, 1 mM DTT, adjusted to pH 7.5 at room temperature). Care was taken to separate NF-κB$_{FL}$ from a breakdown product that eluted at the same volume as NF-κB$_{RHD}$. RelA$_{TAD}$ was purified by size-exclusion chromatography using a Superdex 75 column, followed by a Superdex 200 column (GE healthcare) in the same buffer.

All purification chromatography steps were conducted in a 4 °C cold room. SDS-PAGE assessed the purity of all proteins. The protein concentration was determined by absorption at 280 nm using a NanoDrop spectrophotometer. Purified protein was stored at 4 °C, and all experiments were conducted within 72 hours of purification by size exclusion chromatography.

2.4.2 NF-κB DNA/Nucleosome Assembly Process

The addition of NF-κB to DNA or nucleosome-containing samples was completed in the same manner as previously.[76] The NF-κB was diluted to 300 nM for nucleosome experiments and 600 nM for DNA experiments in NF-κB buffer (25 mM Tris pH 7.5, 150 mM NaCl, 0.5 mM EDTA, 1 mM DTT). The DNA experiments incubated NF-κB at a 2:1 ratio with the DNA for 10 minutes at room temperature. The nucleosome experiments incubated NF-κB at a 1:1 ratio, resulting in 150 nM for both nucleosomes and NF-κB, then incubated for 10 minutes at room temperature.

2.4.3 Rhizavidin Bacterial Transformation Procedures

Four ng of DNA was added to Novablue cells. The cells were heat-shocked by immersion in a 42 °C water bath for 30 seconds. The solution was returned to the ice for 2 minutes. 250 µL of Super Optimal broth with Catabolism suppressor (SOC). The cells were plated with sterilized equipment. Three

quantities were plated and incubated overnight at 37 °C: 10 µL, 50 µL, 170 µL. After one day, 50 µL and 170 µL plates were overgrown due to the high efficiency of transformation. A colony was collected using a 10 µL pipette tip and inoculated into 50 mL of Luria-Bertani (LB) medium.

2.4.4 Rhizavidin Plasmid Purification Procedures

E.Z.N.A.® Plasmid DNA Maxi kit was used to isolate the plasmid DNA. The final DNA concentration was 78.1 ng/µL. Eighteen 50 µL aliquots were made and frozen for future use. BL21(DE3) transformation and plating were conducted on a single aliquot. Four hours at 37 °C vs. overnight at 18 °C test induction was done to determine which method works best for producing the protein inside the bacteria. It was determined that the overnight growth at low temperatures worked best.

A 6L culture was started and induced for overnight growth at 18 °C. The cells were grown overnight at a lower temperature and then quickly subjected to a heat shock followed by cooling on ice to enhance the expression of chaperones. The culture was grown to O.D. 600 nm of 0.870 before induction. After growing overnight, cells were lysed using a French press cell lysis and centrifuged at 40,000 x g for 30 minutes. The results from expression were ~3.5 grams of lysate/2L. The lysate is then dissolved in water and run through an iminobiotin-packed agarose column. The binding buffer for the column was 50 mM ammonium carbonate, pH 11, 500 mM NaCl, and the elution buffer was 50 mM ammonium acetate, pH 4.0, and 500 mM NaCl. Aliquots had 1M Tris pH 7.5 added to them to bring pH to a more neutral level.

2.5 AFM Sample Preparation

2.5.1 Dry AFM Sample Preparation and Imaging

The dry AFM samples are prepared after the assembly of the nucleosomes and are deposited on 1-(3-aminopropyl)silatrane (APS) mica. The addition of APS to mica thereby functionalizes the surface of the mica but creates a positively charged surface instead of a negatively charged mica surface. The stock solutions of nucleosomes (H3 and CENP-A) are stored at 300 nM at 4 °C. In preparation for the stock

solution for imaging, a small aliquot is taken and diluted to 2 nM using imaging buffer (4 mM $MgCl_2$, 10 mM HEPES, and pH 7.4) and deposited on the APS mica. The mica containing the sample is incubated for 2 minutes, washed gently with DI water, and dried with a slow argon flow. The sample is placed in a vacuum and allowed to dry overnight under a vacuum. The dried samples are then imaged on a Multimode AFM/Nanoscope IIId utilizing TESPA probes (Bruker Nano Inc, Camarilla, Ca). The dry sample images were captured at 3 x 3 μm in size with 1536 pixels/line.

2.5.2 High-Speed AFM Sample Preparation and Imaging in Liquid

High-speed AFM imaging was performed as described in our previous literature.[100,101,103] Briefly, a thin piece of mica was punched into circular pieces with a 1.5 mm diameter and then glued onto the sample stage of the HS-AFM (RIBM, Tsukuba, Japan). 2.5 μl of 500 μM APS solution was deposited onto the mica and incubated for 30 min in a wet chamber to functionalize the mica surface. The mica surface was then rinsed with 20 μl of deionized water. Then, 2.5 μl of the DNA or nucleosome sample was deposited onto the APS functionalized mica surface and incubated for 2 min. The sample was then rinsed with buffer and put into the fluid cell containing the imaging buffer described above. HS-AFM carried out imaging using electron beam deposition (EBD) tips. The typical scan size was 400 × 400 nm with an 800 ms/frame scan rate.

2.6 Data Analysis

We utilize the same methods as previously published by our lab.[76,100] The dry sample images captured are analyzed using Femtoscan (Advance Technologies Center, Moscow, Russia), where we can measure the contour lengths of the DNA. The contour length measurements begin at the end of the 3WJ and are measured to the middle of the nucleosome. The second arm measurement starts at the center of the nucleosome and is measured to the 601 terminal end. 5 nm is subtracted from both arm lengths because of the contribution of the DNA to the wrapping around the nucleosome. A conversion factor is calculated from naked DNA to calculate the bp of the measurements. In the dry sample images, measuring the contour lengths of all the free DNA and dividing by the known DNA length (659 bp) will provide a

number around 0.35, which we use to convert nm measurements to bp. The linker length between two nucleosomes is calculated by measuring the DNA length between the center of two nucleosomes and subtracting 10 nm of DNA to account for the contribution of both nucleosomes, as seen in the equation below.

$$Conversion\ Factor = \frac{Measured\ mean\ value\ of\ DNA\ length\ (nm)}{Theoretical\ Length\ of\ the\ designed\ DNA\ substrate\ (bp)}$$

$$Arm\ Length\ (bp) = \frac{(Measured\ from\ DNA\ end\ to\ center\ of\ nucleosomes\ (nm))\ - 5\ nm}{Conversion\ factor\ \left(\frac{nm}{bp}\right)}$$

$$Linker\ Length\ (bp) = \frac{\left(Measured\ center - to - center\ (nm)\right) - 10\ nm}{Conversion\ factor\ \left(\frac{nm}{bp}\right)}$$

In HS-AFM, the contour length is calculated by measuring the DNA length after the nucleosome has evacuated the DNA, and the full-length DNA is accessible for measurement. The averages of the contour lengths are used to calculate the conversion factor. The histograms were created using Origin. Microsoft Excel was used to create scatter plots and bar graphs.

Chapter 3. DEVELOPMENT OF DNA MARKERS

3.1 Introduction

Atomic Force Microscopy (AFM) is a widely used nanotool for single molecule studies of protein–DNA complexes of various types.[104] In many such AFM studies, precise position determination of proteins is of utmost importance, which needs to be retrieved from these experiments. The protein's precise location can only be determined by using large, visible markers on the DNA, and end-labeling the molecule is a simple method. Streptavidin is one such marker, as it specifically binds biotin, that can be incorporated at the end of the DNA template.[105–107] The use of proteins as a marker has several complications. First, binding the protein marker can require a specific buffer composition that can complicate the assembly of the complex under study. Second, the marker can dissociate from the binding site if it is not covalently bound. Third, bulky protein appearance can introduce ambiguity to analysis [108], a problem that led us to utilize rhizavidin, a smaller-sized streptavidin analog [109,110] to reliably distinguish nucleosomal particles due to the similar size of streptavidin from nucleosomes in the AFM images.[98]

An alternative to a bulky protein that binds biotin, rhizavidin can be used as a DNA marker due to the size difference. The rhizavidin (29 kDa) is smaller than streptavidin (51 kDa) for easier and more accurate identification of proteins due to its dimeric state as compared to the tetrameric streptavidin.[109,110]

If the DNA template has a single-stranded end, single-stranded binding proteins such as SSB of *E. coli* can be an attractive marker [111,112], but nonspecific or unwanted interactions can occur.[113] We mentioned the buffer composition above, which can modulate DNA and protein properties.[114–117] This factor is critical in studies of labile and dynamic systems such as chromatin.[118–121] These complications can be avoided if other bulky markers are used. An interesting approach was proposed in [122], where a single-stranded DNA (ssDNA) loop was used as a terminal label for AFM studies, but the labeling yield was low. Later experiments increased the yield of the terminal ssDNA marker to ~70%.[123] However, for some studies, the high flexibility of ssDNA and its relatively low contrast in AFM images compared with dsDNA is a complication in identifying ssDNA loops at the end of DNA duplexes. Reliable visualization

of a terminal label in HS-AFM studies is essential, as multiple frames per second are used to describe the dynamics of a system. The use of a dsDNA-based label could help overcome these complications.

Here, we describe two labeling methods, one based on terminal biotin binding by rhizavidin and a second based on using branched DNA constructs as bulky terminal labels for linear DNA molecules. We used a three-way junction (3WJ) as the simplest branched DNA molecule, which is covalently ligated to a sticky end of the DNA template. We describe a methodology for assembling an appropriate 3WJ, which is stable and easily identifiable with AFM. Our DNA label can be produced efficiently and is a reliable terminal label for DNA and protein–DNA complexes in AFM experiments performed in air and time-lapse HS-AFM studies in an aqueous environment. We tested the use of this labeling in several different protein–DNA systems.

3.2 Experimental Design

3.2.1 Labelling of DNA Substrates with Rhizavidin

AFM experiments utilized biotin attached to one terminal end of the DNA, which can be specifically bound to by rhizavidin and streptavidin. Streptavidin was used for labeling mononucleosomes, and rhizavidin,[109,124] a streptavidin variant with a smaller size, was used for labeling dinucleosomes. Assembled mononucleosomes were incubated with streptavidin for 5 min at room temperature at a molar ratio of 2:1 streptavidin:nucleosome in incubation buffer (10 mM Tris pH 8.0, 125 mM NaCl, 5 mM $MgCl_2$.). Dinucleosomes were incubated with rhizavidin for 5 min at room temperature at a molar ratio of 4:1 rhizavidin:nucleosome in incubation buffer. After incubation, samples were immediately prepared for imaging, as described below.

3.2.2 Oligonucleotides for 3WJ Assembly

Oligonucleotides of the following sequences were acquired commercially from Integrated DNA Technologies (Coralville, IA, USA) with PAGE purification:

Y1: 5′

GCTATACAGCTCGCCGCAGCCGAACGCCCTTGCGCAGCGAGTCAGTGAGATAGGAAGCGGAA

GAGCG-3′

Y2: 5′-

CGCTCTTCCGCTTCCTATCTCACTGACTCGCTGCGCAAGGTTTTTTCTAACAGCATCACACACA

TTAACAATTCTCACATCTGGG-3′

Y3: 5′-

CCCAGATGTGAGAATTGTTAATGTGTGTGATGCTGTTAGGCGTTCGGCTGCGGCGAGCTGTAT-

3′

3.3 Results

3.3.1 Rhizavidin Application Assessed Through AFM Imaging

The addition of rhizavidin required incubation for 15 minutes to get the highest yield of rhizavidin to bind to the DNA. However, the ratio of rhizavidin to DNA necessary to get a good yield of ~40% resulted in the deposit of a lot of rhizavidin binding to the surface of the APS mica (Figure 4).

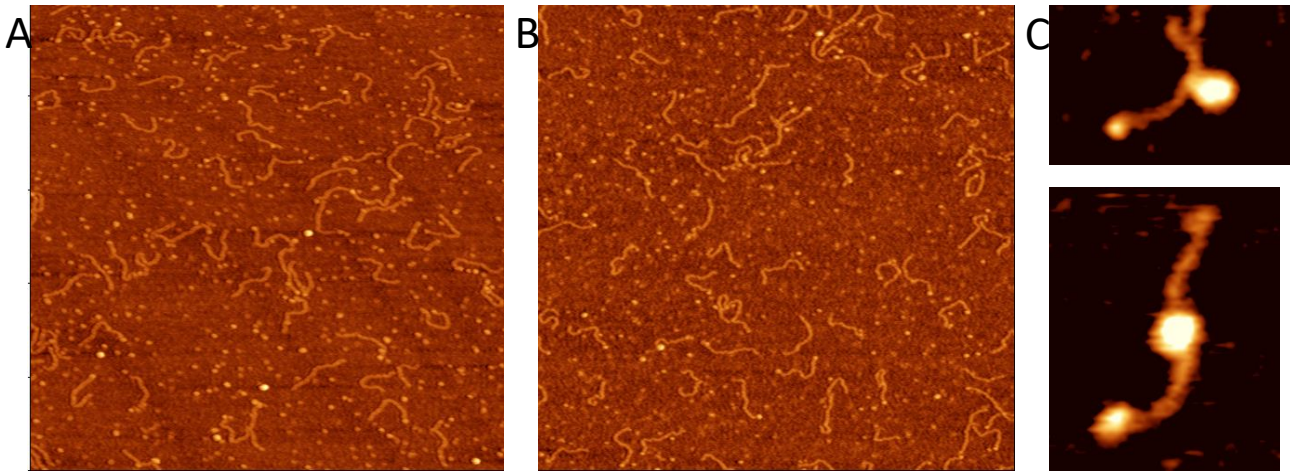

Figure 4- AFM image results of rhizavidin bound to DNA.

AFM images with Rhizavidin bound to DNA containing the 601 sequence (A), random sequence (B), and snapshots rhizavidin bound to the DNA (C). (Unpublished Data)

3.3.3 Coupling of Linear DNA With 3WJ

The 3WJ was assembled by annealing three synthetic DNA oligonucleotides (Figure 1A) to form a construct shown in Figure 1B. Oligonucleotide Y2 contains six T residues to provide additional flexibility to the junction joint.[95,96] The lengths of the arms of the junction are 40 bp, 39 bp, and 20 bp between Y1–Y2, Y2–Y3, and Y1–Y3, respectively. The 3WJ construct was extracted from the gel and ligated to the sticky end of the DNA with its three nucleotide overhang. As described in the methods section, 3WJ containing DNA samples were then deposited on functionalized APS-mica for AFM imaging. One scan of representative AFM images of the labeled DNA is shown in Figure 5A. White arrows indicate the presence of the 3WJ label on the substrate. The yield of DNA labeling was measured by counting the number of clearly defined DNA labels compared with the total of clearly defined DNA molecules. It was determined to be 69% (n = 198), indicating successful label visualization using AFM.

3.3.4 HS-AFM to Visualize the Dynamics of the 3WJ Directly

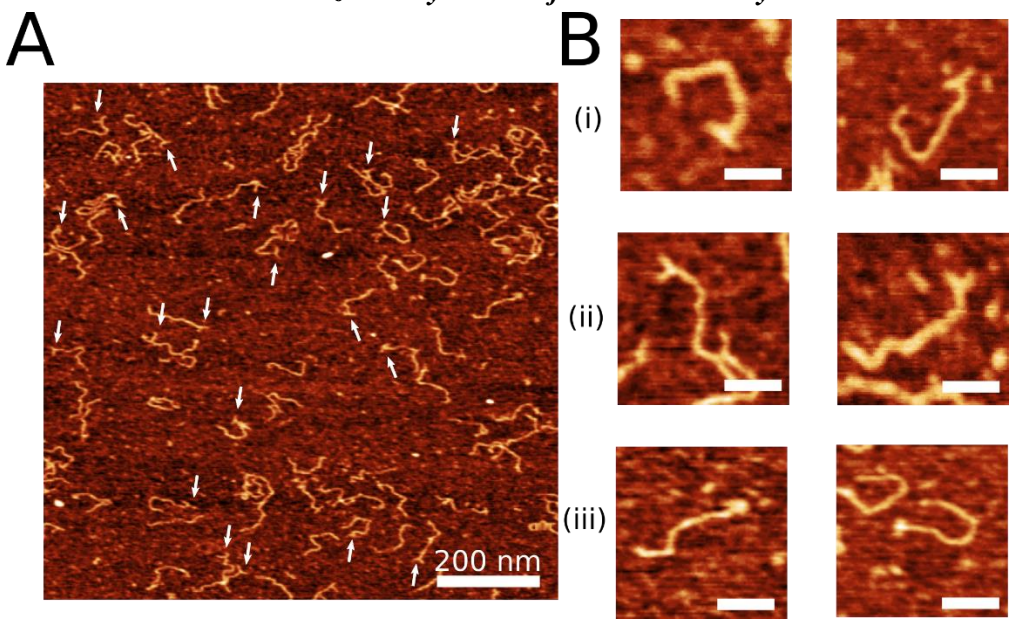

Figure 5- Three-way junction on free DNA.

(A) Representative AFM image of 3WJ label on DNA. White arrows point to the label. The scale bar is 200 nm. (B) Snapshots of DNA with open "T" label conformation (i), bent "Y" label conformation (ii), and condensed "bulge" label conformation (iii). The AFM images are taken in the air. Scale bars indicate 50 nm.

We deposited our labeled DNA on functionalized mica. We imaged it in our imaging buffer on our HS-AFM, which can capture multiple images per second, allowing for the observation of the system's dynamics. The data of the entire set of frames are assembled in Movie S1 of 3WJ. Snapshots from the movie are shown in Figure 6. The label in the "T" conformation from the first frame is immediately observable. It is shown on the right terminus of the DNA molecule. The DNA is shown to be mobile, highlighting the ability of HS-AFM to observe the dynamics of complexes. The unlabeled DNA terminus shows high mobility, curving, and looping throughout the video. The label shows flexibility as well; while the "T" conformation is prominent for the first thirty frames of the video, it briefly adopts a "Y" conformation in frame 31 before reverting to a "T" in frame 33. The DNA and label move throughout the

video, but significantly, the label is visible throughout. In addition to direct visualization of the dynamics of 3WJ, these data illustrate the use of the 3WJ labeling for time-lapse experiments.[95,96,125–127]

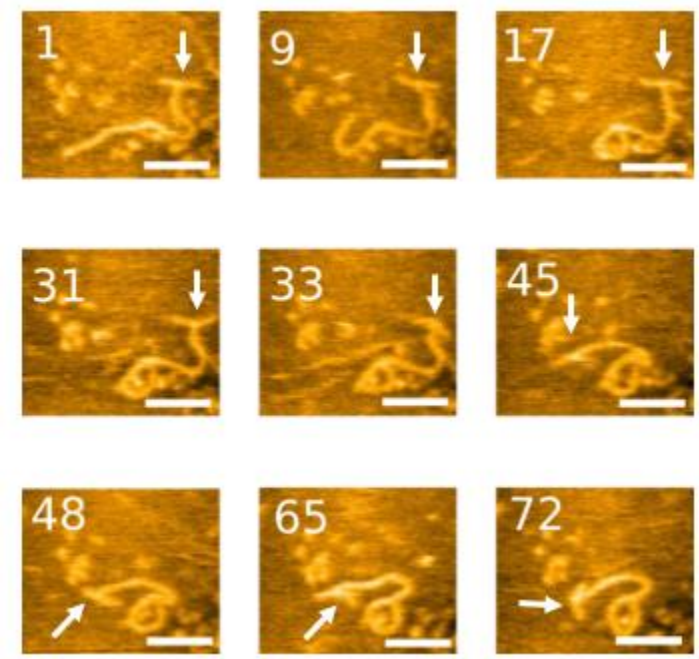

Figure 6- High-speed AFM imaging of labeled DNA substrate.

3WJs are indicated with arrows. The scale bar indicates 40 nm. The numbers in each image are their frame number in the movie file. The complete set of frames can be visualized in Movie S1. The numbers on the snapshots indicate the frame number. A frame is taken every 600 ms.

3.3.5 Assembly of Nucleosomes on 3WJ Substrate

After verifying the successful assembly of our terminally labeled DNA substrate, we aimed to test whether this assembly could be used to study protein–DNA complexes. We chose nucleosomes as our protein–DNA complex of study. Nucleosomes were assembled on the nonspecific 356 bp DNA substrate terminally labeled with the 3WJ using the gradient dialysis approach described in the methods section. After assembly, complexes were diluted to 2 nM, deposited on functionalized mica, and imaged using AFM.

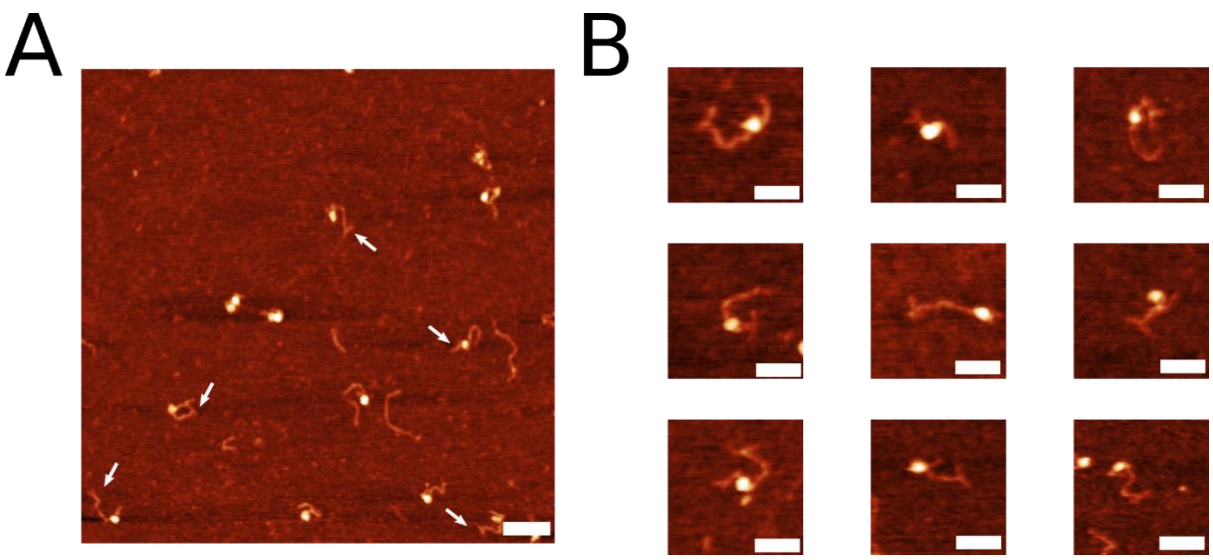

Figure 7- AFM image of nucleosomes assembled on labeled DNA.

*(**A**) A representative frame with images of assembled nucleosomes. White arrows indicate 3WJ labels. The scale bar indicates 100 nm. (**B**) Selected snapshots of nucleosomes with label present. The scale bar indicates 50 nm.*

Representative AFM images of nucleosome assembly with selected snapshots are shown in Figure 7. The bright white features shown in the images are the nucleosome core particles, with DNA flanking on either side. White arrows in Figure 7A indicate the 3WJ labels. Indeed, we can both successfully assemble nucleosome complexes on the labeled DNA substrate and visualize the 3WJ label. Snapshots in Figure 7B show several examples of successfully assembled and labeled nucleosome complexes. The position of the nucleosome varies throughout the different snapshots, as indicated by the distance of the core particle from the labeled end of the DNA. Using the 3WJ as a fiducial marker, one can accurately determine the DNA sequence occupied by the nucleosome based on the position relative to the 3WJ label.

Next, we utilized the 3WJ label to characterize the role of the DNA sequence on the nucleosome assembly. We constructed the DNA substrate comprising the 601 nucleosome-specific sequence and a 372 bp segment with no specific affinity to the histone core termed random sequence to accomplish this goal. A diagram of the DNA construct can be seen in Figure 3 and labeled with the 3WJ as described in the methods. This DNA construct has sufficient space for binding at least two nucleosomes. A 147 bp

sequence 601-motif with a very high affinity to the nucleosome assembly was placed 80 bp from the opposite side as the 3WJ label. We assembled nucleosomes on the substrate and imaged the complexes. AFM images are shown in Figure 8, with selected snapshots to the right. These images show that mononucleosomes are assembled at the position distant to the label with 98% preference, indicating a strong affinity of the nucleosome assembly on the 601-motif.

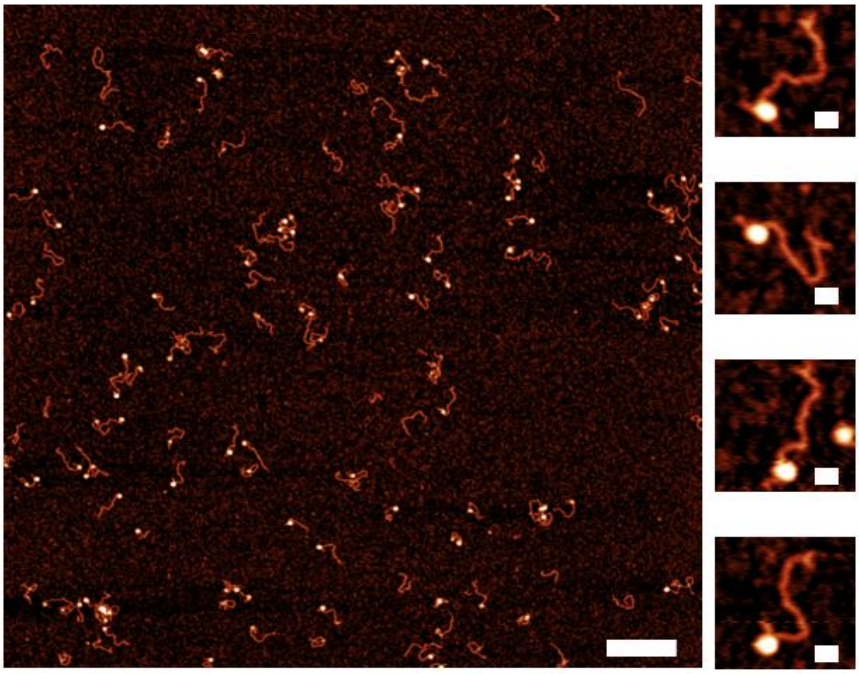

Figure 8- AFM image of nucleosome assembled on dinucleosome construct.

AFM images of dried nucleosome sample assembled on a dinucleosome construct containing the Widom 601 sequence. The snapshots display nucleosomes bound to the Widom 601 sequence and a clear 3WJ. The scale bars are 300 and 25 nm for the larger image and snapshots, respectively.

This conclusion is supported by the mapping results shown in Figure 9. In this graph, the center of the nucleosome positions (orange dots) are located at the 601-sequence, with a few nucleosomes bound to the non-specific DNA sequence. There was no binding of the nucleosomes to the 3WJ label. These

results indicate that the 3WJ is a reliable terminal label, able to facilitate studies of sequence-dependent protein–DNA interactions by allowing the precise determination of the protein position.

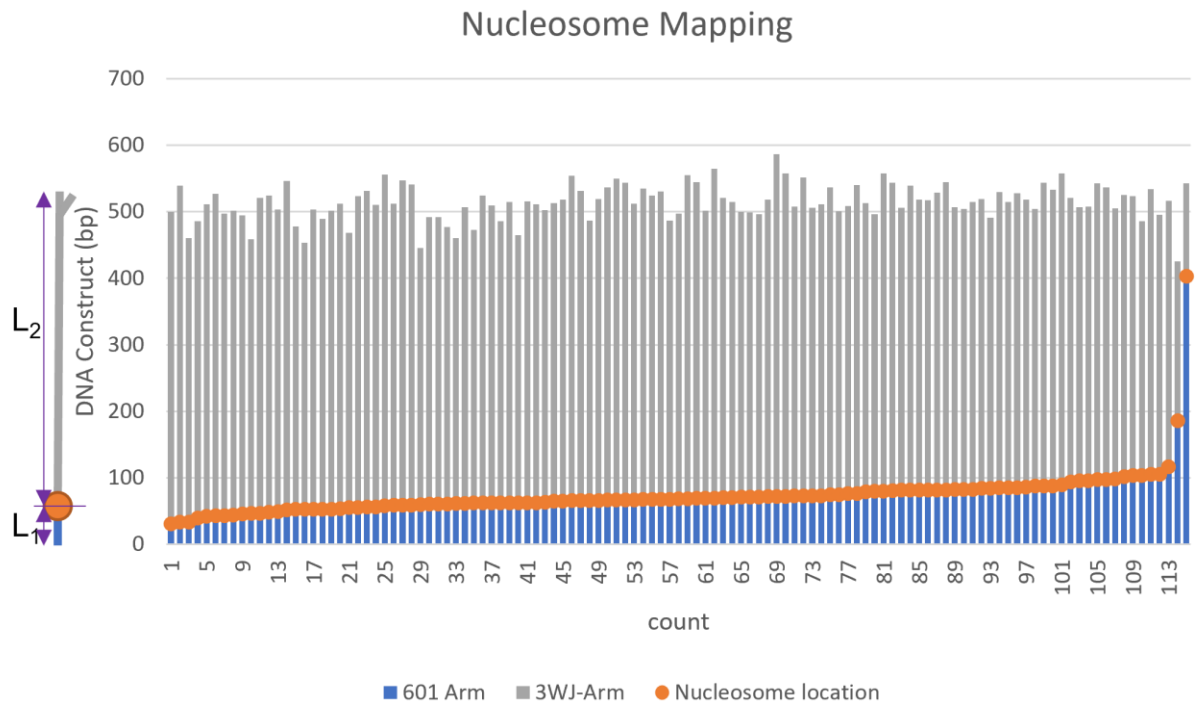

Figure 9- Nucleosome mapping data from dinucleosome construct.

Mapping data from the analysis of nucleosomes assembled on the DNA template containing the nucleosome-specific and non-specific sequences. On the left is a schematic of the DNA construct with the nucleosome bound (orange dot). The nucleosome position was measured from the center of the nucleosome particle to the DNA end. The grey bars (L_2) correspond to the distance measured from the end of the 3WJ to the center of the nucleosome, and the blue bars (L_1) show the distance from the center of the nucleosome to the unlabeled end of the DNA. 5 nm was subtracted from the measurement of each DNA flank to account for the size contributed by the nucleosome core. The variable overall contour lengths of the DNA are due to the varying wrapping efficiency of the nucleosome.

3.3.5 Dynamics of the Nucleosome

We continued our HS-AFM experiments to characterize the dynamics of the nucleosome arrays. In one set of experiments, we followed the dynamic unraveling of a mononucleosome assembled on the labeled DNA substrate. The video is shown as a movie in Movie S2, and selected snapshots from this video are shown in Figure 10. In frame 1, an assembled nucleosome is shown as the bright globular feature indicated with an arrow. The DNA label, which is distant from the nucleosome, remains in the "T" conformation. Over time, the nucleosome undergoes unraveling, identified by decreasing nucleosome height and increasing arm lengths. The unwrapping of DNA from the histone core starts after frame 10, with a complete dissociation in frame 25. This conclusion is supported by the height measurements of nucleosomes shown in Figure 11. The initial height of the nucleosome with the value of 2.5 nm gradually decreases to 1 nm (frame 17), after which the core dissociates. Note that the 3WJ label in this frame is still clearly visible, with primarily a T-shape briefly adopting a "Y" conformation, as shown in frame 20.

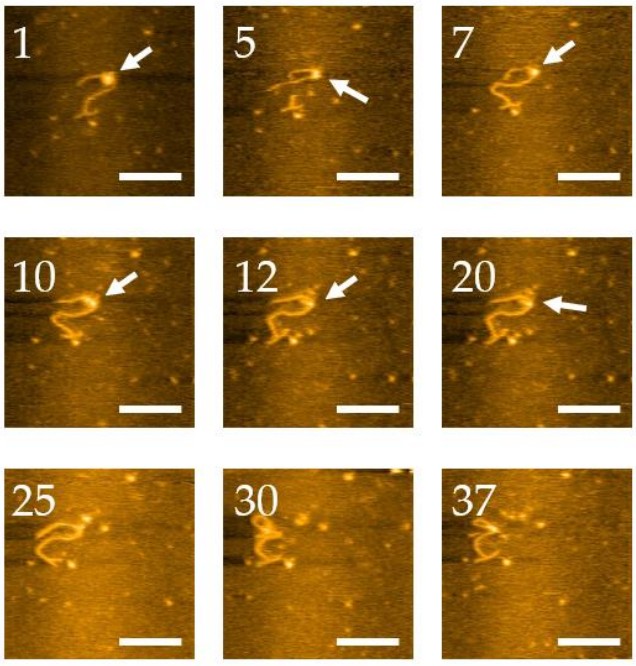

Figure 10- High-speed AFM imaging of nucleosome dynamics on labeled DNA.

The nucleosome is indicated with arrows. Scale bars indicate 50 nm. The numbers in each image are their frame number in the movie. The numbers in each image are their frame number in the movie. The complete set of frames can be visualized in Movie S2.

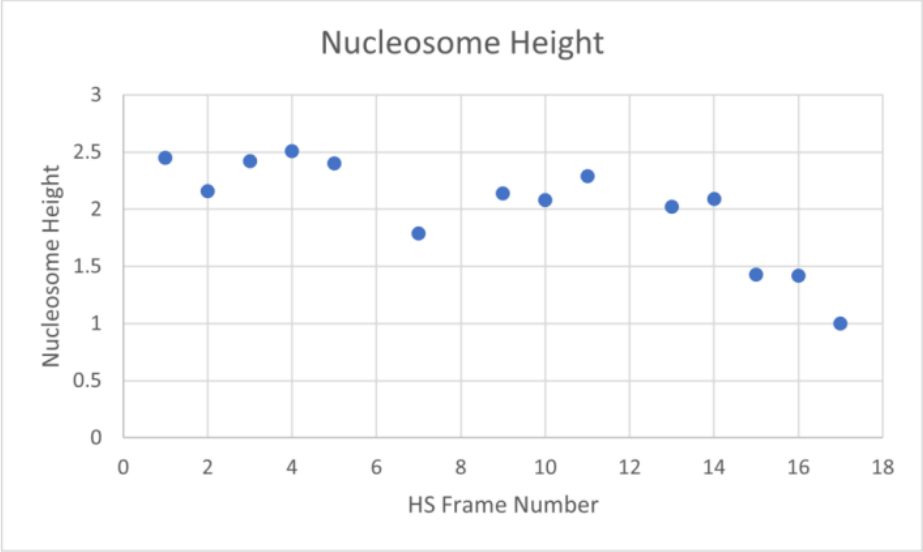

Figure 11-Nucleosome Height Measurements. *The height values remained relatively stable for the first five frames, and then the nucleosome began to unravel, lowering the nucleosome height in the following frames.*

3.4 Discussion

3.4.1 Advantages of 3WJ

We presented here a methodology for the DNA end labeling with a feature routinely identifiable with AFM. We selected the simplest branched DNA molecule, the 3WJ. This approach has several attractive features. First, most topographic AFM studies are performed with protein molecules as a label.[107,128,129] On AFM, these labels appear as globular features. The branched morphology of the 3WJ label is distinct from the globular features of proteins and allows for no ambiguity in identifying the label compared with the protein. We illustrated this benefit by imaging nucleosomes appearing as globular features on the linear DNA template. Second, the 3WJ label is covalently attached to the end of DNA, so buffer composition is not an issue for this type of labeling. This property is essential for studies of protein complexes, as the stability of such complexes can depend dramatically on the buffer composition.

The 3WJ is a dynamic structure with preferable pyramidal conformation with 60° between the arms.[95,96] The unpaired bases at the joint point switch the equilibrium to the T-conformation of the paired arms, and we observed this type of conformational transition with AFM. Such conformational transition does not affect the label's visualization, although the junction's T-conformation is simpler to visualize.

Time-lapse AFM imaging is highly attractive for biological studies, as it allows one to perform imaging close to physiological conditions by avoiding sample drying.[103,130] HS-AFM instrumentation is especially attractive, as it will enable the direct visualization of dynamics at a high data acquisition rate.[99,131,132] We demonstrated that labeling with 3WJ is fully compatible with such AFM instrumentation. The high labeling yield is another attractive feature of the described approach that we would like to emphasize.

The 3WJ is visible through most of the frames despite its dynamics. The arm can be off the surface, becoming non-visible, but appears on the following frame, allowing for unambiguous identification of the DNA end. Once we know which end is the 3WJ end, we can track it through each frame, even if the 3WJ is not visible on AFM in some frames.

We have also utilized the 3WJ to accurately map out the exact location of nucleosomes on a DNA sequence. These results showed that 98% of the H3 nucleosomes bound to the 601 sequence, indicating a high affinity for the sequence with H3 nucleosomes and demonstrating the potential usefulness of this application in further nucleosome analyses.

The DNA template as prepared remains stable during the typical storage of DNA without requiring special conditions for the sample storage. The ligation of 3WJ to the DNA with sticky ends requires adjustment of the junction sequences to the DNA template sequence. However, incorporating the restriction site sequence into the primer for the PCR synthesis of the DNA template allows one to use the unmodified 3WJ with any DNA substrate desired, provided that the substrate does not already contain the SapI restriction site. In the case where another restriction enzyme is required, the 3WJ sequence can be easily modified. This modularity is another convenience, as assembled 3WJ can be used to label a nearly unlimited number of DNA templates.

3.4.2 Disadvantages With Rhizavidin

Although the protein was able to be expressed, purified, and even bound to the biotin-labeled ends of the DNA, the overall yield of the rhizavidin binding to the DNA was too low. In order to get a usable amount of protein bound to the DNA, the ratio of protein to DNA was often 5:1, and with the excess protein binding to the APS mica in the background, it was determined that the protein would not work for our use case. With the high concentrations of proteins, there was also a concern about unwanted side reactions that could occur with the protein.

3.5 Conclusion

The 3WJ resulted in a very versatile and modular technique later used in Chapter 4. INTERNUCLEOSOMAL INTERACTIONS. The 3WJ had an excellent yield of terminal labeling; it was stably bound to the DNA and eliminated the need for another protein to be in the system, which can cause unwanted side reactions. The durability and yield were demonstrated in both static and HS-AFM imaging. The 3WJ labeling has much potential for many projects in the future when labeling is needed.

Despite rhizavidin being a theoretically good DNA marker, the yield was ultimately too low for practical usage with AFM imaging. Rhizavidin required too high of a concentration to get a good yield of bound protein to DNA, which resulted in a background with high concentrations of protein-bound, an undesirable effect or look for AFM images.

Overall, we successfully designed and implemented an efficient and clearly identifiable 3WJ DNA label. This label is observable in the majority of complexes imaged and was shown to be useful in both AFM and HS-AFM studies. Thus, the results presented in this section can be utilized in a vast array of AFM studies in the future, particularly those involving nucleosomes and other protein–DNA complexes.

Chapter 4. INTERNUCLEOSOMAL INTERACTIONS

4.1 Introduction

Nucleosomes are the fundamental nano assemblies in chromatin, the assembly of which is the first step for packing DNA in the nucleus.[22,133] Interaction between nucleosomes is a fundamental property that defines the assembly and function of chromatin. Studies over the past two decades have revealed highly dynamic features of nucleosomes that can explain regulatory processes at the chromatin level (e.g., see recent reviews [104,134,135]). However, structural details and the mechanism underlying the assembly of nucleosomes in higher-order structures of chromatin and their dynamics remain unexplained. Many cellular processes, such as transcription, require the dissociation of DNA from nucleosomes, which is achieved through nucleosome dynamics and remodeling machinery.[136,137] Structural and single-molecule studies of these processes have been critical in developing current nucleosome models [138]; however, the strong reliance on nucleosome positioning sequences for these techniques raises the question of how nucleosome structure and dynamics differ for those assembled on positioning vs. non-positioning DNA sequences.[104] We used DNA templates with different sequences and AFM visualization to directly characterize the role of the DNA sequence on the positioning of nucleosomes and their interactions.[98,104,139–142] In paper [142], we used DNA templates with different sequences. We found that nucleosomes are capable of close positioning with no discernible space between them, even in the case of assembled dinucleosomes. This array morphology contrasts with that observed for arrays assembled with repeats of the nucleosome positioning motifs separated by uniform spacers.[143] Simulated assembly of tetranucleosomes by random placement along the substrates revealed that the interaction of the nucleosomes promotes nucleosome array compaction.[142] In this paper, we developed a theoretical model capable of accounting for the role of DNA sequence and internucleosomal interactions in forming nucleosome structures. These findings suggest that, in the chromatin assembly, the affinity of the nucleosomes to the DNA sequence and the strengths of the internucleosomal interactions are the two major factors defining the compactness of the chromatin.

Canonical nucleosomes ($H3_{nuc}$) are found throughout the chromosome and consist of two of each histone (H2A, H2B, H3, and H4).[144–146] The H2A and H2B form dimers and interact with the entry-exit site opposite the H3/H4 tetramer arranged at the dyad.[147] The $H3_{nuc}$ wrap ~147 bp of DNA corresponding to ~1.7 turns around the octameric histone core.[148–151] A unique area of the chromosome is the centromere, which is responsible for holding together the sister chromatid and then must be pulled apart during replication.[45,152,153] In the centromere nucleosomes, a variant of H3 histone is replaced with its variant CENP-A in the octameric core. CENP-A nucleosomes ($CENP\text{-}A_{nuc}$) typically wrap 121 bp.[48,154] Both types of nucleosomes are dynamic, and in our AFM experiments[139], we found that CENP-A nucleosomes are capable of spontaneous unwrapping, which is the major dynamics pathway. [100,101,139,155] Unwrapped CENP-A nucleosomes can undergo long-range translocation by traveling over ~200 bp; this process is also reversible.[100,155] Additionally, CENP-A stabilizes nucleosome core particles against complete dissociation even when not fully wrapped with DNA.[100,155]

Here, we compared nanoscale features of both types of nucleosomes assembled on identical DNA templates. Using the DNA template with segments with different nucleosome affinity capable of forming two nucleosomes, we compared the interactions and dynamics properties of both types of nucleosomes assembled on the same DNA templates. Internucleosomal interaction was estimated by measuring the internucleosomal distance, revealing the elevated interactions between canonical nucleosomes compared with CENP-A ones. Time-lapse, high-speed AFM (HS-AFM) was applied to characterize the nucleosome's unraveling dynamics, allowing us to reveal similarities and differences between canonical H3 and CENP-A nucleosomes.

4.2 Experimental Design

4.2.1 DNA construct

A description and diagram of the 3WJ used in these experiments can be seen in Chapter

2.2.2 3WJ DNA Full Construct Preparation

.

4.2.2 Assembly of H3 and CENP-A nucleosomes

A description of $H3_{nuc}$ and CENP-$_{Anuc}$ assembly can be seen in Chapter 2.3 Nucleosome Assembly.

4.2.3 Dry AFM sample preparation

Chapter 2.5.1 Dry AFM Sample Preparation and Imaging contains the dry AFM sample preparation description.

4.2.4 High-Speed Atomic Force Microscopy Imaging in Liquid

A description of high-speed AFM sample preparation can be seen in Chapter 2.5.2 High-Speed AFM Sample Preparation and Imaging in Liquid.

4.2.5 Data Analysis

A description of Data Analysis can be seen in Chapter 2.6 Data Analysis.

4.3 Results

4.3.1 DNA Substrate

We designed a DNA template capable of assembling two nucleosomes containing the nucleosome-specific 601 motif and non-nucleosome-specific random sequences to accomplish our goal. Schematically, the construct is shown in Figure 12A. At the end of the DNA, opposite the location of the 601 motif, we placed a three-way junction DNA segment forming a Y-shape, which served as the marker for mapping the nucleosomes on the DNA.[141] The nucleosomes were assembled as described in the methods section using a 2:1 molar ratio of the nucleosome core and DNA. The samples with CENP-A and canonical $H3_{nuc}$ were assembled in parallel and prepared for AFM imaging as described earlier.[76,101]

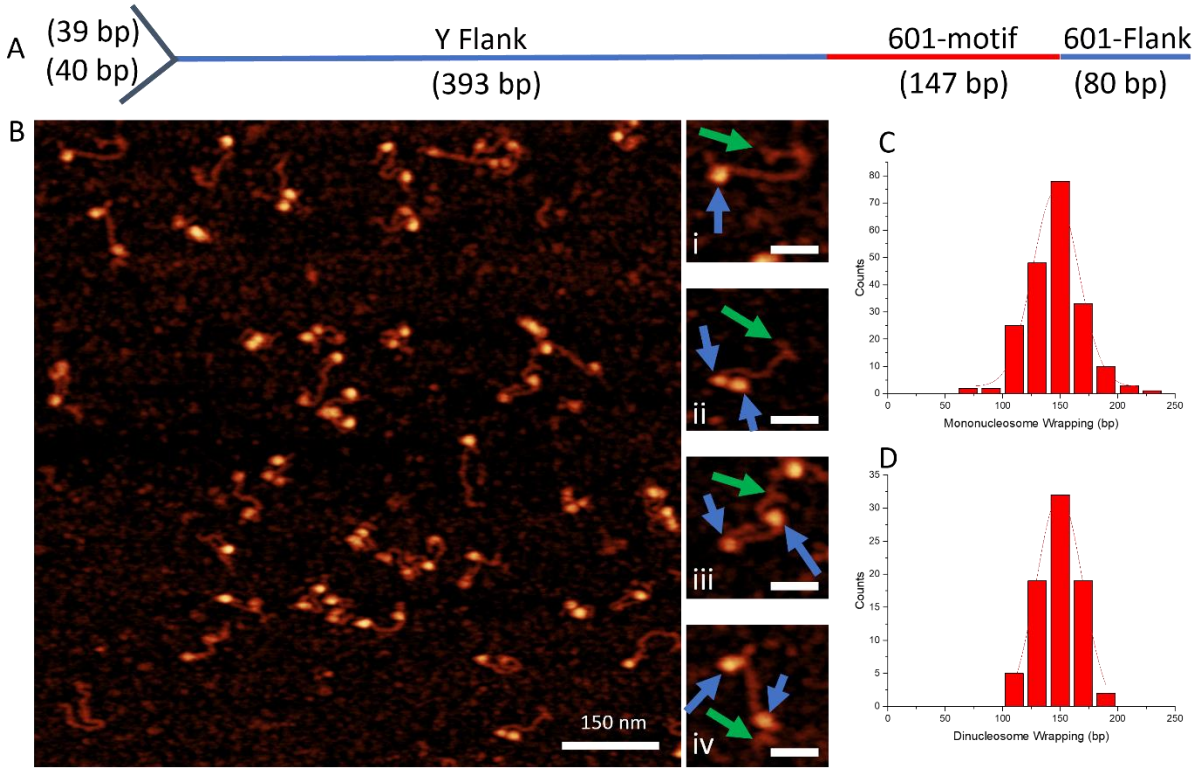

Figure 12- AFM imaging of H3 Dinucleosomes.

(A) DNA construct containing a three-way junction at one terminal end as a fiducial marker, and the 601 motif is shown in red. (B) AFM image 1000 nm x 1000 nm. Selected zoomed images of monoH3$_{nuc}$(i) and diH3$_{nuc}$(ii, iii, and iv) subsets are shown to the right of the main AFM image. Nucleosomes and 3WJ are indicated with blue and green arrows, respectively. (C, D) histograms for wrapping efficiencies of mononucleosomes (C) and the dinucleosomes (D).

4.3.2 Positioning for Canonical H3 Nucleosomes

Figure 12B shows typical topographic AFM images for the array with canonical H3$_{nuc}$ sample. Nucleosomes appear as bright globular features, and mononucleosome samples are seen along with dinucleosomes. Selected images for mono and dinucleosomes are shown to the right of the scan. The frame (i) shows a mononucleosome AFM image in which the nucleosome is indicated with a blue arrow, whereas the green arrow points to the Y-end of the DNA. Three other frames (ii) – (iv) illustrate dinucleosome samples with different distances between the nucleosomes indicated with blue arrows. The

nucleosomes were found in close locations (frame (ii)) or far from each other, frames (iii) and (iv). The AFM images were analyzed to characterize the arrays.

First, the length of DNA wrapped around the nucleosome was measured to determine the length of DNA wrapped around the core, wrapping efficiency. It was done by subtracting the total contour lengths of DNA segments attached to the nucleosome core from the total length of the free DNA. The mono- and dinucleosome sample data are shown in Figure 12C and D, respectively. These data demonstrate that the mono$H3_{nuc}$ wrap 145 ± 23 bp and the di$H3_{nuc}$ wrap 149 ± 24 bp, which are in the expected 147 bp value range.[156,157]

Next, we mapped the position of nucleosomes for both types of samples. The data visualizing the positions of the center of the nucleosomes for the mononucleosome samples are shown in Figure 13A. The green boxed-in area indicates the 601 location on the DNA construct, and the orange dots indicate the center position of the nucleosome. Therefore, if the orange dot is within the green boxed-in area, this shows the nucleosome is bound to the 601 location of the DNA. The zero position on the Y-axis corresponds to the DNA end opposite the 3WJ. The primary binding location of nucleosomes are to the

601 sequence (orange dots)—only three nucleosomes out of 202 (99%) bind to the locations outside the 601 region. The histogram of the nucleosome position in Figure 13B produces a narrow distribution.

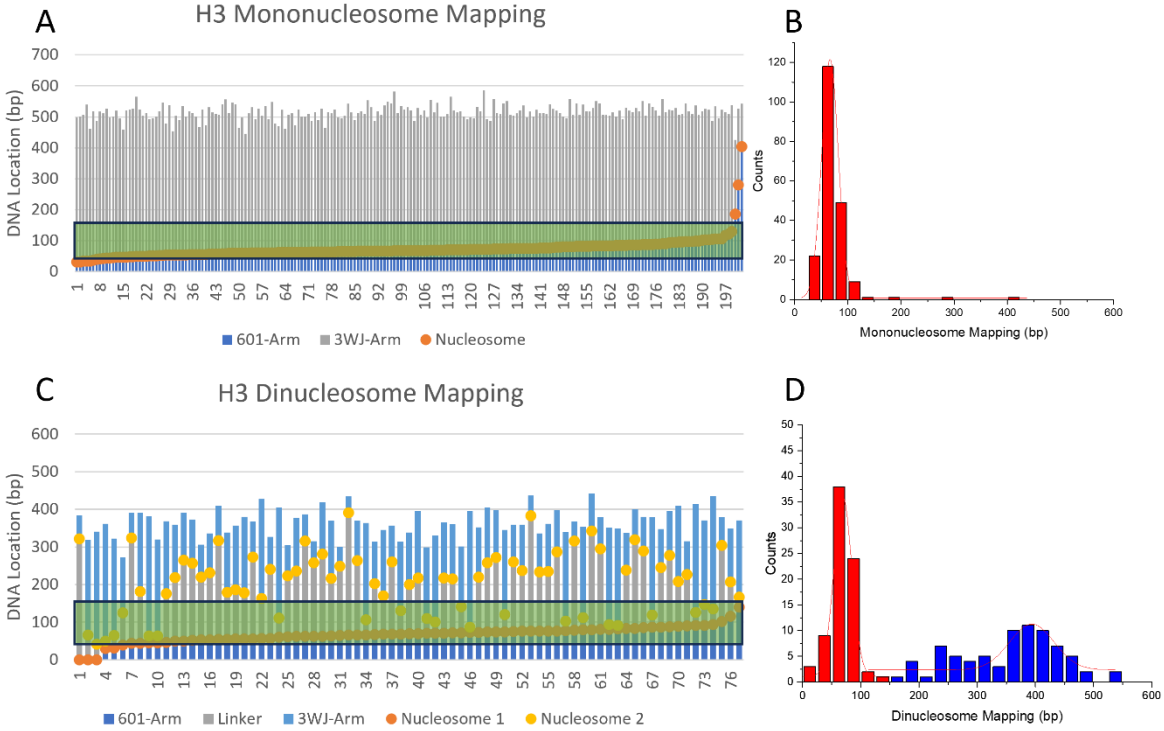

Figure 13- Nucleosome Mapping of H3 nucleosomes.

The dry sample AFM of monoH3$_{nuc}$ (A) and diH3$_{nuc}$ (B) mapping location binding on the DNA construct. The orange and yellow dots are nucleosome binding locations. The Y-axis is the DNA location, where 0 indicates the 601 terminal end and the 601 motif starts 80 bp from 0. The green boxed-in area represents the 601 portion on the DNA. (C, D) depict histograms for mapping data for mononucleosomes (C) and dinucleosomes (D). Different colors in C and D correspond to nucleosome position on 601 motif (red) and the rest of the DNA template (blue).

A similar mapping analysis was performed for the dinucleosome samples, and the results are assembled in Figure 13C. Nucleosomes bound to the 601 region are depicted in orange dots, and the position of the second nucleosome is shown as yellow dots. The positions of the yellow dots are not specific, so these are scattered over the rest of the DNA template. The histograms for the nucleosome positions assembled as histograms are shown in Figure 13D. A narrow peak (red) corresponds to the nucleosome assembled at the 601 sequence, and the positions of the second nucleosome shown in blue are not well defined, producing a broad peak.

4.3.3 Positioning for CENP-A Nucleosomes

Typical AFM images for the CENP-A_{nuc} samples are shown in Figure 14A with selected zoomed images of the subset's mono- and dinucleosome species. In frame (i), a mononucleosome (blue arrow) can be seen bound to the 601 site, far from the 3WJ (green arrow) at the opposite end of the DNA. In frame (ii), two nucleosomes are relatively close to one another. In frame (iii), there is one stable nucleosome fully wrapped nucleosome near the 601 site, and near the 3WJ, there is an unwrapped nucleosome. In frame (iv), two partially unwrapped nucleosomes are bound to the DNA.

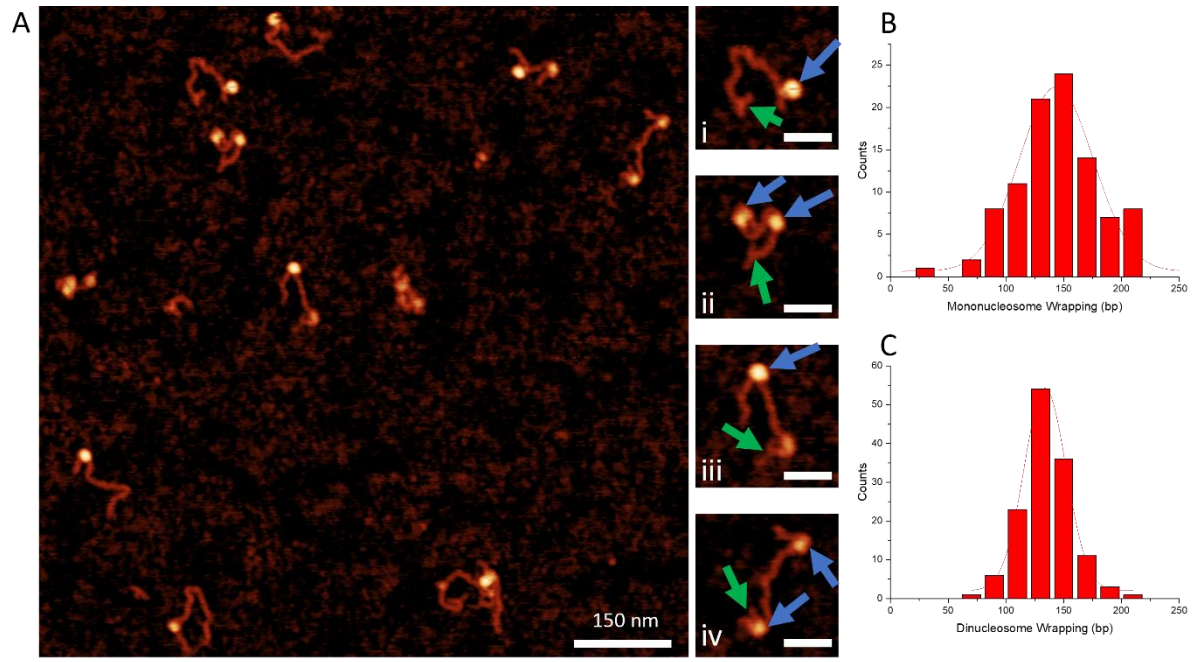

Figure 14- AFM imaging of CENP-A nucleosomes.

(A) AFM image 1000 nm x 1000 nm. Selected zoomed images of monoCENP-A_{nuc} (i and iii) and diCENP-A_{nuc}(ii and iv) subsets are shown to the right of the main AFM image. Nucleosomes and 3WJ are indicated with blue and green arrows, respectively. (B, C) histograms for wrapping efficiencies of mononucleosomes (B) and dinucleosomes (C).

The measurements of the DNA wrapping efficiency for CENP-A_{nuc} were done the same way as for the $H3_{nuc}$ samples. The monoCENP-A_{nuc} samples had a DNA wrapping efficiency of 137 ± 43 bp; the standard deviation for the monoCENP-A_{nuc} wrapping is much larger than the $H3_{nuc}$ counterpart. The

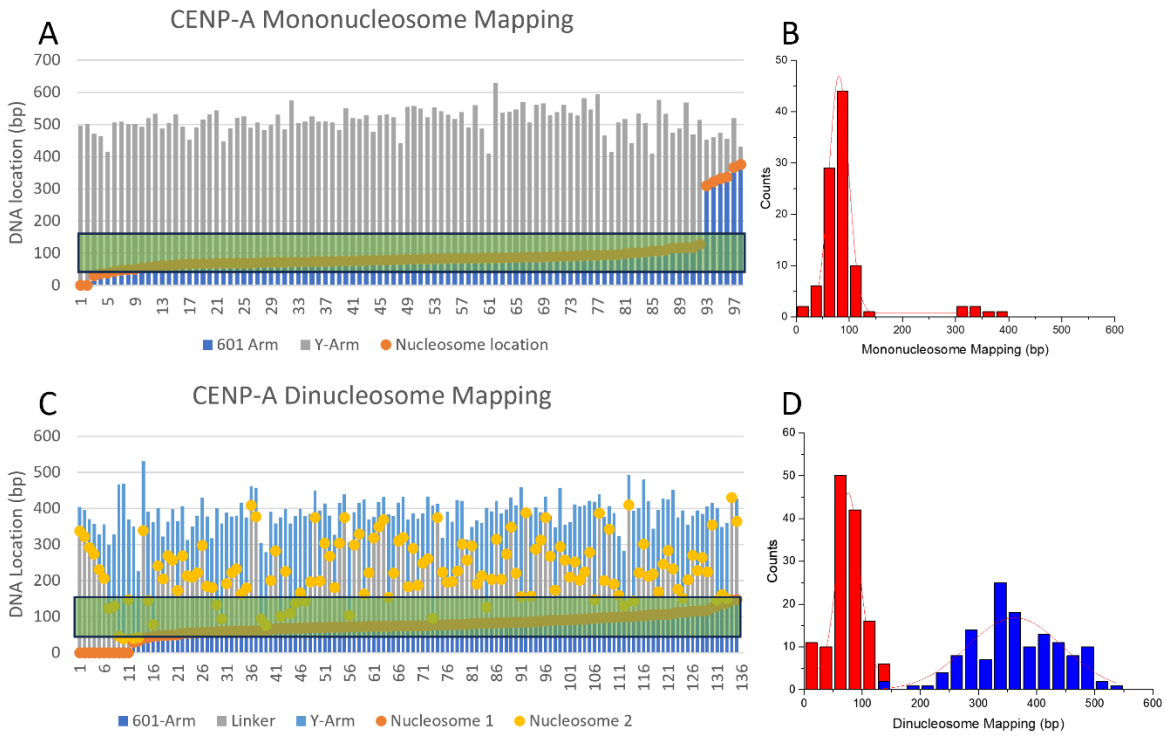

Figure 15- AFM mapping of CENP-Anuc.

The dry sample AFM of monoCENP-A_{nuc} (A) and diCENP-A_{nuc} (B) AFM mapping location binding on the DNA construct. The orange and yellow dots are nucleosome binding locations. The Y-axis is the DNA location, where 0 indicates the 601 terminal end and the 601 motif starts 80 bp from 0. The green area represents the 601 area on the DNA. (C, D) depict histograms for mapping data for mononucleosomes (C) and dinucleosomes (D). Different colors in C and D correspond to nucleosome position on 601 motif (red) and the rest of the DNA template (blue).

dinucleosome assemblies of CENP-A_{nuc} DNA wrapping efficiency was 130 ± 1.4 bp (SEM). Histograms for the bp wrapping of mononucleosomes and dinucleosomes can be seen in Figure 14B and C.

The mapping of CENP-A_{nuc} was completed on the same DNA construct as the $H3_{nuc}$. The monoCENP-A_{nuc} mapping results can be seen in Figure 15A. The green highlighted area shows the location of the 601 sequence on the DNA construct. The orange dots represent the center of the nucleosome binding location. The blue arm represents the DNA from the center of the nucleosome to the non-3WJ terminal end, and the grey bars represent the DNA from the center of the nucleosome to the 3WJ terminal end. The high affinity of the nucleosomes to the 601 motif is seen in these nucleosomes,

although there is a decrease to 92% binding to the specific sequence as compared to 99% for $H3_{nuc}$. A histogram representation of the CENP-A_{nuc} binding location can be seen in Figure 15B, showing the specific binding to the 601 region.

The mapping results for the dinucleosome CENP-A_{nuc} sample ($diH3_{nuc}$) are shown in Figure 15C. The orange dots are the nucleosomes bound closer to the non-3WJ end, which results in 93% of the nucleosomes binding to the 601 sequence. The yellow dots represent the nucleosomes binding closer to the 3WJ end, which is comprised of non-specific DNA; therefore, the nucleosomes have random binding locations. Interestingly, there is an elevated affinity of the CENP-A_{nuc} assembly at the end of the DNA template.

4.3.4 Internucleosomal Interactions for H3 and CENP-A Nucleosomes

Nucleosomes in the AFM images (e.g., plate (ii) in Figure 12B) are located close to each other, pointing to the interaction between the nucleosomes. Such events can be identified in dinucleosome maps (Figure 16) by the co-localization of two nucleosomes. We used the values for the centers of the nucleosome locations to measure the linker length's internucleosomal distance to characterize the ratio of such close contacts.[98] The results of such measurements for canonical H3 dinucleosomes are shown as histograms in Figure 16A. The first bar in the histogram corresponds to the close location of the nucleosome, which, according to our publication [98], points to the formation of close internucleosomal contacts. The yield of nucleosomes with a linker length of less than 50 bp was 23%. A similar analysis was done for the CENP-A dinucleosomes, and the histogram is shown in Figure 16B. Although the bar corresponding to the distance below 50 nm is detectable, its height is twice lower than that for $H3_{nuc}$ (Figure 16A), pointing to the weaker internucleosomal interactions for CENP-A_{nuc} compared with $H3_{nuc}$ ones.

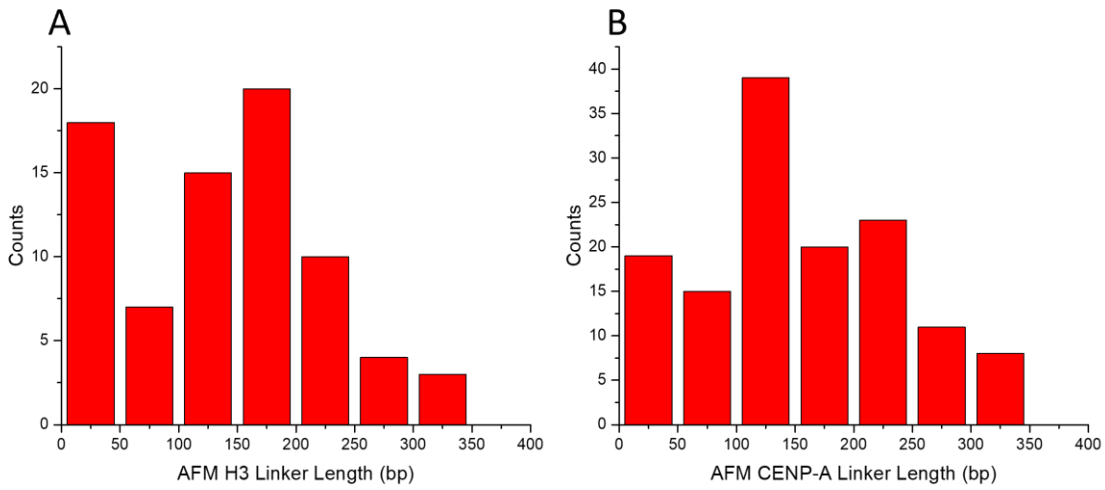

Figure 16- Dinucleosome linker length results.

The $H3_{nuc}$ linker length (A) shows a preferential linker length of less than 50 bp and a gaussian distribution of around 170 bp. The CENP-A_{nuc} linker length (B) demonstrated a lower yield of linker lengths less than 50 bp and the largest population of around 125 bp.

4.3.5 Time-lapse AFM to Probe Nucleosome Dynamics

Nucleosomes are dynamic complexes capable of spontaneous dissociation, which were directly characterized by single-molecule approaches.[132,158] AFM is attractive among these methods because it can directly visualize the spontaneous unraveling of nucleosomes using the time-lapse AFM approach.[132,159,160] In this approach, the sample is placed on the substrate, and continuous scanning over the same area allows one to observe the dynamics of various systems, including nucleosomes.[160] We applied high-speed AFM capable of data acquisition in the millisecond time scale [103,161] to compare the dynamics of two types of nucleosomes characterized above. Multiple frames are acquired, and a set of time-lapse images over the same area is shown in Figure 17 to illustrate a spontaneous unraveling of the nucleosome—the complete set of datasets with 211 frames assembled as Movie S3 is shown in the

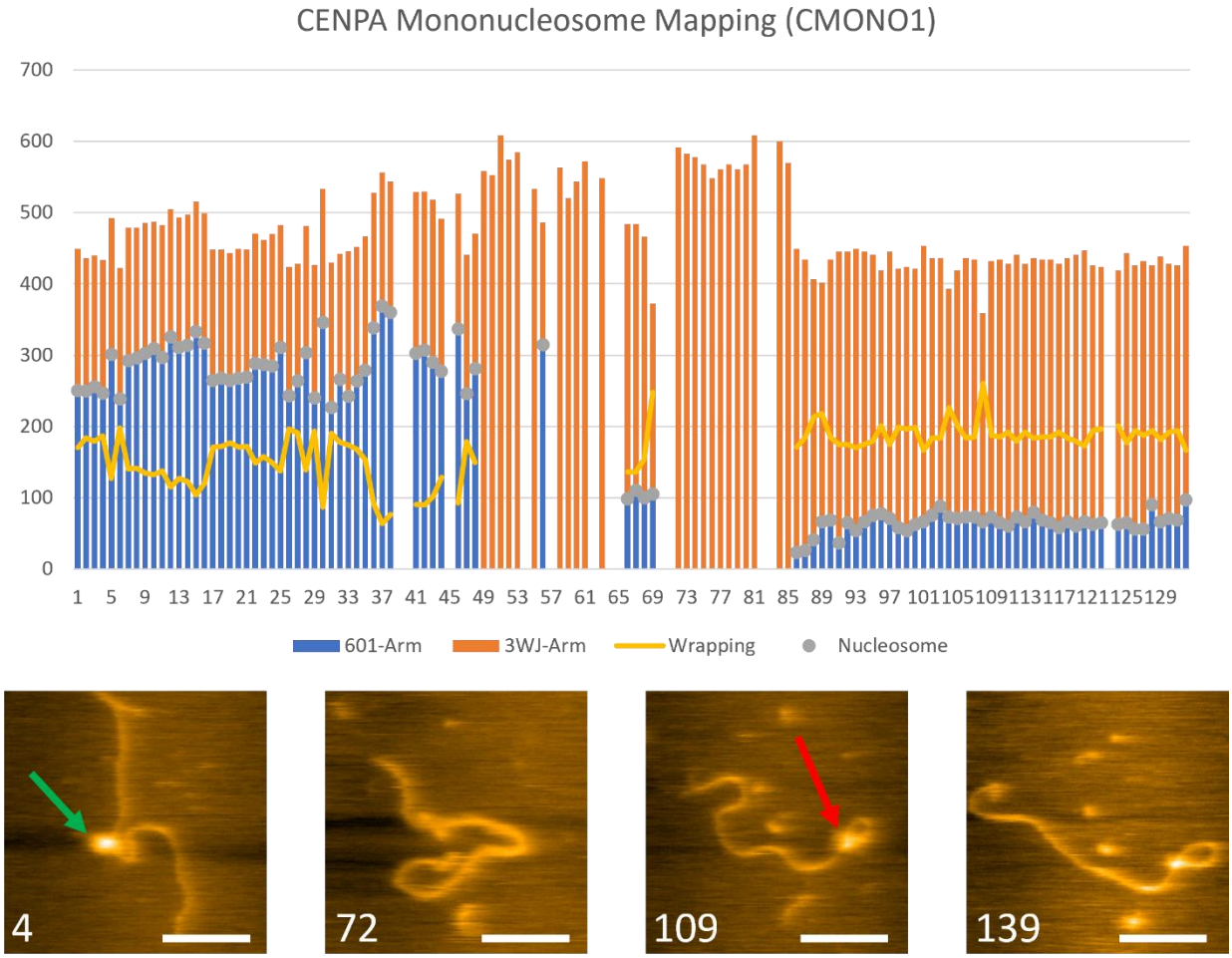

Figure 17- High-speed AFM video analysis.

The Movie S3 analyzed, showing the mapping (bar graph) and snap shots of particular frames. The grey dots in the bar graph indicate the nucleosome bound to the DNA. The yellow line shows the wrapping of the CENP-A nucleosome. The number in white in the bottom left of the snap shots indicates the frame the image is from. In frame 4, the nucleosome is fully wrapped in a random location (green arrow) in the middle of the DNA. In frame 72, the nucleosome has disassociated completely from the DNA. In frame 109, a nucleosome rewraps DNA, spontaneous assembling a nucleosome. This assembly remains stably wrapped up to frame 139. Scale bar is 50 nm.

supplement. There were approximately 100 videos analyzed in total for $H3_{nuc}$ and CENP-A_{nuc}, which resulted in 4113 total frames analyzed.

4.3.5.1 Dwell Time for Nucleosomes Unraveling

One of the parameters we analyzed was the dwell time of the nucleosome, defined by the time required for the complete unraveling of the nucleosome. First, we compared the dwell times of mono and dinucleosomes, and the results for $H3_{nuc}$ can be seen in Figure 18A and B, respectively. For mono$H3_{nuc}$, we found that 38% of the videos analyzed lasted 20 or more frames. This dwell time was increased by 48% for the di$H3_{nuc}$, suggesting the nucleosome stability increased by the internucleosome interactions.

A similar analysis was done for CENP-A_{nuc} samples, and the data are summarized as histograms in Figure 18C and D. For the monoCENP-A_{nuc}, 52% of the videos analyzed lasted longer than 20 frames, and 66% for the dinucleosomes. CENP-A_{nuc} followed a similar trend as $H3_{nuc}$, but this time, there was an increase of 14% from mononucleosomes to dinucleosomes. Also of interest is that the CENP-A_{nuc} averaged longer dwell times than the $H3_{nuc}$, for mono$H3_{nuc}$ with 38% and CENP-A_{nuc} with 52% of videos with longer than 20 frames in a video. The difference between $H3_{nuc}$ and CENP-A_{nuc} is 14%. The same trend is visible for the dinucleosome results, with a difference of 18% more diCENP-A_{nuc} lasting longer than 20 frames than $H3_{nuc}$. According to these studies, CENP-A_{nuc} are more stable than $H3_{nuc}$ nucleosomes.

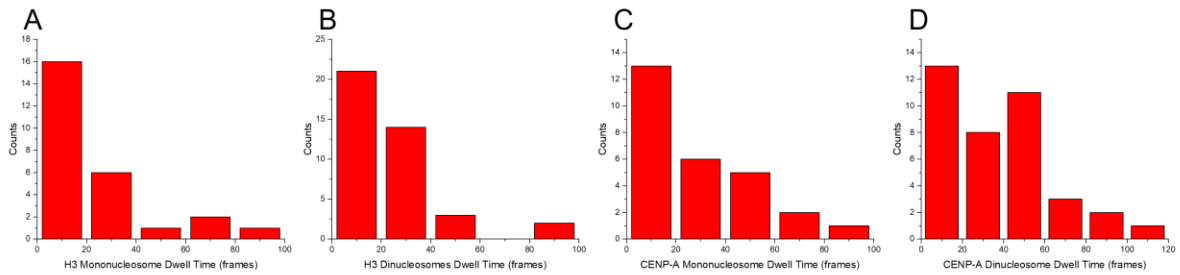

Figure 18- Nucleosome dwell times on HS-AFM.

The monoH3$_{nuc}$ results (A) showed most nucleosomes lasting 20 frames or less. The diH3$_{nuc}$ results (B) showed a shift to the right, indicating that the dinucleosomes have a longer dwell time than the mononucleosomes. The monoCENP-A$_{nuc}$ results (C) showed that most nucleosomes lasted less than 20 frames. The diCENP-A$_{nuc}$ results (D) showed a shift to the right, indicating that the dinucleosomes have a longer dwell time than the mononucleosomes.

4.3.5.2 Dynamics of Nucleosomes Core During Unraveling

This large set of data revealed that unraveling is a non-gradual process. It is illustrated in Figure 8. One set of images is shown in Figure 19A (Movie S4). It can be seen that there is an H3$_{nuc}$ (green arrow) that is wrapped at the 601 location (frame A1). In the following frames (A2 and A20), the histone (blue arrow) has vacated the octameric core, but the partial core remains to wrap the DNA. In frame A36, the DNA unwraps the partial core, resulting in a wrapping of ~100 bp, and the free histone remains near the DNA filament. In the last frame, A66, the DNA loosens even more, effectively no longer tightly wrapping DNA around the core. Another example of a histone exiting the octameric core can be seen in Figure 19B (Movie S5). This H3$_{nuc}$ (green arrow) starts fully wrapped at the 601 location (frame B1). In frames B4 and B7, it can be seen that a histone blue arrow) left the core particle and now drifts nearby. During this process, unwrapping of the DNA took the ~150 bp wrapping down to ~100 bp in frame B4. This unwrapping continues, and by frame B11, the core particle no longer wraps any DNA. Lastly, in frame B14, the histones have wholly vacated the DNA, and only a couple of histones can be seen floating nearby, the original location of the octameric nucleosome core.

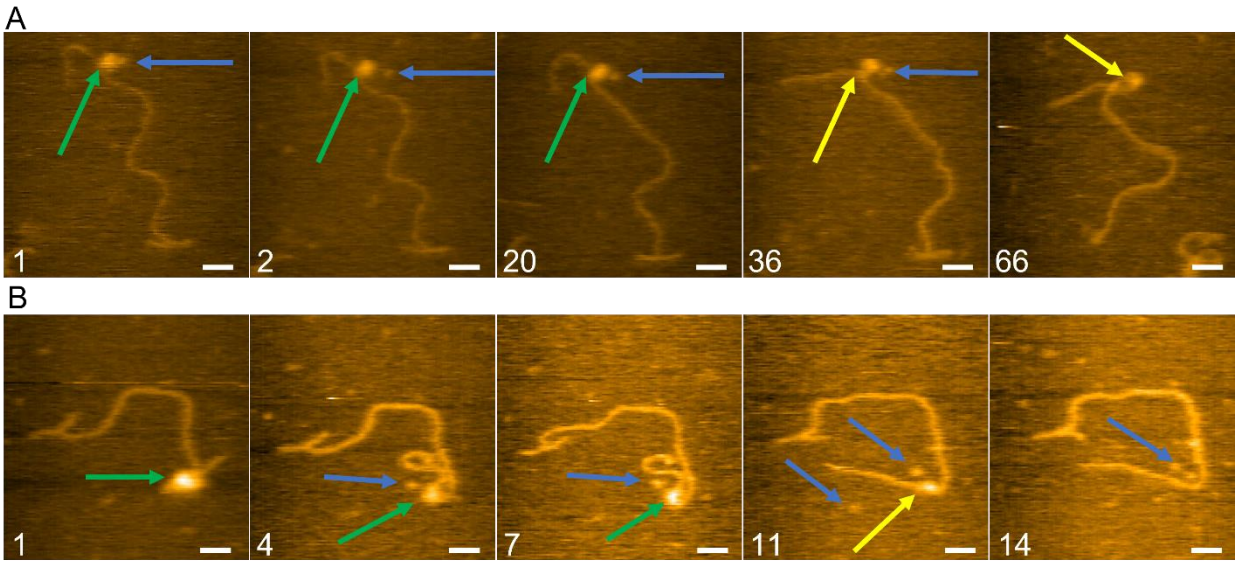

Figure 19- HS-AFM analysis of $H3_{nuc}$ unwrapping.

HS-AFM videos analyzed, showing the protein unwrapping pathway of $H3_{nuc}$(green arrows) with histones (blue arrows) leaving the nucleosome core particle. Once the DNA unwraps the non-octameric core, they are indicated with yellow arrows—the frames in A come from Movie S4. In frame, A1, the nucleosome is bound to the 601 location, and the histone can be seen bulging out, indicated with the blue arrows. This histone moves in frames A2 and A20 while the DNA and nucleosomes remain in the same location. In frame A36, the DNA unravels the nucleosome; by frame, A66, only the tetramer can be seen still bound to the DNA. The frames in B come from the video of Movie S5. In frame, B1, the green arrow indicates a fully wrapped nucleosome bound to the 601 location. In frames B4 and B7, the histone (green arrow) can be seen to have left the nucleosome core particle, leaving a partial core. By frame B11, the DNA has unwrapped the partial core, and the tetramer remains bound. By frame B14, all histones have evacuated the DNA. The scale bar represents 25 nm.

Next, we looked at the unwrapping pathways of CENP-A_{nuc} on the same DNA construct. Figure 20A (complete set of frames in Movie S8), frame A1 shows a fully wrapped CENP-A_{nuc} (green arrow) bound to the 601 site. The nucleosome remains stably wrapped in frames A4 to A18. In frame A20, the nucleosome (yellow arrow) spontaneously unwraps, resulting in a decreased wrapping of ~110 bp. The CENP-A_{nuc} remains wrapped at ~110 bp through the next frame shown, A37. The example in Figure 20B (Movie S9) shows a CENP-A_{nuc} bound near the 3WJ (frame B3). The CENP-A_{nuc} (green arrow) remains stably wrapped at this location through frames B8 to B11. In frame B13, the nucleosome (yellow arrow)

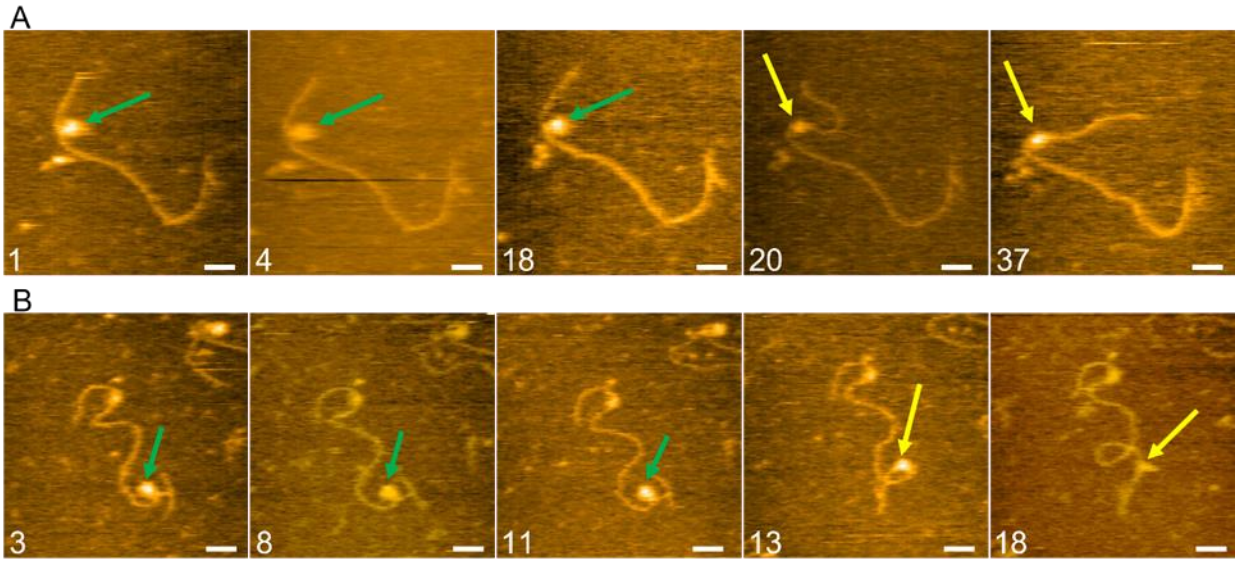

Figure 20- HS-AFM analysis of CENP-Anuc unwrapping.

AFM videos were analyzed, showing the DNA unwrapping pathway of CENP-A_{nuc} (green arrows). Once the DNA unwraps the nucleosome core particle, they are indicated with yellow arrows—the frames in A come from Movie S8. In frame A1, the nucleosome can be wrapped fully at the 601 location. The nucleosome remains fully wrapped in frames A4 and A18. Suddenly in frame A20, the DNA unwraps, leaving the nucleosome core partially wrapped (~110 bp), indicated by the yellow arrow. The nucleosome particle remains partially even into frame A37 (~100 bp). The frames in B come from the video of Movie S9. In frame, B3, the green arrow indicates a fully wrapped nucleosome bound near the 3WJ. In frames, B8 and B11, the nucleosome (green arrow) is still fully wrapped. By frame B13, the DNA has unwrapped the nucleosome (~100 bp). By frame B18, the nucleosome no longer wraps any DNA. The scale bar represents 25 nm.

undergoes unwrapping, resulting in a wrapping of ~100 bp. By frame B18, the nucleosome no longer wraps any DNA. Notably, no octamer dissociation is observed during the entire unraveling process.

The nucleosome core stability of $H3_{nuc}$ was found to be weaker through our analysis of the HS-AFM videos. We found that out of 69 total movies of $H3_{nuc}$ analyzed, 53 (77%) of them resulted in the nucleosome core losing histones during the unwrapping, as indicated in Figure 16A and B, the blue arrows are pointing to the histones leaving the nucleosome core. In contrast, CENP-A_{nuc} had 63 nucleosomes analyzed, and only 6 (10%) had histones leave the core during the unwrapping event, indicating that the DNA was able to unwrap the nucleosome core without the octameric core falling apart.

These results lead us to believe that the CENP-A_{nuc} core particle is significantly more stable than the $H3_{nuc}$, which likely plays a role in its necessity of having a strong interaction to withstand the kinetochore pulling the sister chromatid apart. This overall higher stability of CENP-A_{nuc} is also supported by the longer dwell times found with CENP-A_{nuc} compared to the $H3_{nuc}$, as seen in Figure 18.

4.3.5.3 A Step-Wise Unraveling of Nucleosomes

AFM images shown above point to the step-wise process of the nucleosome unraveling. To characterize this phenomenon, we measured the lengths of the DNA arms for each frame and plotted these measurements as a set of bars with different colors. These data are shown in Figure 21A, and a few snapshots are displayed in Figure 21B. The complete set of frames are assembled into Movie S6. The blue bars represent the distance from the 601 end of the DNA to the center of the nucleosome (grey dot). The orange bar represents the distance from the center of the nucleosome to the end of the 3WJ. The yellow line shows the DNA wrapping values calculated from the length measurements of the arms. In this set of images in frame (2), the nucleosome can be seen to be overwrapped. These data show that there was a partial unwrapping event that started in frame (11) and proceeded to frame (13), where the nucleosome went from a state of overwrapped (~210 bp) and, throughout three frames, it decreased to an under

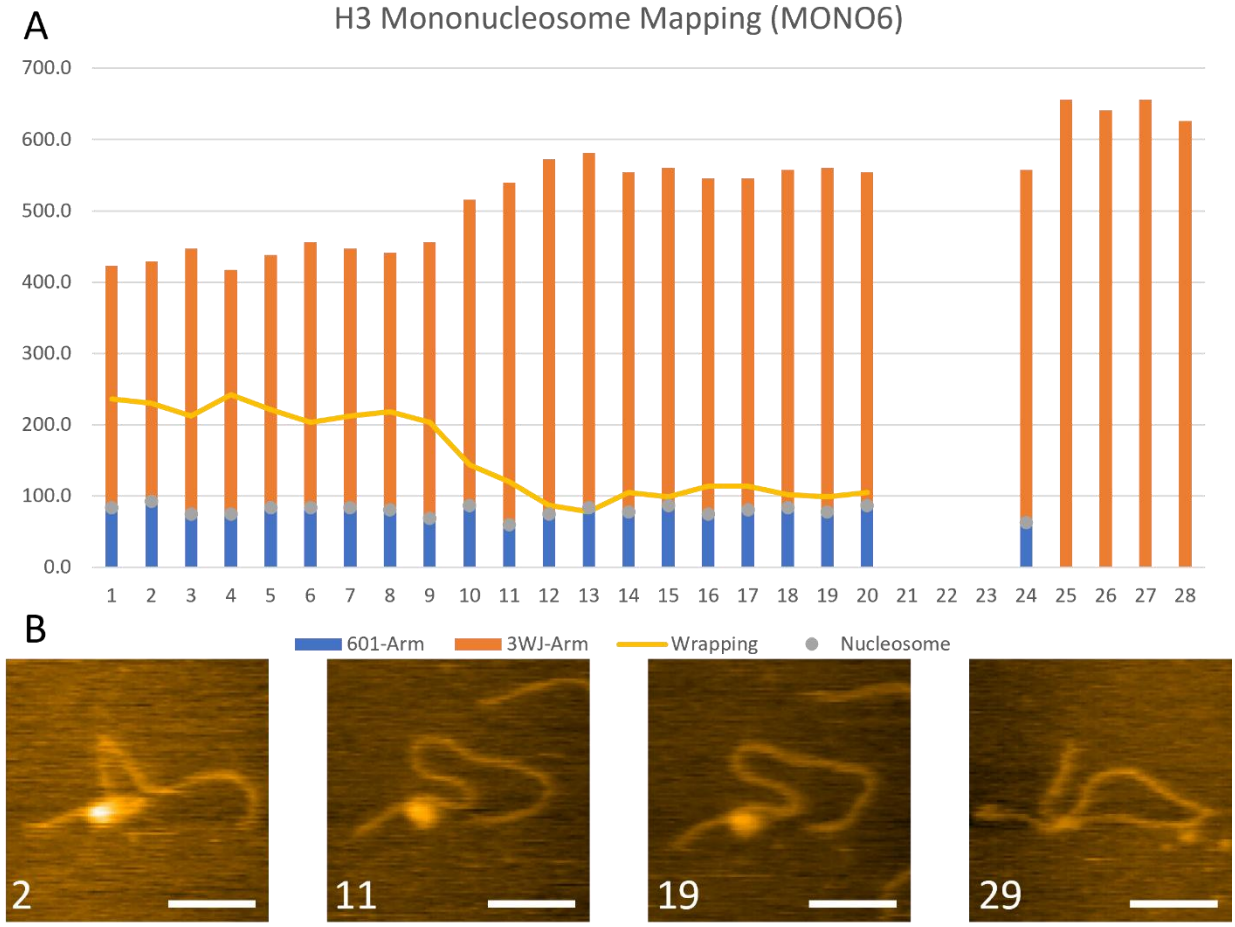

Figure 21- HS-AFM video of H3nuc analyzed with snapshots.

The Movie S6 was analyzed, showing the mapping (bar graph) and snapshots of particular frames. The orange bars represent the DNA from the 3WJ end to the center of the nucleosome (grey dot). The blue bar represents the 601 DNA, from the 601 end to the center of the nucleosome. The yellow line shows the wrapping of the $H3_{nuc}$. The number in white in the bottom left of the snapshots indicates the frame of the image.

wrapped state (~100 bp), where it remained bound for another 7 frames. The last frame 29 shows the nucleosome wholly disassociated from the DNA.

A similar event is shown in the Figure 22 and in the Movie S7. It was demonstrated that the initial overwrapped state (~200 bp) in frame 10 dropped quickly to an under-wrapped state (~100 bp), where it remained for another 6 frames.

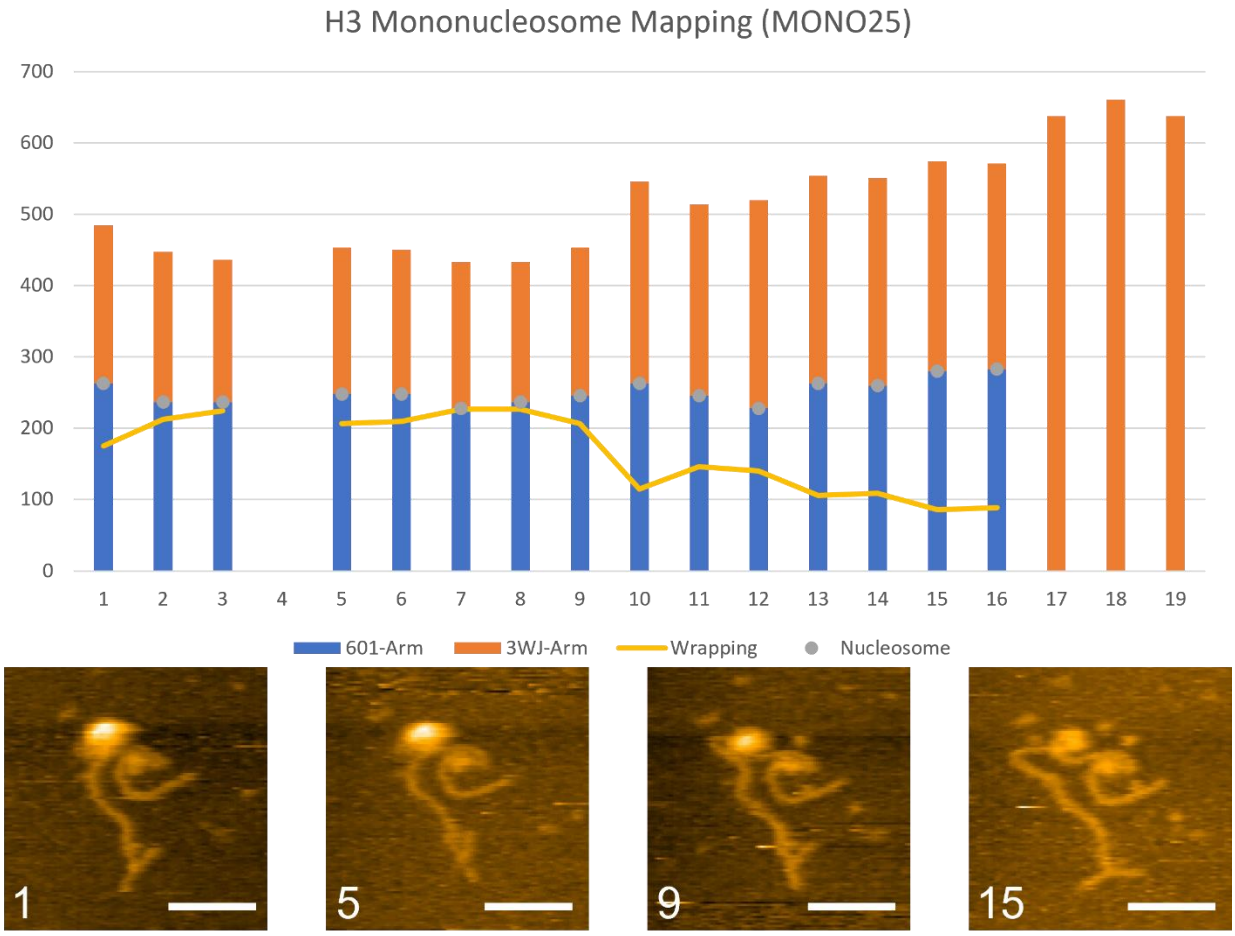

Figure 22- HS-AFM analysis of $H3_{nuc}$.

The Movie S7 video analyzed, showing the mapping (bar graph) and snap shots of particular frames. The grey dots in the bar graph indicate the nucleosome bound to the DNA. The yellow line shows the wrapping of the $H3_{nuc}$. The number in white in the bottom left of the snap shots indicates the frame the image is from.

Both videos demonstrated an intermediate step in $H3_{nuc}$ disassembly, a state in which the nucleosome is considerably stable. There was a variation in the time that these unwrapping events took place. In Movie S6, the unwrapping took place over 3 frames (2.4 s), whereas in Movie S7, the unwrapping took place over 1 frame (0.8 s). The difference in time to unwrap indicates there is still something not completely understood in this process.

A similar analysis was done on CENP-A nucleosomes. The data are shown in Figure 23, where the results of measurements are shown (Figure 23A), and snapshots are displayed below (Figure 23B). The complete set of frames are assembled into Movie S10. In the snapshots shown, frames (4) to (36) show a fully wrapped nucleosome, and frame (43) shows an increase in DNA length and a decrease in bp wrapping around the nucleosome. Finally, frame (79) shows histones bound to the DNA without wrapping. According to Figure 23A, the CENP-A_{nuc} was stability-wrapped (~130 bp) for 41 frames; at this point, it went to an unwrapped state (~90 bp). The unwrapping process took only a single frame (0.8 s).

In a recently published paper[162], they found a step-wise unraveling that resulted in the formation of hexasomes and stable tetrasomes for H3 nucleosomes. These results align with our results of the visualization of histones leaving the H3 nucleosome.

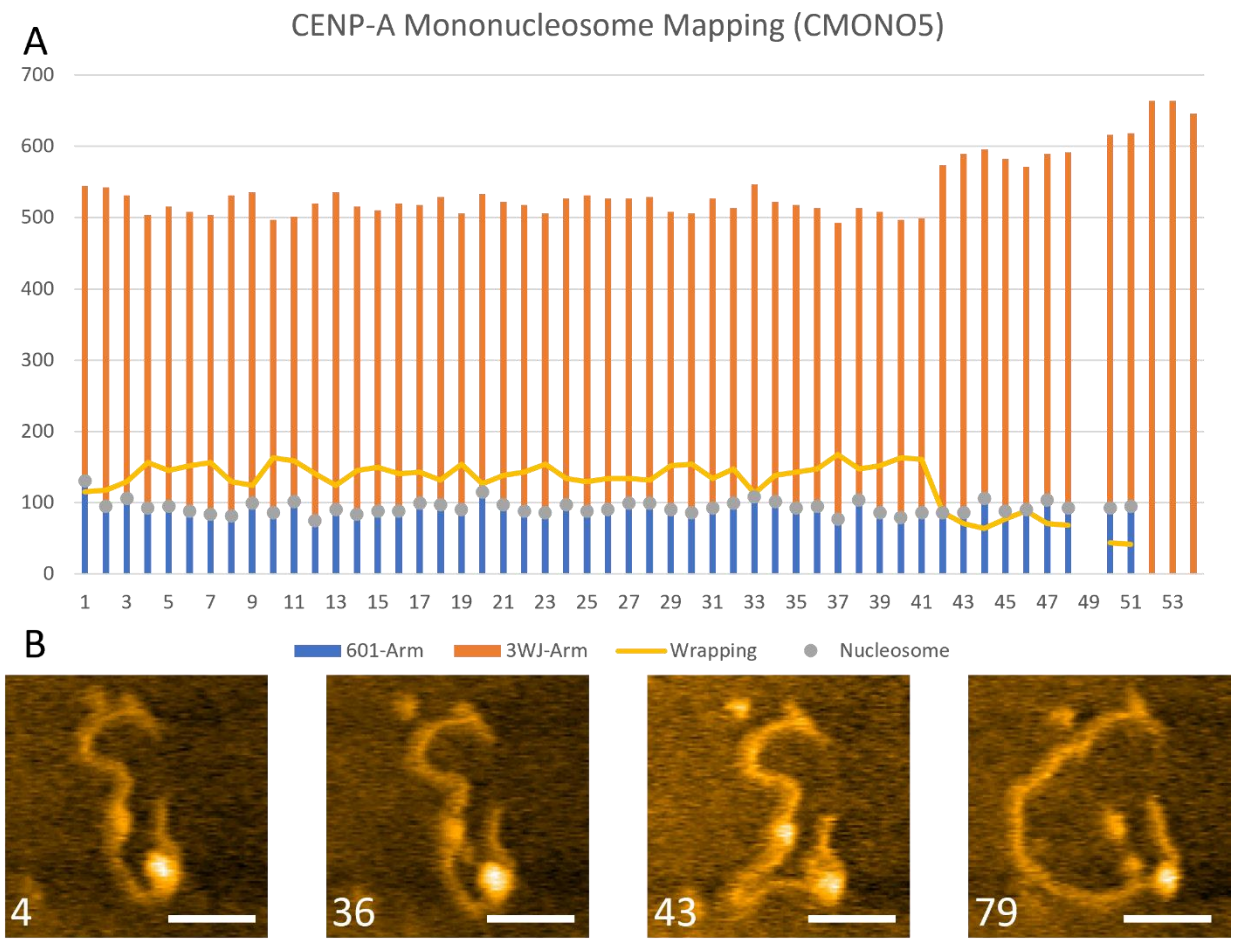

Figure 23- HS-AFM video of CENP-Anuc analyzed with snapshots.

The Movie S10 was analyzed, showing the mapping (bar graph) and snapshots of particular frames. The grey dots in the bar graph indicate the nucleosome bound to the DNA. The orange bars represent the DNA from the 3WJ end to the center of the nucleosome (grey dot). The blue bar represents the 601 DNA, from the 601 end to the center of the nucleosome. The yellow line shows the wrapping of the CENP-A$_{nuc}$. The number in white in the bottom left of the snapshots indicates the frame of the image.

Another video with the same analysis was done to confirm the step-wise disassembly process of the previous video, seen in Figure 24. This video demonstrates an event similar to Figure 23. The nucleosome began in an over-wrapped state (~200 bp), remaining for 33 frames. The nucleosome was

unwrapped from frame 33 to 35 to ~100 bp, staying for another 12 frames before completely disassociating.

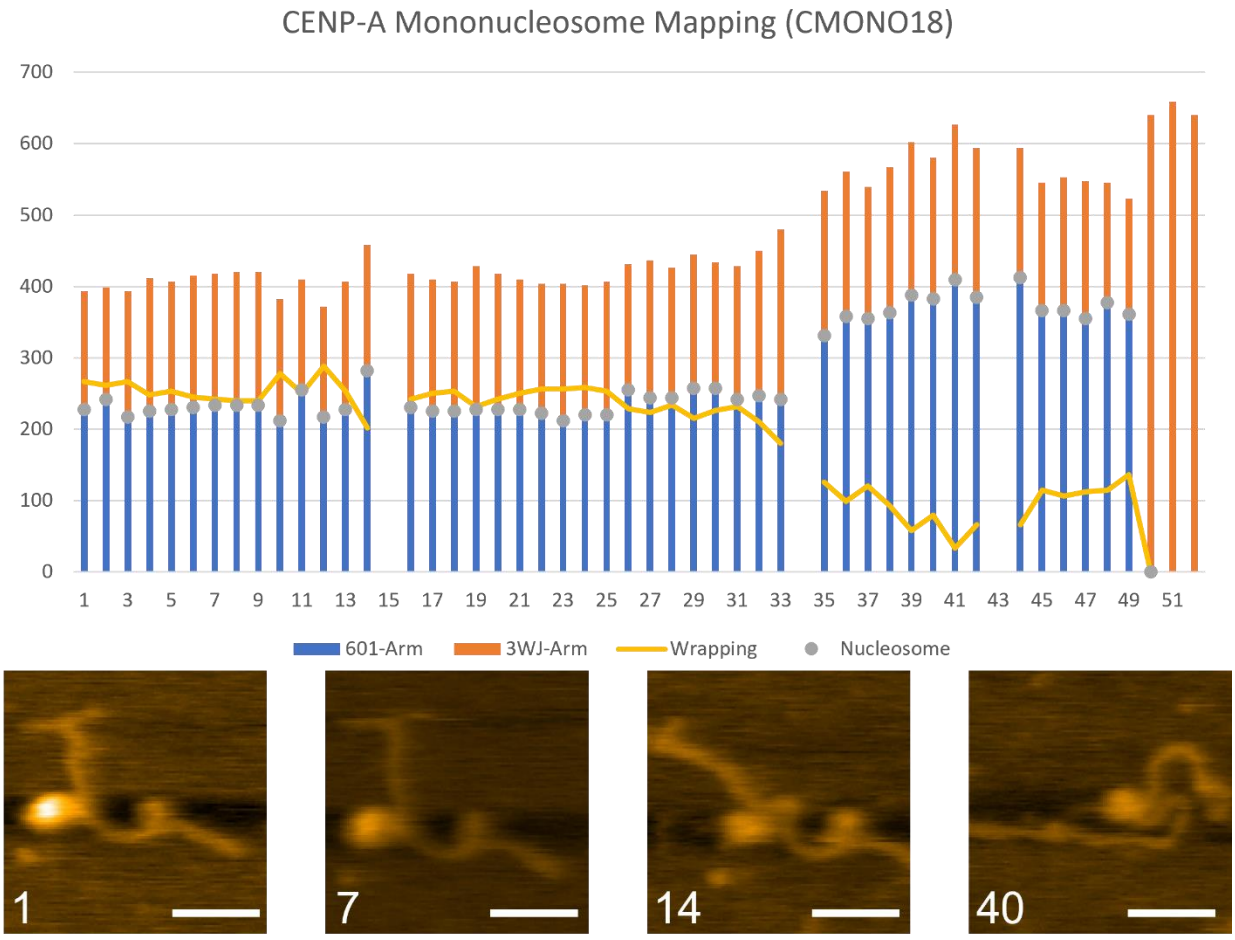

Figure 24- HS-AFM analysis of CENP-A_{nuc}.

The Movie S11 video analyzed, showing the mapping (bar graph) and snap shots of particular frames. The grey dots in the bar graph indicate the nucleosome bound to the DNA. The yellow line shows the wrapping of the CENP-A_{nuc}. The number in white in the bottom left of the snap shots indicates the frame the image is from.

4.3.5.4 Asymmetric Unraveling of Nucleosomes

A closer analysis of the $H3_{nuc}$ (Figure 21 and Figure 22) and CENP-A_{nuc} (Figure 23 and Figure 24) movies revealed that the unwrapping process is asymmetric, so one arm increases the size without changing another arm in length. In Figure 21A, the $H3_{nuc}$ short 601 arm (blue) remains constant throughout the video, but the 3WJ arm (orange) increases in length during the unwrapping. Similar

asymmetry was observed for the nucleosome initially assembled away from the 601 motif (Figure 22). The blue arm fluctuated, but the orange bar grew as unwrapping occurred (yellow line in Figure 22A).

The asymmetry in the unwrapping was observed for CENP-A nucleosomes, which is illustrated in Figure 11. The nucleosome is bound to the 601 site, and the short arm (blue) remained constant throughout the video, but the 3WJ arm (orange) grew in length during the unwrapping. In Figure 24, the CENP-A_{nuc} was assembled near the middle of the DNA template, away from the 601 motif. The nucleosome length of both arms remained relatively consistent until the unwrapping event, which caused the blue arm to grow in length with the orange bar remaining constant. Thus, the asymmetric unwrapping events do not have a preference for the DNA sequence.

In the analysis of 98 total unwrapping events, asymmetric unwrapping was found in 87% of cases for $H3_{nuc}$ and 88% of the CENP-A_{nuc}. The symmetric unwrapping was observed in 13% and 12% for $H3_{nuc}$ and CENP-A_{nuc}, respectively. In the recently published paper [162], they also found that the nucleosomes were unwrapped asymmetrically as the disassembly of the nucleosomes occurred. They also correlated the asymmetrical unwrapping to the asymmetrical dissociation of the H2A/H2B dimer from a chromatosome.

4.4 Discussion

The dinucleosome approach using end-labeled DNA revealed several different features of CENP-A_{nuc} and bulk $H3_{nuc}$. Although both nucleosome types can form tight contact with no visible space between nucleosomes (Figure 12B, frame (ii)), CENP-A_{nuc} indicated a lower effect than $H3_{nuc}$ ones (Figure 16). We have demonstrated that the balance between energies of internucleosomal interaction and the affinity of the nucleosome core to the DNA sequence previously defines the formation of tight contacts between the nucleosomes.[98,142] The balance favors the dinucleosome assembly for non-specific DNA sequences. We have shown that the number of such contacts increases in nucleosomes assembled with truncated H4 histone, suggesting that histone tails contribute to the tightening of dinucleosomes.[98]

Therefore, we hypothesize that the lower yield of dinucleosome complexes for CENP-A_{nuc} can be due to the repulsion generated by the CENP-A tail, and we plan experiments to test this hypothesis.

The DNA sequence is the primary factor defining the nucleosome positioning in the chromatin, and the 601 motif is the strongest nucleosome positioning sequence—our AFM data in Figure 12B and Figure 14A visually support it, illustrating the almost exclusive formation of mononucleosomes on the position of the 601 motif. At the same time, there is a difference between both types of nucleosomes. The yield of $H3_{nuc}$ bound to the 601 site in the mononucleosome and dinucleosome samples was 99% (Figure 13B and D). The CENP-A_{nuc} were mapped similarly to $H3_{nuc}$ and found bound to 601 site at 92% for mononucleosomes and 93% for the dinucleosomes (Figure 15B and D). These differences in the binding affinity to 601, although marginal ~6%, were consistent in both the mono and dinucleosomes results. Although the DNA sequence and specifically the TA dinucleotides provide such a high affinity of 601 to the formation of nucleosomes, it was shown in[163] that interaction with histones contributes to the nucleosome positioning and H3–H4 tetramer dominates in the DNA sequence dependency effect. Replacement of H3 histone with CENP-A histone can decrease this DNA affinity effect.

The elevated affinity of CENP-A_{nuc} to the DNA ends is another property of these nucleosomes, illustrated in Figure 14. DNA wrapping around CENP-A_{nuc} is less than for $H3_{nuc}$, 137 bp +/-20 bp vs. 145 +/- 23 bp, respectively, which is consistent with previous publications.[140,155]

Time-lapse HS-AFM studies revealed different stabilities of H3 and CENP-A nucleosomes. The data in Figure 18 demonstrate that CENP-A_{nuc} appear more stable under the scanning conditions than $H3_{nuc}$. In the dwell time analysis on the HS-AFM, we found that 38% of mono$H3_{nuc}$ lasted longer than 20 frames, whereas 52% of monoCENP-A_{nuc} lasted longer than 20 frames, a substantial increase of 14%. The dinucleosomes dwell comparison also showed that $H3_{nuc}$ had a dwell time of more than 20 frames only 48% of the time compared to the CENP-A_{nuc} at 66%, a dramatic increase of 18%. This finding seems counterintuitive as the wrapping efficiency of CENP-A_{nuc} is less than $H3_{nuc}$. However, CENP-A nucleosomes are not simply partially unwrapped H3 nucleosomes. Structures of CENP-A and H3

nucleosomes are different, pointing to different contacts between the DNA and histones, so this structural property of these two types of nucleosomes explains their different stabilities. For example, the CENP-A nucleosomes have increased flexibility of the DNA ends, the octameric core is more rigid, and has a different surface charge (positive) at the interface of the L1 of CENP-A and L2 of H4; in contrast, this surface is negatively charged in $H3_{nuc}$.[48,164]

Most commonly, the $H3_{nuc}$ found in the unwrapped state also appeared to have lost some of the histones from the nucleosome core, an H2A/H2B dimer. The loss of the dimeric histone caused the nucleosome core to become unable to maintain the fully wrapped ~147 bp and loosen to a state of ~100 bp wrapping. The remaining dimer sits at the entry-exit site opposite the tetrameric H3/H4 dimer at the nucleosome's dyad. In the $H3_{nuc}$, a hexasome with a single dimeric H2A/H2B can maintain the integrity of a single DNA wrap around the histones.

In Figure 19A, it can be seen that there is an $H3_{nuc}$(green arrow) that is wrapped at the 601 location (frame A1). In the following frames (A2 and A20), the histone (blue arrow) has vacated the octameric core, but the partial core remains to wrap the DNA. In frame A36, the DNA unwraps the partial core, resulting in a wrapping of ~100 bp, and the free histone remains near. In the last frame, A66, the only histone remaining appears to be the tetramer. These predictions on the dimer being the first to leave the octameric core are based on the size of the histone leaving, the location, and the assembly process of nucleosomes, showing that dimers are the last ones to leave; it would make sense that they would be the first histones to leave.

$H3_{nuc}$(green arrow), in Figure 19B, starts fully wrapped at the 601 location (frame B1). In frames B4 and B7, it can be seen that a histone (blue arrow) left the core particle and now drifts nearby. During this process, unwrapping of the DNA took the ~150 bp wrapping down to ~100 bp in frame B4. This unwrapping continues, and by frame B11, the core particle no longer wraps any DNA. We assume that the octameric core splits into its three components: H2A/H2B dimers (blue arrows) and H3/H4 tetramers (yellow arrows).

The CENP-A_{nuc}, conversely to the H3nuc, had a much lower occurrence of the histones vacating the octameric core. In Figure 20A, the CENP-A_{nuc} (green arrow) can be seen sitting at the 601 location in frames A1, A4, and A18. In frame B20, the DNA on the short arm can be seen to have lengthened, indicating an unwrapping of the nucleosome (yellow arm now). Of note, no histones left the nucleosome during this unwrapping transition. The under-wrapped nucleosome can be seen stably bound to the DNA in frame A37, still at the 601 location.

Another example of the CENP-A_{nuc}, unwrapping without the loss of a histone, is seen in Figure 20B. In this example, the CENP-A_{nuc} is not bound to the 601 site but near the 3WJ, indicating that this process is not DNA sequence-dependent. In frames B3, B8, and B11, the CENP-A_{nuc} is fully wrapped and stably wrapping the DNA. In frame 13, the DNA is unwrapped from the short arm (3WJ arm), but once again, the nucleosome (yellow arrow) does not lose any histones in the process. The nucleosome is eventually evacuated from the DNA in frame 18 (yellow arrow).

These differences between the H3 and CENP-A nucleosomes indicate an intrinsic difference between the interactions of the DNA and the nucleosomes. Despite the lower wrapping efficiency of CENP-A nucleosomes compared with $H3_{nuc}$, we have shown here that the nucleosomes not only have longer dwell times on the DNA, but their octameric structural integrity is greater than that of $H3_{nuc}$.

We also found that a step-wise disassembly process occurs in both $H3_{nuc}$ and CENP-A_{nuc}, resulting in a stable under-wrapped state of ~110 bp. This step-wise disassembly is only unwrapped from a single side, as seen in Figure 21 and 11. Therefore, these nucleosomes had an entry/exit DNA that remains completely intact, while the other unraveled between 20 and 40 bp. These results give insight into how the nucleosomes may be translocated in a rolling fashion, breaking only the contacts at a single entry/exit site. The exciting thing about this under-wrapped state is that it appears more stable than the fully wrapped state, with more time for both nucleosomes to be under-wrapped instead of the fully wrapped state.

The asymmetric unwrapping of nucleosomes is another property observed in both nucleosome types. The asymmetry is the preferential pathway for the nucleosome unwrapping observed in 87% of cases for $H3_{nuc}$ and 88% of the CENP-A_{nuc}. Previously, asymmetry was observed for the initial stage of unwrapping for the breathing of DNA.[165] Other published work discovered that the histone dimers (H2A/H2B) are the first to leave the octameric core, guided by the asymmetrical unwrapping of the DNA.[166,167] Here, we observed the asymmetry in the nucleosome unwrapping over the entire unraveling process. Also, we observed the asymmetry in unwrapping for CENP-A nucleosomes, where the core remains intact, suggesting that the core dissociation is not a factor contributing to the asymmetry of the nucleosome unwrapping.

Overall, a variety of unique structural characteristics of canonical and centromere nucleosomes at the nanoscale have been found. We found that CENP-A nucleosomes are more stable than canonical nucleosomes, regardless of their lower wrapping efficiency. Moreover, time-lapse experiments demonstrate that nucleosomes with ~100 bp DNA wrapped are in a transient state with elevated stability. These findings suggest that the amount of DNA wrapped around the histone core is not the only factor defining nucleosome stability; instead, other interactions between the histone cores and DNA contribute to its stability. The unwrapping process is highly asymmetric, and it was observed with both types of nucleosomes, revealing a novel property of the nucleosome dynamics. Additionally, HS-AFM revealed higher stability of CENP-A nucleosomes compared with H3 nucleosomes, in which dissociation of the histone core occurs prior to the H3 nucleosome dissociation. The histone core of CENP-A nucleosomes remains intact even after the dissociation of DNA, so the re-assembly of the CENP-A nucleosomes is facilitated. This feature of CENP-A nucleosomes can be important for the centromere dynamics during mitosis and chromatin replication.

4.5 Conclusions

We found that universally, there was an asymmetric unwrapping that occurred in both nucleosomes despite the difference in the unwrapping pathways. The H3 nucleosome unwrapping

pathway typically involved the loss of histones, which then led to the first step in unwrapping the nucleosome. In contrast, the CENP-A nucleosomes had a more stable nucleosome core that retained the histones during the first step of unwrapping, which was surprising due to the lower wrapping efficiency found in CENP-A nucleosomes. These first steps in unwrapping resulted in a nucleosome with ~100 bp of DNA wrapped, in which the nucleosomes, or potentially hexasome/tetrasome for H3 nucleosomes, could stably wrap this DNA for many more frames. The dwell times of CENP-A nucleosomes were discovered to have a longer dwell time than H3 nucleosomes, which also demonstrates that CENP-A nucleosomes are more stable than H3 nucleosomes. We also found that H3 nucleosomes had a higher preference for the 601 sequence vs. CENP-A nucleosomes, with 99% vs. 92%, respectively, being bound to the nucleosome-specific sequence. Many of these findings were found in another lab, where they found both the asymmetric unwrapping and the capability of H3 nucleosomes to lose histones during the unwrapping process but still wrap DNA even without the full octamer.[162] Interestingly, their experiments utilized bare mica, a negatively charged surface, whereas our experiments utilized APS functionalized mica, a positively charged surface. However, our experimental results aligned well, further validating the experiments.

Chapter 5. TRANSCRIPTION FACTOR NF-κB AND NUCLEOSOMES

5.1 Introduction

Transcription is a necessary part of biology that takes information from DNA, creates mRNA with the same information, and then potentially turns it into proteins.[168] This process of transcription, by transcription factors such as NF-κB, must overcome barriers of DNA accessibility to execute this process, and for DNA to fit in the nucleus of cells, it must be compacted by histones.[169,170] With the majority of DNA being wrapped around nucleosomes in the cell, the accessibility of binding sites for transcription factors is questioned: how do transcription factors bind to these sites that are currently wrapping around nucleosomes? We recently published that NF-κB, a notorious transcription factor involved in inflammation, is a pioneer transcription factor.[76]

The centromere consists of a complex network of proteins, DNA sequences, and chromatin structures that interact to form a cohesive unit responsible for accurately segregating chromosomes performed by the kinetochores.[33,152,171] The centromere chromatin consists of two types of nucleosomes: CENP-A (CENP-A_{nuc}) and canonical $H3_{nuc}$ nucleosomes.[172] The centromere of most higher eukaryotes are comprised of alpha satellite (α-sat) motifs of a 171 bp DNA sequence.[173–175] It is a biologically relevant sequence that is tandemly repeated hundreds to thousands of times, comprising 0.2-5 Mb stretches depending on the chromosome.[176–178]

$H3_{nuc}$ nucleosomes are composed of 147 bp DNA wrapped around a protein core of histone proteins (H2A, H2B, H3, and H4) and compact the genome into a more manageable structure.[144,146,179] This compact structure is essential in protecting the genome from damage and plays a critical role in gene regulation.[87,148,150,151]

In centromeric CENP-A octameric nucleosomes, H3 histones are replaced with CENP-A histones, an H3 homolog.[45,152,153,178,180] These two homologs share a 50% similar homology in the C-terminal histone fold domain but vary drastically in the N-terminal tail in both size and sequence.[47,181] These and

other structural differences between CENP-A and H3 result in an unfixed 13 bp at both entry/exit of the CENP-A nucleosome, so centromeric CENP-A_{nuc} octameric nucleosomes wrap ~ 20 bp less DNA than bulk H3 nucleosome.[100,140]

Studies show that transcription does occur in the centromere, yielding different products depending on the number of repeats of a-sat.[182,183] The transcription occurring in the centromere yields lncRNAs, which functionally load both CENP-A and CENP-C.[180] However, there is a 200-300 fold difference between bulk chromatin and centromere transcription.[178,180,184(p20)]

The accessibility of transcription factors to the bulk vs. centromere chromatin may be one of the explanations, so to test this hypothesis, we investigated the interaction of NF-κB transcription factor with both types of nucleosomes. NF-κB is a transcription factor that recognizes κB sites in the DNA and is crucial in regulating the immune response and inflammation. The α-sat sequence contains many half κB sites, which are also known to bind NF-κB.[178,180,185,186] We previously reported that NF-κB binds and unravels $H3_{nuc}$ nucleosomes assembled with the Widom 601 DNA motif.[76] Here, we tested how NF-κB interacts with nucleosomes assembled on the centromere-specific a-sat sequence. Both $H3_{nuc}$ and CENP-A_{nuc} were assembled on the same DNA substrate, and the interaction of the nucleosomes with NF-κB was studied using AFM. Analysis of AFM data revealed that NF-κB unravels $H3_{nuc}$ but does not appear to bind or unravel CENP-A_{nuc} nucleosomes.

5.2 Experimental Design

5.2.1 DNA substrate

A description of the DNA substrate can be seen in Section 1.1. The DNA schematic can be seen in Figure 25A.

5.2.2 NF-κB

A description of the NF-κB procedures can be found in Chapters 2.4.1 NF-κB Preparation and 2.4.2 NF-κB .

5.2.3 Dry AFM sample preparation

Chapter 2.5.1 Dry AFM Sample Preparation and Imaging contains the dry AFM sample preparation description.

5.2.4 Data Analysis

A description of Data Analysis can be seen in Chapter 2.6 Data Analysis.

5.3 Results

5.3.1 NF-κB Binding to the Alpha satellite DNA substrate

In these studies, we used a DNA construct containing an alpha satellite (α-sat) sequence, 171 bp long, present exclusively in the centromere part of the chromosome flanked with the DNA segments that are not specific for nucleosome binding. Schematics of the DNA are shown in Figure 25A. α-sat segment was placed in the middle of the construct, indicated with a gray bar below. Green and orange bars indicate

the positions of the NF-κB half recognition sequences. Both the central α-sat segment and flanks contain NF-κB binding sites.

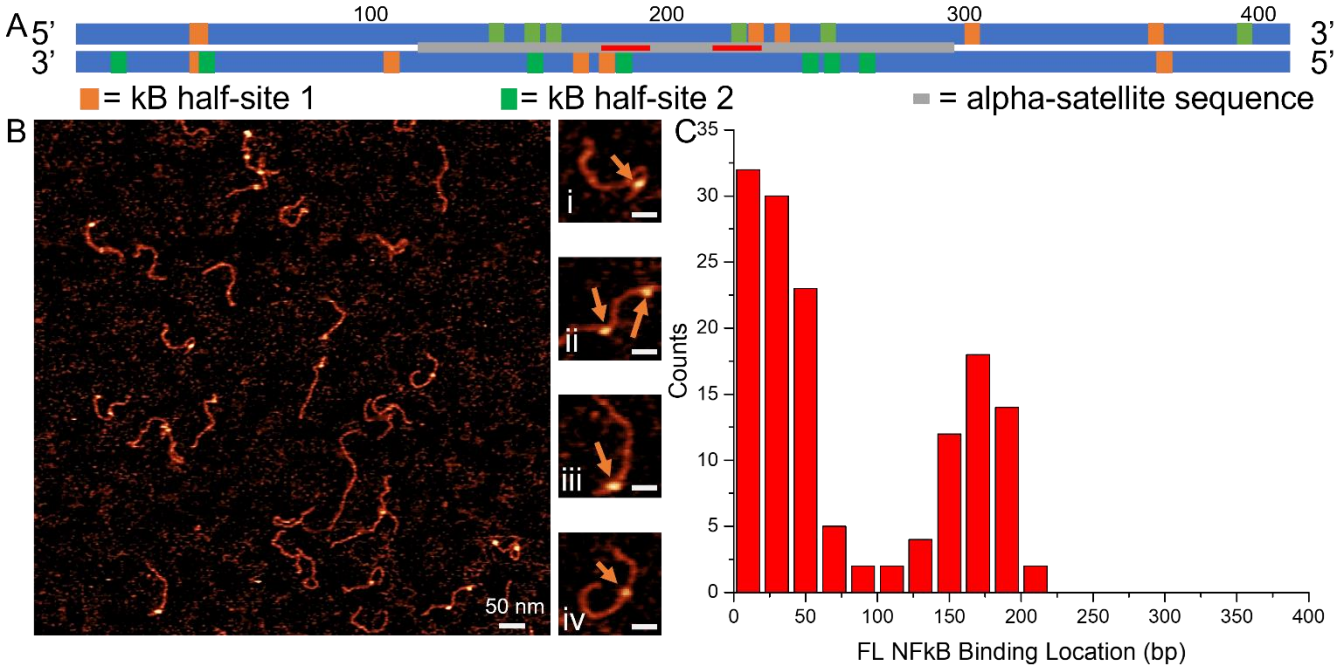

Figure 25- DNA Construct and AFM image with NF-κB$_{FL}$ results.

DNA construct (A) containing the alpha-satellite sequence in the middle of the sequence (grey bar), to analyze if there was any preferential binding at half sites, they are displayed in the "forward" 5' -> 3' direction and again in "reverse" 3' ->5', and the half-sites were marked (green and orange). The κB half-sites 1 (GGGRN) were labeled with orange boxes, and the κB half-sites 2 (YYYCC) were labeled with green boxes. The results indicate a large cluster of half-sites near the middle of the DNA strand. The CENP-B box was marked in red. AFM images of NF-κB$_{FL}$ at a 1 to 2 ratio(B) binding on the DNA substrate. Snapshots shown to the right of large AFM images (i, iii, and iv) show a single NF-κB$_{FL}$ bound to the DNA, and image (ii) shows two NF-κB$_{FL}$ bound to the DNA. The orange arrows indicate an NF-κB$_{FL}$ bound to the DNA. The large AFM image is a 1 x 1 μm scan size with a 50 nm scale bar. The snapshots are 100 x 100 nm scan area and 25 nm scale bars. The binding location results for a single NF-κB$_{FL}$ can be seen in the histogram (C), indicating a preference for terminal and a second peak around ~170 bp.

The DNA was complexed with NF-κB$_{FL}$ using a 1:1 protein-to-DNA molar ratio and imaged with AFM. AFM images are shown in Figure 25B. Protein bound to DNA appears as a globular feature on the DNA filament. Similar to our previous study [76], NF-κB does not alter the length of the DNA, suggesting that there is no wrapping DNA around the protein. A few zoomed images are displayed to the right

(frames i-iv), and the protein position is indicated with arrows in these images. Complexes of the DNA with one or two NF-κB_{FL} molecules are seen, and both types of complexes are shown in selected frames. Protein can appear close to the end of the DNA (frames i and iii) or inside the DNA (frame iv). A similar arrangement was observed for two protein molecules bound to DNA (frames ii). Locations of the protein were mapped, and the results are shown as a histogram in Figure 25C. Two peaks correspond to the NF-κB_{FL} binding to the DNA ends (0-50 bp) and the central location (~ 170 bp). The mapping results correlate with NF-κB binding sites shown in Figure 25A. Note that the left and right ends of the DNA cannot be distinguished in the AFM images, so the end-bound peak corresponds to complexes of NF-κB with left-right binding sites on the DNA construct. Similarly, the peak at 170 bp corresponds to NF-κB bound to half-κB sites (green or orange bars) on both DNA strands between 100 and 200 bp and to 200-300 segments of the DNA. The binding affinity for NF-κB between the peaks is low, which is in line with the lack of NF-κB sites on both DNA strands in the construct. These results agree with other papers demonstrating the need for a half κB site for binding.[187,188]

Similar experiments were performed with the NF-κB$_{RHD}$ variant in which the 228 amino acids of the TAD region were deleted. Regardless of the deletion, NF-κB$_{RHD}$ demonstrates sequence-specific affinity very similar to the one for the full-length NF-κB heterodimer (Figure 26). These findings suggest that the C-terminal RelA TAD is not critical for the interaction of the NF-κB heterodimer with the DNA.

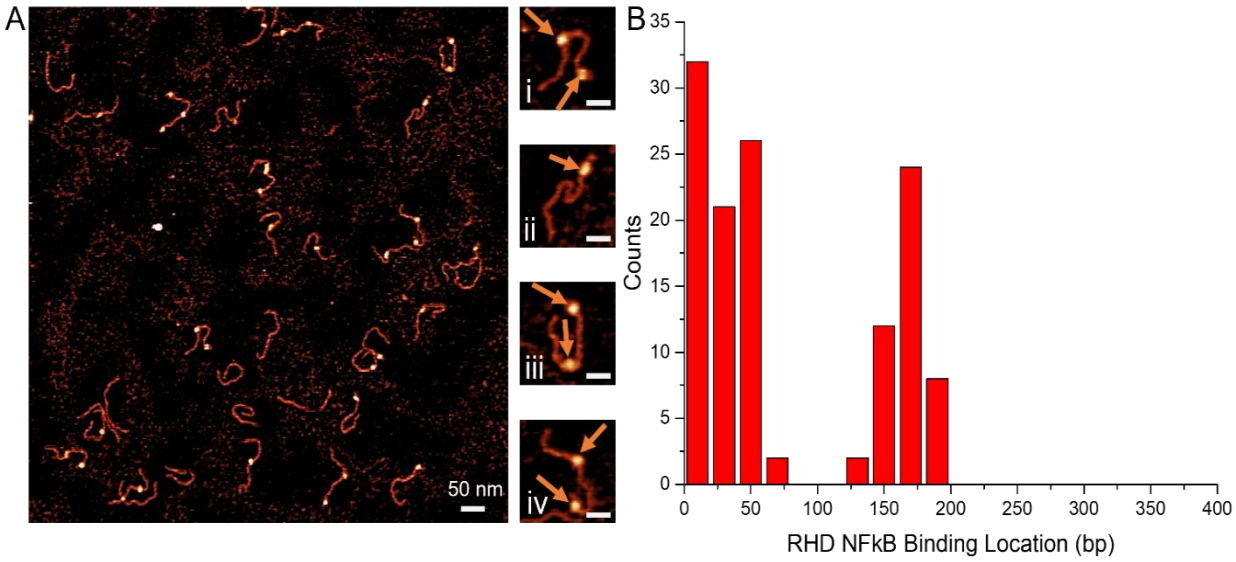

Figure 26- Alpha satellite DNA with NF-κB$_{RHD}$.

AFM images of NF-κB$_{RHD}$ (A) on the DNA substrate. The orange arrows indicate an NF-κB$_{RHD}$ bound to the DNA. The snapshots to the right of the large AFM image show various binding locations of individual NF-κB$_{RHD}$. In the snapshots (i, iii, and iv), two nucleosomes are bound to the DNA, with one near the end of the DNA and the other near the middle. In snapshot (ii), a single protein is bound near the terminal end of the DNA. The large AFM image is a 1 x 1 µm scan size with a 50 nm scale bar. The snapshots are 100 x 100 nm scan area and 25 nm scale bars. Analysis of AFM images yielded the results of the NF-κB$_{RHD}$ binding locations to have a preferential terminal binding when a single NF-κB is bound to the DNA (B) and a secondary peak near 170 bp.

5.3.2 NF-κB interaction with canonical nucleosomes H3

Canonical nucleosomes H3$_{nuc}$ were assembled on the DNA substrate described above by the self-assembly process described in the methods section using an octameric histone core containing H2A, H2B, H3, and H4. The AFM images of nucleosomes are shown in Figure 27A, with a few selected frames to the right of the large scan. Nucleosomes are indicated with blue arrows. In addition to terminal locations in frames (ii and iv), nucleosomes occupy positions near the middle of the sequence (frames i and iii). The

various positions of the nucleosomes located in the middle of the α-sat segment demonstrate that the α-sat segment is not a nucleosome-specific sequence. This conclusion aligns with our previous publication in which a similar DNA substrate was used. [98] We also measured another parameter of the nucleosome, the length of DNA wrapped around the core, termed the wrapping efficiency. This value was obtained by subtracting the lengths of the DNA not wrapped around the nucleosome core from the total length of the DNA. As shown in Figure 27B, the wrapping efficiency for the $H3_{nuc}$ sample is 146 ± 1.6 bp (SEM), which is in line with previous measurements on different DNA substrates, including the nucleosome-specific 601 motif.[76]

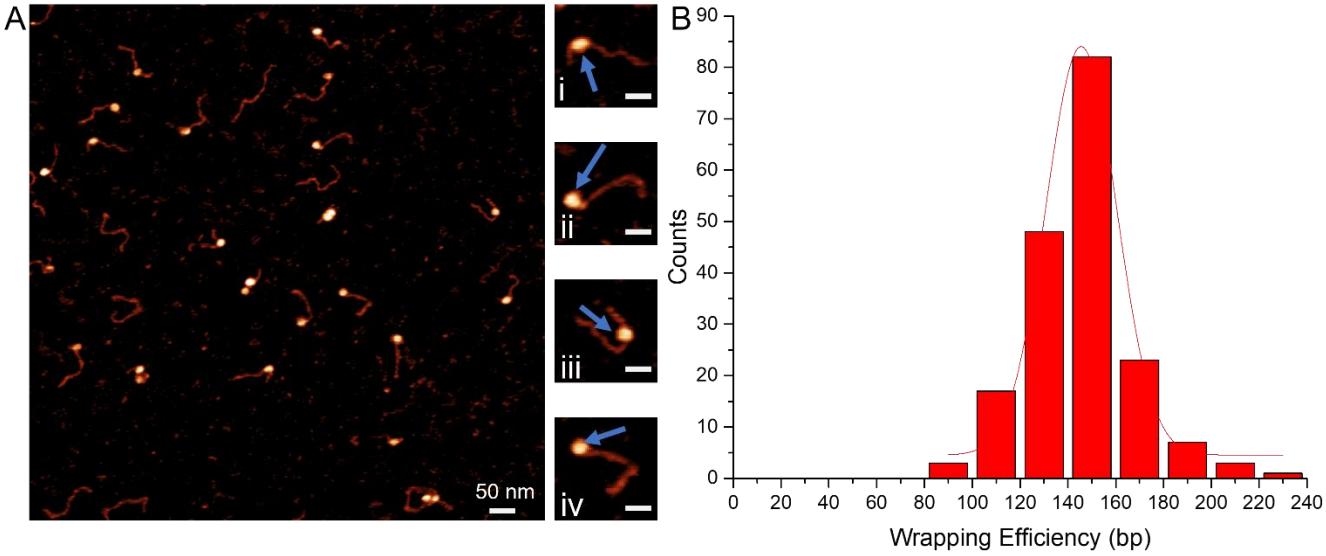

Figure 27- AFM image with zoomed-in snapshots of canonical $H3_{nuc}$

AFM image (A) of the canonical $H3_{nuc}$ assembled on the DNA construct. The large AFM image is a 1 x 1 mm scan size with a 50 nm scale bar. The snapshots to the right of the large AFM show the varying nucleosome binding locations. The snapshots are 100 x 100 nm scan area and 25 nm scale bars. Snapshots (ii and iv) show terminally bound nucleosomes, and (i and iii) are closer to the middle but are not terminally bound. The blue arrows indicate the location of a nucleosome. The wrapping efficiency of the nucleosomes on the DNA substrate was 146 ± 1.6 bp (SEM), as seen in the histogram (B).

Next, we added NF-κB_{FL} to the assembled $H3_{nuc}$ sample in a 1:1 nucleosome:protein ratio, incubated the mixture for 10 min, and prepared the sample for AFM as in previous studies. AFM images are shown in Figure 28A, in which selected typical images of the complexes are shown to the right of the

large AFM scan. Frame (i) shows a single centrally bound $H3_{nuc}$ (blue arrows), frames (ii and iv) show a terminally bound $H3_{nuc}$ with an NF-κB_{FL} protein adjacent to it (orange arrows), and frame (iii) shows a terminally bound nucleosome with an NF-κB_{FL} on the opposite end of the DNA. The nucleosomes and NF-κB_{FL} can be visually differentiated based on their overall sizes, with NF-κB being significantly smaller than the nucleosome.

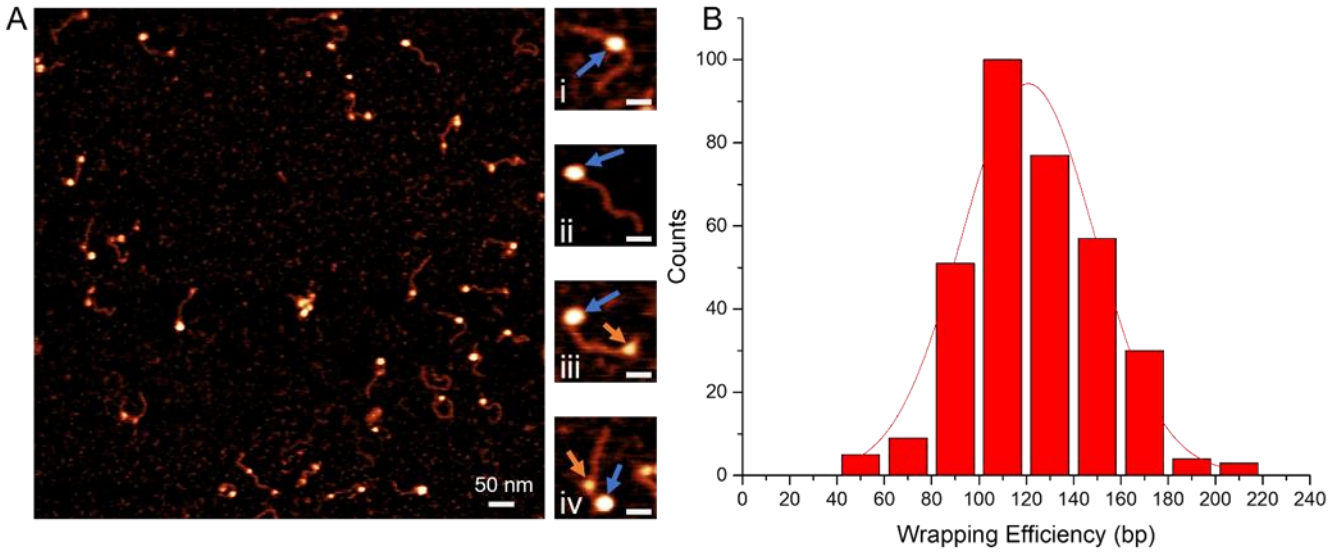

Figure 28- AFM image with zoomed-in snapshots of canonical $H3_{nuc}$ with NF-κB_{FL}.

AFM images of $H3_{nuc}$ assembled on the DNA construct with NF-κB_{FL} added at a 1 to 1 ratio(A). The large AFM image is a 1 x 1 mm scan size with a 50 nm scale bar. The snapshots to the right of the larger AFM image show varying situations. The snapshots are 100 x 100 nm scan area and 25 nm scale bars. In (i and ii), there is a nucleosome bound near the center of the DNA, with no NF-κB visible. In (iii), the nucleosome is bound to one side of the DNA, and the NF-κB is bound to the other side. In (iv), there is a terminally bound nucleosome with an NF-κB_{FL} bound adjacent. The orange arrows indicate NF-κB_{FL} bound to the DNA, and the blue arrows indicate the nucleosome. The wrapping efficiency was found to be decreased to 125 ± 2.2 bp (SEM), as seen in (B).

Next, we calculated the wrapping efficiency from these data as described above. The histogram from multiple measurements is shown in Figure 28B. The distribution was fit to a Gaussian distribution, yielding a mean value of the wrapping efficiency of 125 ± 2.2 bp (SEM). This number is considerably lower than the wrapping efficiency of the control sample, 146 ± 1.6 bp (SEM). This suggests that in the presence of NF-κB_{FL}, the nucleosomes are unraveled by some 21 ± 3.8 bp (SEM). The p-value between

these two populations was 9.6×10^{-10}, indicating a statistically significant difference between the control and the NF-κB$_{FL}$ containing population.

We completed a parallel experiment that tested the effects of adding additional NF-κB to the nucleosome sample. In these experiments, we had a nucleosome: NF-κB ratio of 1 to 2 to check if increasing the concentration would affect the unwrapping effect of NF-κB. The AFM image can be seen in Figure 29A. In frame (i), a single nucleosome bound near the middle of the DNA can be seen. In frames (ii and iii), there is one H3$_{nuc}$ and one NF-κB$_{FL}$. In frame (iv), there is an H3$_{nuc}$ and two NF-κB$_{FL}$ bound to both sides of the nucleosome. The histogram of the wrapping results can be seen in Figure 29B. The unwrapping effect of the nucleosomes resulted in a wrapping efficiency of 125 ± 2.2 bp (SEM) regardless of the increased ratio of NF-κB. The yield of NF-κB bound to DNA flanks on the same strand as a nucleosome was calculated to be 43% and 85% for 1 to 1 and 1 to 2, respectively, which is in line with the use of higher concentration of the NF-κB.

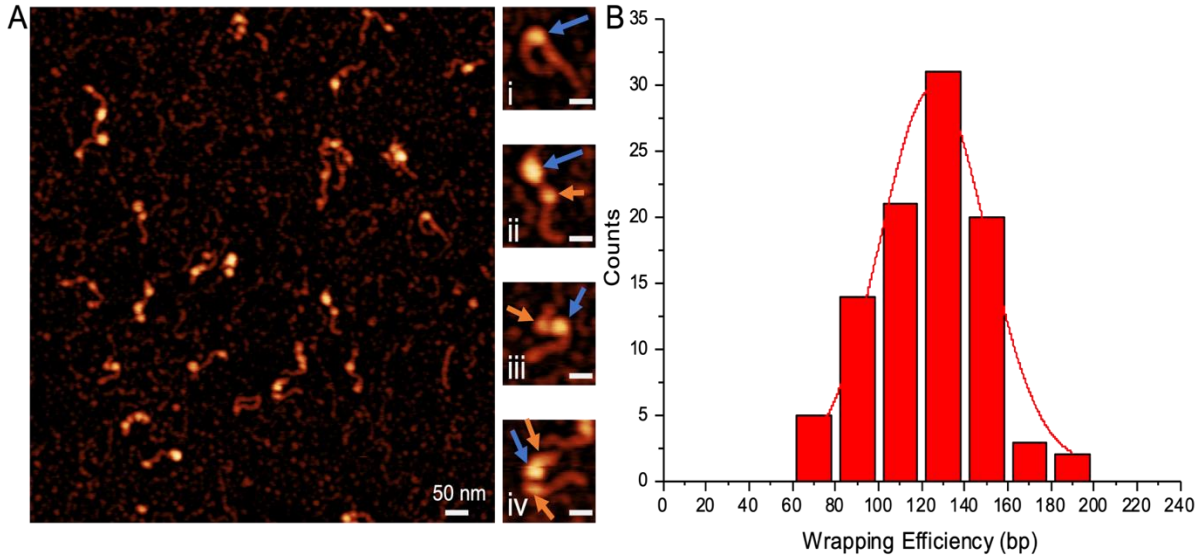

Figure 29- AFM image with zoomed-in snapshots of canonical $H3_{nuc}$ with NF-κB_{FL}.

AFM images of $H3_{nuc}$ assembled on the DNA construct with NF-κB_{FL} added at a 1 to 2 ratio (A). The large scan in (A) is 1 x 1 µm, and the scale bar is 50 nm. The snapshots to the right of the larger AFM image show varying situations. The snapshots are 100 x 100 nm, and the scale bar is 25 nm. In (i), there is a nucleosome bound near the center of the DNA. In (ii and iii), the nucleosome is bound to the DNA, and the NF-κB is bound near the nucleosome. In (iv), the nucleosome has an NF-κB_{FL} bound to both sides of the nucleosome. The orange arrows indicate NF-κB_{FL} bound to the DNA, and the blue arrows indicate the nucleosome. The wrapping efficiency was found to be decreased to 125 ± 2.2 bp (SEM), as seen in (B).

Although NF-κB bound to the nucleosome itself cannot be visualized with AFM directly, its contribution to the particle size can be evaluated with AFM by the height or volume measurements. [189] The height of NF-κB_{FL} bound to DNA was measured, as well as the DNA height on each AFM image. The average DNA height was subtracted from the height measurements of NF-κB_{FL} bound to the DNA and was found to be 0.55 ± 0.02 nm (SEM) (n = 82). The height measurements for the set of 183 particles for the $H3_{nuc}$ control produced the value 1.9 ± 0.02 nm (SEM). Similar measurements for the nucleosome particles (n = 157) in the presence of NF-κB led to the value 2.3 ± 0.04 nm (SEM), which is statistically significant from the control measurements. The p-value between these two populations was 5.4×10^{-23},

indicating a statistically significant difference between the control and the NF-κB$_{FL}$ containing population. These data are in Figure 30A-C and summarized in

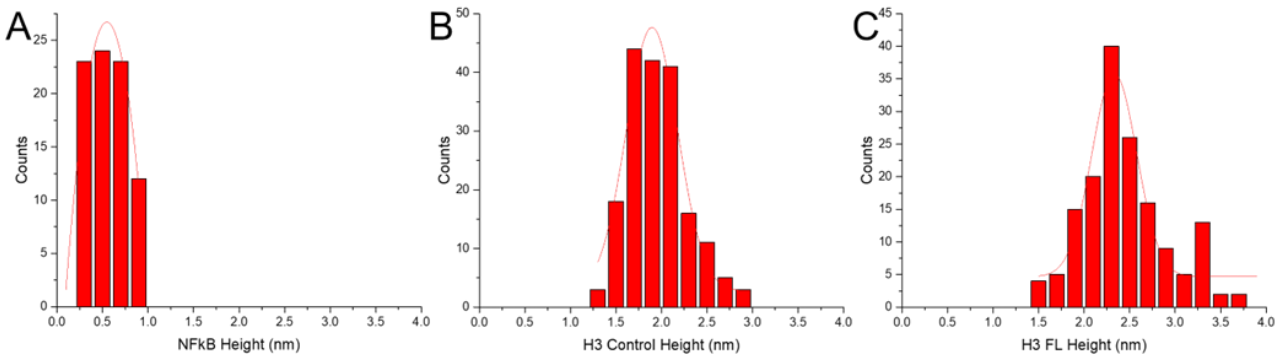

Figure 30- Height results of NF-κB$_{FL}$, H3$_{nuc}$, and H3$_{nuc}$ + NF-κB$_{FL}$.

The height results for the NF-κB$_{FL}$ protein only (A), H3$_{nuc}$ control (B), and H3$_{nuc}$ in the presence of NF-κB$_{FL}$ (C). The mean height of NF-κB$_{FL}$ protein only, H3$_{nuc}$ control, and H3$_{nuc}$ in the presence of NF-κB$_{FL}$ were 0.55 ± .02 nm, 1.9 ± 0.02, 2.3 ± 0.04 nm (SEM), respectively. Histograms for all the heights measured with a gaussian distribution are shown.

	H3 Nucleosomes		**CENPA Nucleosomes**	
	Control	FL 1to1	Control	FL 1to1
Wrapping Mean (bp)	146 ± 1.6	125 ± 2.2	130 ± 1.4	129 ± 2.2
Height Mean (nm)	1.9 ± 0.02	2.3 ± 0.04	2.2 ± 0.02	2.2 ± 0.04
Volume Mean (nm^3)	355 ± 9	469 ± 9	351 ± 5	338 ± 8

Table 2- Results summary of H3 and CENP-A nucleosomes.

We also completed a volume analysis of the control $H3_{nuc}$ and the $H3_{nuc}$ in the presence of NF-κB_{FL} and found that 355 ± 9.4 nm^3 (SEM) and 469 ± 9.0 nm^3 (SEM), respectively. A histogram distribution of these results can be seen in Figure 31A-D. The p-value between these two populations was 1.8×10^{-15}, indicating a statistically significant difference between the control and the NF-κB_{FL} containing population.

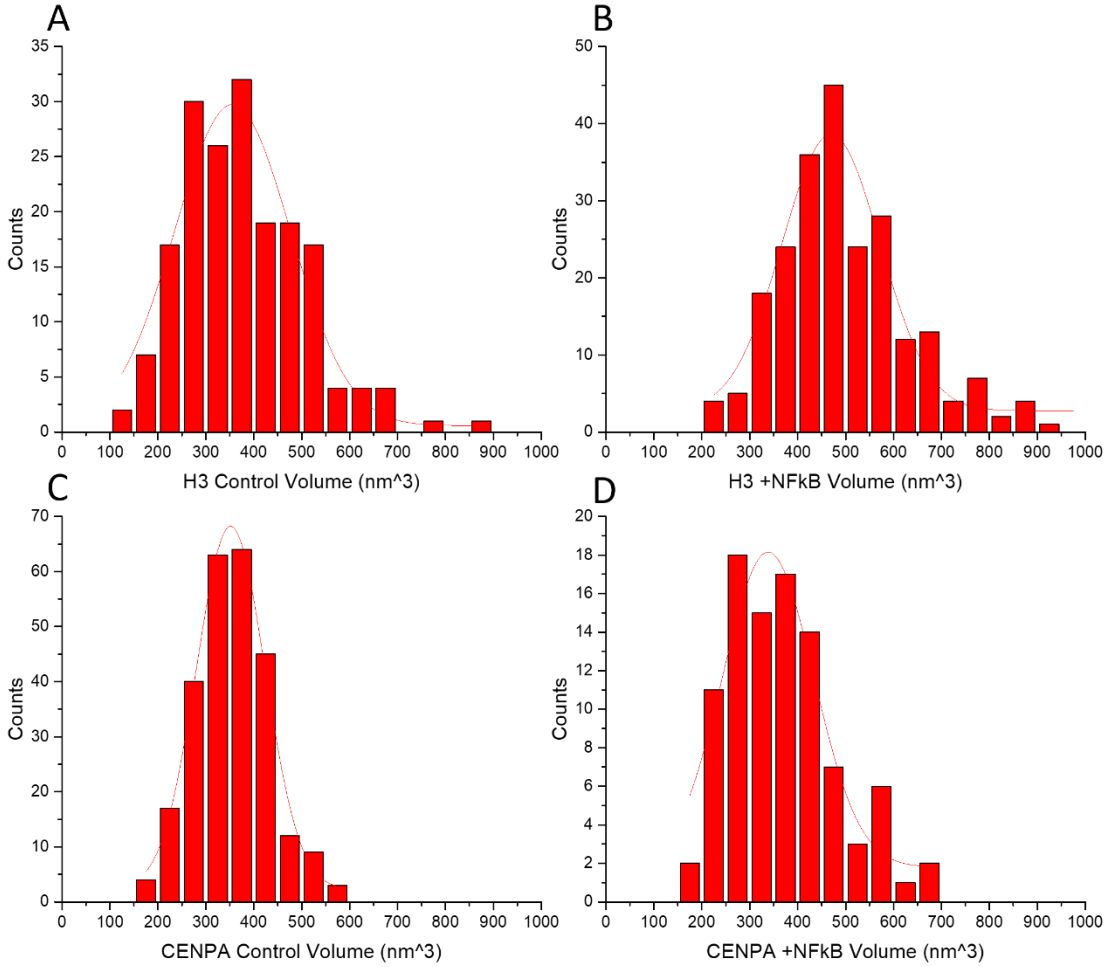

Figure 31- Volume analysis of H3 and CENP-A nucleosomes.

The histograms show the results of the volume analysis of $H3_{nuc}$ control (A), $H3_{nuc}$ + NF-κB_{FL} (B), CENP-A_{nuc} control (C), and CENP-A_{nuc} + NF-κB_{FL} (D). The average volume of the H3 Control, H3 + NF-κB_{FL}, CENP-A control, and CENP-A + NF-κB_{FL} was 355 ± 9.4 nm^3, 469 ± 9.0 nm^3, 351 ± 4.9 nm^3, and 338 ± 8.2 nm^3 (SEM), respectively.

Similar studies were performed with truncated NF-κB_{RHD} protein. Images of the sample with snapshots can be seen in Figure 32A, where the nucleosomes are indicated with a blue arrow, and the NF-

κB_{RHD} are marked with orange arrows. The snapshots from the larger AFM image can be seen to the right, where frames (i and iii) show nucleosomes in different places on the DNA. In frames (ii and iv), a nucleosome is either terminally bound or close to the end of the DNA with an NF-κB_{RHD} protein bound on the DNA flank. The wrapping efficiency of the complex was decreased to 126 ± 1.5 bp (SEM) (Figure 32B). These data suggest that the C-terminal RelA TAD does not contribute to the unraveling property of NF-κB. The height measurements for the NF-κB_{RHD}-bound nucleosomes was 1.9 ± 0.02 nm (SEM)(Figure 32C). The control for the subpopulation of $H3_{nuc}$ with 129 ± 1.5 bp wrapping efficiency resulted in a height of 1.8 ± 0.03 nm (SEM). This value is less than the height of complexes of NF-κB_{RHD} protein with nucleosome, suggesting that the truncated NF-κB_{RHD} is bound to the nucleosome.

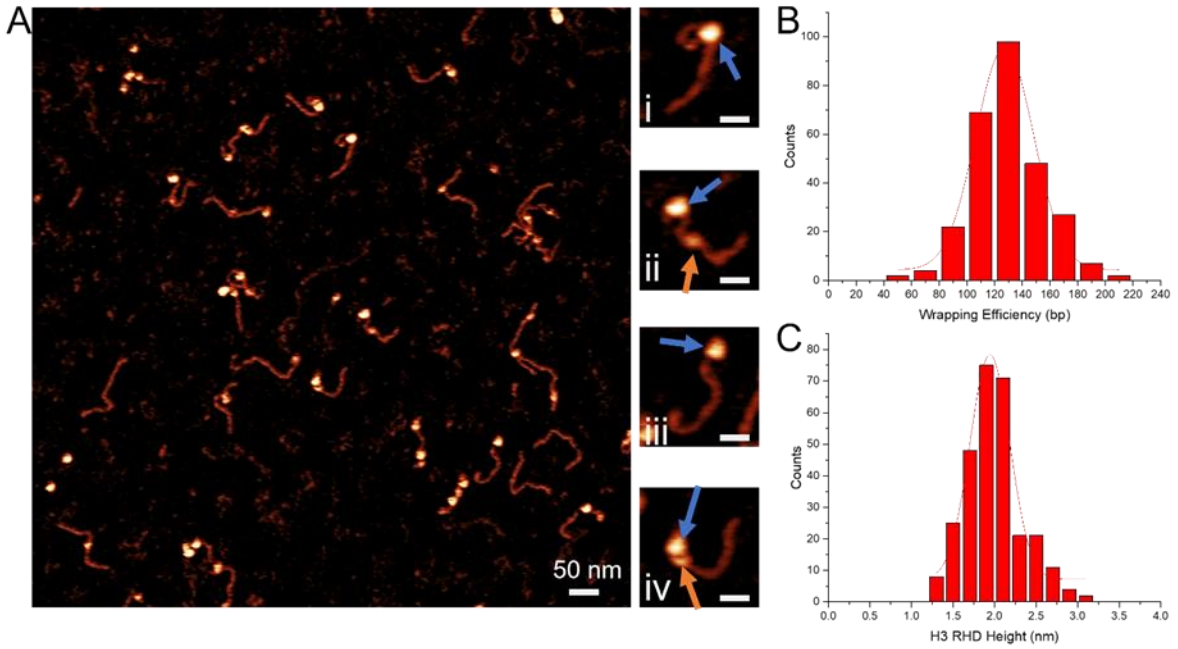

Figure 32- AFM image with zoomed-in snapshots of canonical $H3_{nuc}$ with NF-κB_{RHD}.

AFM image of $H3_{nuc}$ assembled on the DNA construct with added NF-κB_{RHD}(A). Snapshots of the image scanned can be seen to the right of the large AFM image, with images (i and iii) showing a nucleosome bound to the DNA and in (ii and iv) a nucleosome bound with an NF-κB_{RHD} bound to the flank of the DNA. The large scan in (A) is 1 x 1 µm, and the scale bar is 50 nm. The snapshots are 100 x 100 nm, and the scale bar is 25 nm. The orange arrows indicate NF-κB_{RHD} bound to the DNA, and the blue arrows indicate the nucleosome. The wrapping efficiency was found to be decreased to 126 ± 1.5 bp (SEM), as seen in (B). The histogram shows the nucleosome height for $H3_{nuc}$ with NF-κB_{RHD} (C). The mean height for H3nuc with NF-κB_{RHD} was 1.9 ± 0.02 nm (SEM).

Therefore, NF-κB leads to a substantial unraveling of $H3_{nuc}$. The unraveling of nucleosome by NF-κB was reported in our recent publication [76], in which the nucleosome-specific 601 motif was used, but in this case, NF-κB unwrapped the 601 DNA to a lesser extent, only 135 ± 3 bp (SEM). Our data obtained on the physiologically-relevant DNA substrate indicates that the nucleosome unraveling is a property of NF-κB, but the effect quantitatively depends on the DNA sequence.

5.3.3 NF-κB Interaction With Centromeric CENP-A Nucleosomes

Centromeric-specific CENP-A_{nuc} were assembled on the α-sat DNA substrate mentioned above (Figure 25A) in a similar manner as the $H3_{nuc,}$ with the exception that the CENP-A_{nuc} requires an extra step in the self-assembly process of mixing 2:1 molar concentrations of the dimeric H2A/H2B and tetrameric CENP-A/H4 (see the methods section for details). The AFM images of the nucleosomes are shown in Figure 33A, with a few snapshots selected to the right. The snapshots of the assembled CENP-A nucleosomes shown in frames (i and ii) show nucleosomes bound close to the DNA ends, and frames (iii and iv) show nucleosomes closer to the middle of the DNA sequence. The nucleosomes are indicated with blue arrows. The wrapping efficiency of the CENP-A_{nuc} was 130 ± 1.4 bp (SEM) (Figure 33B), which is in line with our previous publications in which 601 motif DNA substrate along with non-specific DNA sequences were used.[76,100,140]

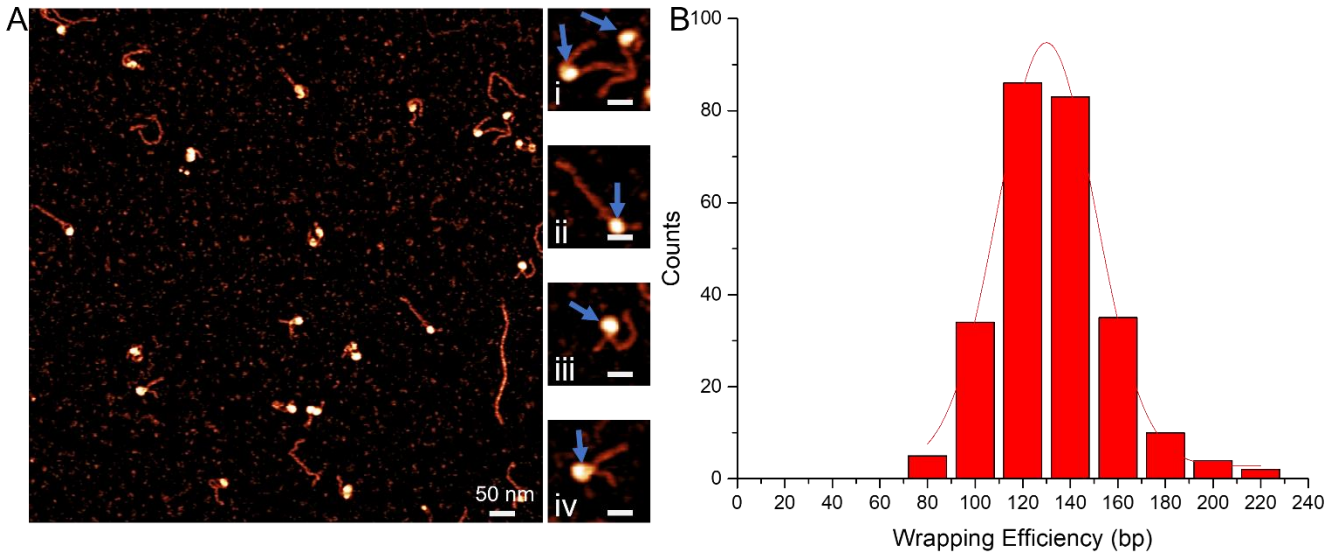

Figure 33- AFM image with zoomed-in snapshots of centromeric CENP-A_{nuc}.

AFM image of CENP-A_{nuc} assembled on the DNA construct is shown in (A). The large AFM image is 1 x 1 µm, and the snapshots are 100 x 100 nm. The scale bars are 50 and 25 nm for the large AFM image and snapshots, respectively. The snapshots to the right of the large AFM image show typical nucleosomes assembled on the DNA construct. In (i), there are two nucleosomes, one close to the end and one more centrally bound. In (ii) and (iii), nucleosomes are close to the terminal end. In (iv), the nucleosome is closer to the middle of the DNA. The histogram to the right (B) represented the Gaussian distribution of the wrapping efficiency of the assembly, which was 130 ± 1.4 bp (SEM). The scale bar is 50 and 25 nm for the large image and snapshots, respectively.

Next, NF-κB_{FL} was added to CENP-A_{nuc} in a nucleosome-to-protein molar ratio of 1:1. The AFM results from the CENP-A_{nuc} and NF-κB_{FL} can be seen in Figure 34A, where selected complexes can be seen in the snapshots shown to the right of the large AFM image. In frame (i), the CENP-A_{nuc} is bound near the end of the DNA, and the NF-κB_{FL} is adjacent to the CENP-A_{nuc}. In frame (ii), the CENP-A_{nuc} is bound to the middle, with the NF-κB_{FL} bound to the end of the DNA. In frame (iii), the CENP-A_{nuc} and the NF-κB_{FL} are bound to opposite ends of the DNA. Frame (iv) shows a CENP-A_{nuc} bound to the middle of the DNA, with no NF-κB_{FL} on the DNA flanks. The blue arrows indicate CENP-$A_{nuc,}$ and the orange arrows indicate the NF-κB_{FL} bound to DNA flanks. The wrapping efficiency of the nucleosomes at a 1 to

1 ratio was calculated as described above, and the histograms of multiple measurements can be seen in Figure 34B. The mean wrapping efficiency was 129 ± 2.2 bp (SEM).

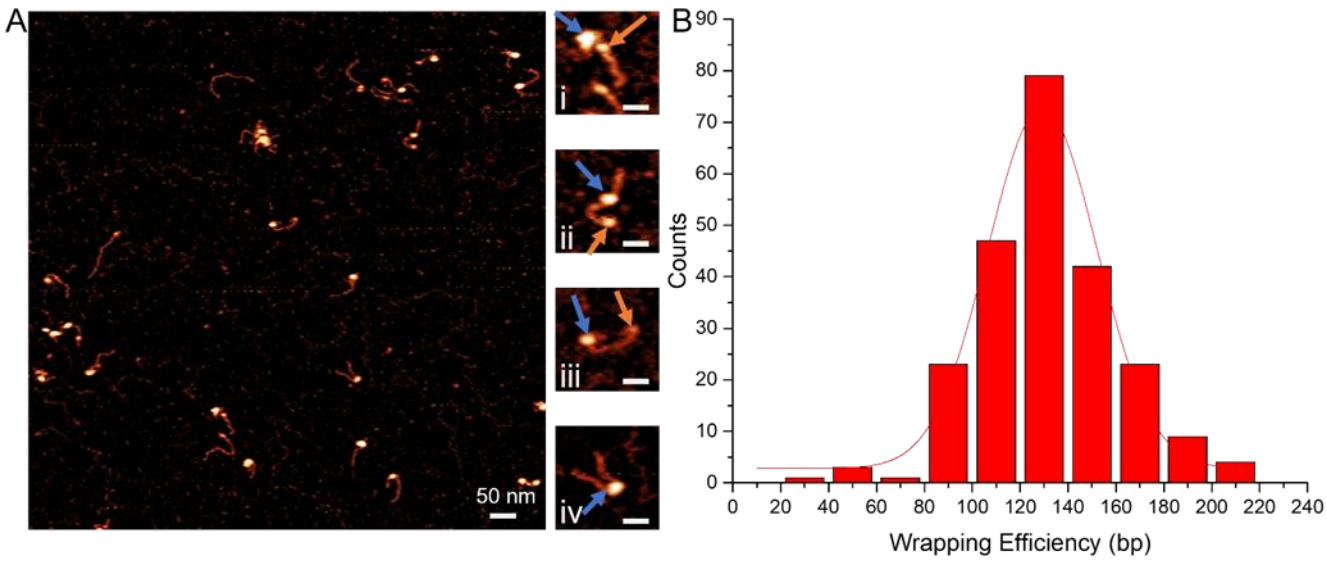

Figure 34- AFM image with zoomed-in snapshots of centromeric CENP-A$_{nuc}$ with NF-κB$_{FL}$.

AFM image of CENP-A$_{nuc}$ assembled on the DNA construct with 1 to 1 NF-κB$_{FL}$ on the left (A) and histogram of wrapping efficiency on the right (B). The larger AFM image has a scan size of 1 x 1 µm, and the snapshots are 100 x 100 nm and scale bars of 50 nm and 25 nm, respectively. The snapshots to the right of the large AFM image have NF-κB$_{FL}$ added to the assembled nucleosomes and can be seen easily, represented by the orange arrows. The blue arrows represent the nucleosomes. The snapshots show nucleosomes binding near the terminal and can be seen in (i and iii), whereas centrally bound nucleosomes can be seen in (ii and iv). The CENP-A$_{nuc}$ wrapping efficiency was 129 ± 2.2 bp (SEM).

The wrapping efficiency of the nucleosomes at a 1 to 2 ratio is shown in Figure 35A. In frame (i), a single CENP-A$_{nuc}$ is bound to the DNA. In frames (ii and iii), there is a single CENP-A$_{nuc}$ bound near the end of the DNA, with a single NF-κB$_{FL}$ bound on the flank of the DNA. In frame (iv), there is an NF-κB$_{FL}$ bound to both sides of the CENP-A$_{nuc}$. The wrapping efficiency of the 1 to 2 experiments can be seen in Figure 35B, which resulted in a wrapping efficiency of 131 ± 2.3 bp (SEM). Both the 1 to 1 and the 1 to 2 wrapping efficiencies were unchanged from the results found in the control sample, suggesting that in the presence of NF-κB, there is no unwrapping to the CENP-A$_{nuc}$. The number of NF-κB on the DNA flanks with the CENP-A$_{nuc}$ was 46% and 80% for molar ratios of 1:1 and 1:2, respectively. The p-

value between the control and the 1 to 1 NF-κB$_{FL}$ wrapping populations was 0.49, indicating no difference between the control and the NF-κB$_{FL}$ populations. This increased binding of NF-κB to DNA

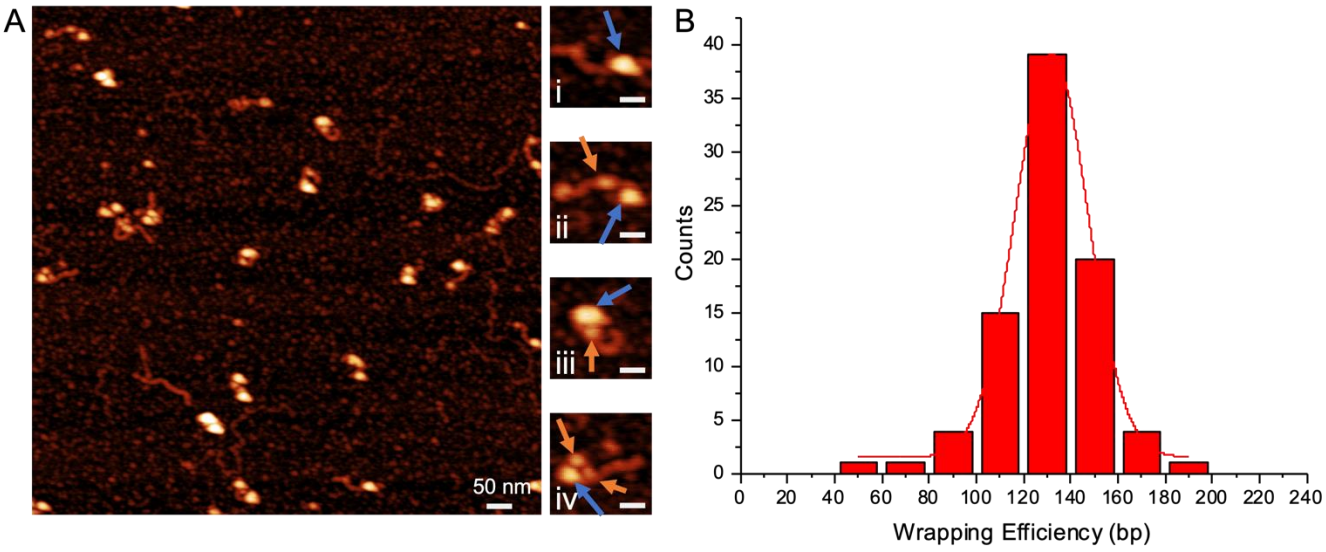

Figure 35- AFM image with zoomed-in snapshots of centromeric CENP-A$_{nuc}$ with increased NF-κB$_{FL}$ ratio.

AFM image of CENP-A$_{nuc}$ assembled on the DNA construct with NF-κB$_{FL}$ added at a 1:2 ratio with AFM images on the left (A) and histogram of wrapping efficiency on the right (B). The snapshots to the right of the larger AFM image show varying situations, NF-κB$_{FL}$ represented by orange arrows. The blue arrows represent the nucleosomes—the snapshots to the right show various binding locations of the nucleosomes and NF-κB$_{FL}$. In (i), there is a nucleosome bound near the end of the DNA. In (ii and iii), the nucleosome is bound to the DNA, and the NF-κB is bound near the nucleosome. In (iv), the nucleosome has an NF-κB$_{FL}$ bound to both sides of the nucleosome. The large AFM image has a scan size of 1 x 1 µm, and the snapshots are 100 x 100 nm and a scale bar of 50 nm and 25 nm, respectively. The wrapping efficiency was 131 ± 2.3 bp (SEM).

indicates at least twice as many NF-κB seen bound to the DNA, which does not include the NF-κB that is potentially bound to the nucleosomes.

Next, we looked for evidence of NF-κB$_{FL}$ binding to the CENP-A$_{nuc}$ through analysis of the nucleosome's measured heights, which can be seen in Figure 36A-C. The NF-κB$_{FL}$ protein bound to the DNA, minus the height of the DNA, was measured and found to be 0.54 ± 0.03 nm (SEM). The CENP-

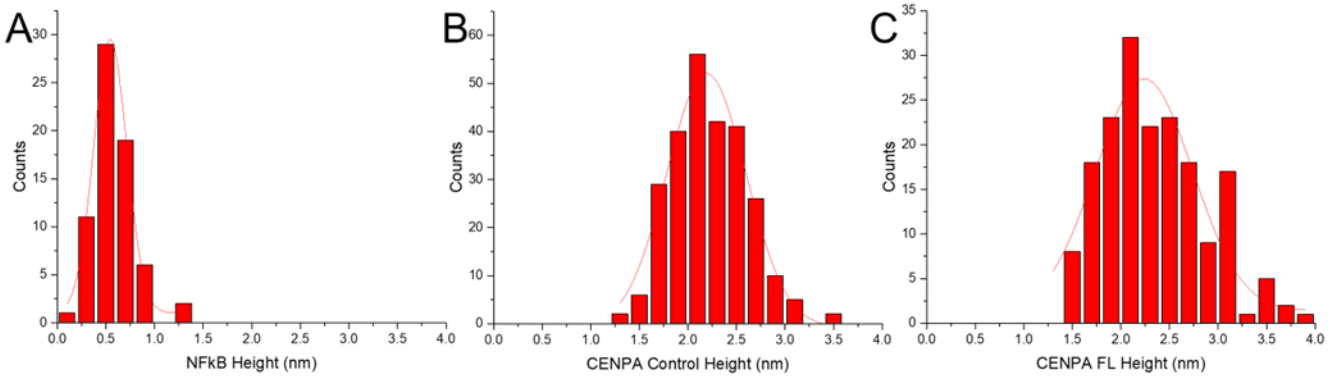

Figure 36 - Height results of NF-κB$_{FL}$, CENP-A$_{nuc}$, and CENP-A$_{nuc}$ + NF-κB$_{FL}$.

The height results for NF-κB$_{FL}$ protein only (A), CENP-A$_{nuc}$ control (B), and CENP-A$_{nuc}$ in the presence of NF-κB$_{FL}$(C). The mean height of NF-κB$_{FL}$ protein only, CENP-A$_{nuc}$ control, and NF-κB$_{FL}$ were 0.54 ± 0.03, 2.2 ± 0.02, and 2.2 ± 0.04 nm (SEM), respectively. Histograms for all the heights were measured with a gaussian distribution shown.

A$_{nuc}$ control nucleosomes had a height of 2.2 ± 0.02 nm (SEM), and with the addition of NF-κB$_{FL}$, the height was 2.2 ± 0.04 nm (SEM). The p-value between these two populations was 0.008, indicating little statistically significant difference between the control and the NF-κB$_{FL}$ containing population. These results differ from the H3$_{nuc}$, where an increase could be seen from the control upon the addition of NF-κB$_{FL}$. With the CENP-A$_{nuc}$, there was no increase in height with the addition of NF-κB$_{FL}$, indicating no NF-κB$_{FL}$ binding to the CENP-A$_{nuc}$.

We also completed a volume analysis of the control H3$_{nuc}$ and the H3$_{nuc}$ in the presence of NF-κB$_{FL}$ and found that 351 ± 8.2 nm^3 (SEM) and 338 ± 4.9 nm^3 (SEM), respectively. A histogram distribution of these results can be seen in Figure 31C and D. The p-value between these two populations was 0.27, indicating little statistical difference between the control and the NF-κB$_{FL}$ containing population.

Similar experiments were completed with the modified NF-κB$_{RHD}$. Images and snapshots can be seen in Figure 37A. The snapshots can be seen to the right of the large AFM image. In frames (i and ii), the CENP-A$_{nuc}$ is bound to the DNA without any NF-κB$_{RHD}$ bound to the flanks. In frames (iii and iv),

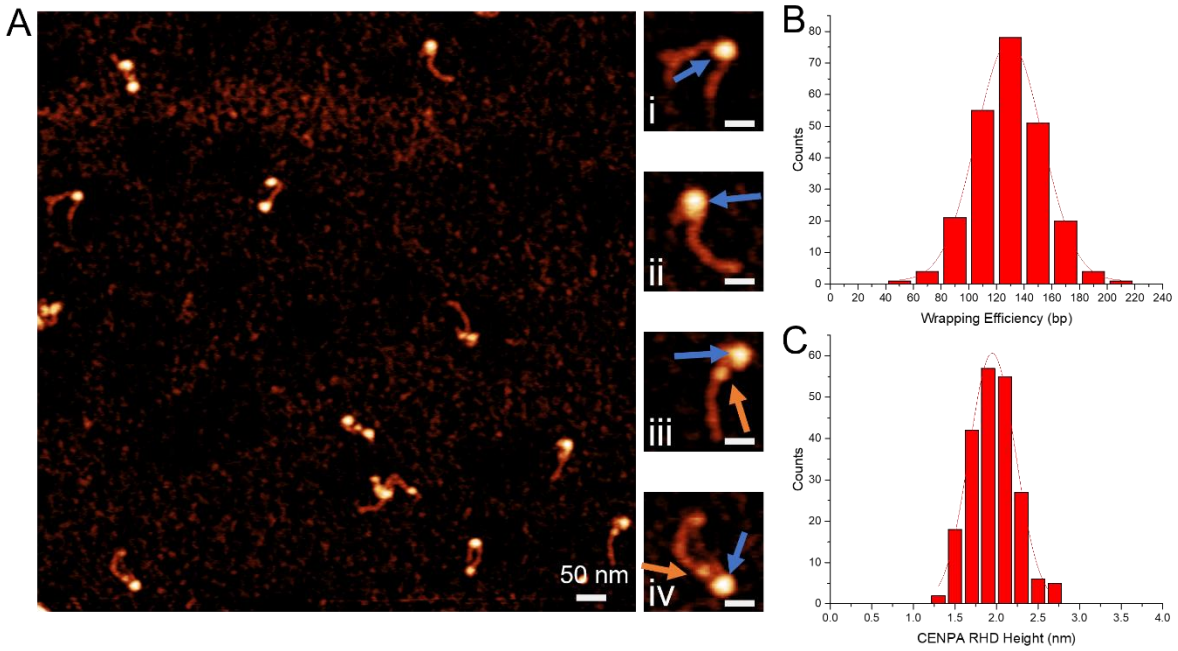

Figure 37- AFM image with zoomed-in snapshots of centromeric CENP-A_{nuc} with NF-κB_{RHD}.

AFM image of CENP-A_{nuc} assembled on the DNA on the left (A) and histogram of wrapping efficiency in the upper right (B). NF-κB_{RHD} was added to the assembled nucleosomes and can be seen easily in the snapshots, represented by the orange arrows. In snapshots (i and ii), the nucleosome is bound to the DNA, with (i) being more centrally bound and (ii) being closer to the terminal end. In (iii and iv), terminal or nearly terminal bound nucleosomes have an adjacent NF-κB_{RHD} bound. The blue arrows represent the nucleosomes. The large AFM image has a scan size of 1 x 1 µm, and the snapshots have a size of 100 x 100 nm and a scale bar of 25 nm. The wrapping efficiency was 129 ± 1.6 bp (SEM)—the histogram showing the nucleosome height for CENP-A_{nuc} with NF-κB_{RHD} can be seen in (C). The mean height for CENP-A_{nuc} with NF-κB_{RHD} was 1.9 ± 0.02 nm (SEM).

the CENP-A_{nuc} are bound near the terminal end of the DNA with the NF-κB_{RHD} bound adjacent to the CENP-A_{nuc}. The nucleosomes are indicated with a blue arrow, and the NF-κB_{RHD} are marked with orange arrows. The wrapping efficiency of CENP-A_{nuc} with NF-κB_{RHD} was 129 ± 1.6 bp (SEM)(Figure 37B), indicating no unwrapping. The height values of the nucleosomes were measured for the NF-κB_{RHD} containing samples and found to be 1.9 ± 0.02 nm (SEM)(Figure 37C) for CENP-A_{nuc}. These results show that NF-κB does not unravel CENP-A_{nuc} nor bind to the nucleosome.

5.3.4 Comparison of nucleosome positioning with NF-κB

We mapped the position of the nucleosome in these complexes, as shown in Figure 38A-C. Interestingly, the data show a lower population of nucleosomes at the DNA end when NF-κB is bound. This value was reduced to 16 % compared with 27 % for the control, which decreased even more with a 1 to 2 ratio decreasing to 9%. These results suggest that the NF-κB can cause displacement of the nucleosomes from the end of the DNA.

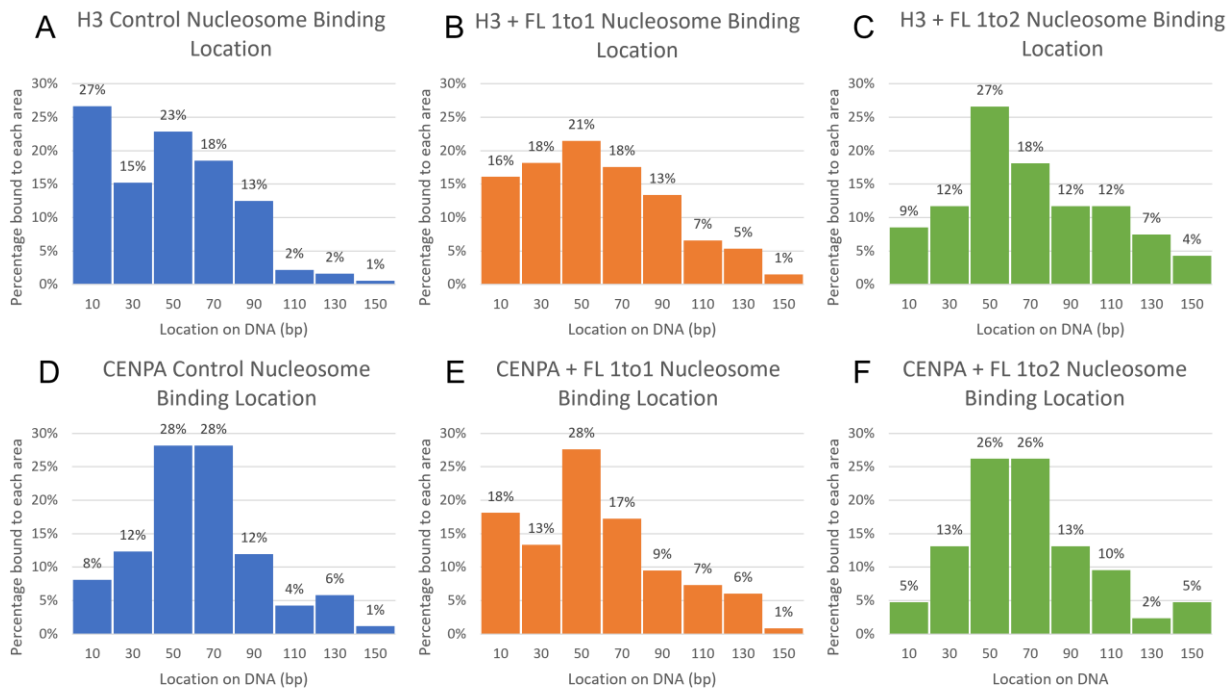

Figure 38- Nucleosome binding locations with varying concentrations of NF-κB$_{FL}$.

Canonical nucleosome binding locations along the DNA construct: H3$_{nuc}$ Control (A), H3$_{nuc}$ with 1 to 1 NF-κB$_{FL}$ (B), and H3$_{nuc}$ with 1 to 2 NF-κB$_{FL}$ (C). The H3nuc control had a terminal binding percentage of 27%, drastically decreasing to 16% in samples with NF-κB$_{FL}$. The 1 to 2 NF-κB$_{FL}$ had an end binding of 9%, an even greater decrease in terminal binding than the 1 to 1 sample. Centromeric nucleosome binding locations along the DNA construct: CENP-A$_{nuc}$ control (D), CENP-A$_{nuc}$ with 1 to 1 NF-κB$_{FL}$ (E), and CENP-A$_{nuc}$ with 1 to 2 NF-κB$_{FL}$ (F). The CENP-A$_{nuc}$ control had an end binding percentage of 8%, which was increased to 18% in samples with NF-κB$_{FL}$, at a 1 to 2 ratio, the terminal bound CENP-A$_{nuc}$ decreased to 5%.

The mapping results of the CENP-A$_{nuc}$ control and CENP-A$_{nuc}$ in the presence of NF-κB$_{FL}$ can be seen in Figure 38D-F. There was no consistent change in the mapping profile for the CENP-A nucleosomes in the presence of NF-κB.

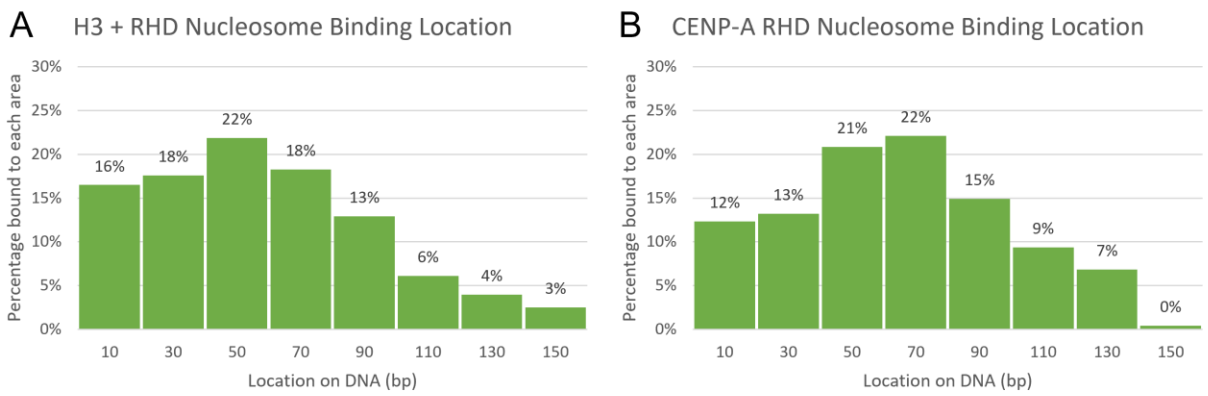

Figure 39- Nucleosome positioning at 1 to 1 nucleosome:protein of NF-κB$_{RHD}$.

The results of the nucleosome positioning in the presence of NF-κBRHD were similar to those achieved in the presence of NF-κBFL. The H3nuc (A) decreased the end binding of the nucleosomes, and the CENP-Anuc (B) had a slight increase in end binding.

The mapping data of H3$_{nuc}$ with NF-κB$_{RHD}$ added is shown in Fig. S8A, which is very close to the data obtained for the full-length NF-κB. Similarly, the CENP-A mapping results with the NF-κB$_{RHD}$ were comparable to the effects of NF-κB$_{FL}$, with 12% terminal binding compared to 18% (Fig. S8B).

An analysis of the height compared to the position of the nucleosome showed no correlation between the two. A scatter plot of the comparison for H3$_{nuc}$ can be seen in Figure 40A-F. This indicates that nucleosome repositioning does not solely occur when NF-κB is bound to the nucleosome itself but can also occur when NF-κB is bound at the flanking DNA.

We considered the possibility that the observed repositioning was actually a result of nucleosome removal. The results show that whether NF-κB was not present (control) or was present at a nucleosome:protein ratio of 1:1 or 1:2, the yield of H3$_{nuc}$ were 62%, 62%, and 63%, respectively. These results indicate that the NF-κB is not removing the nucleosomes from the DNA but rather causes

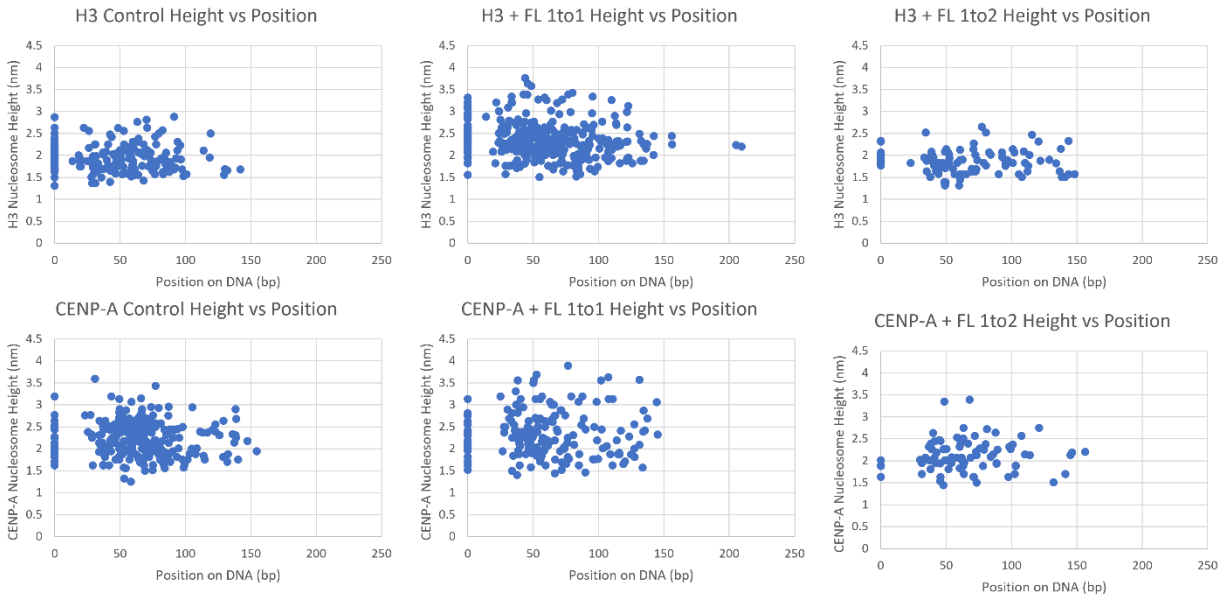

Figure 40- Analysis of the nucleosome's height as a comparison to the position on the DNA.

There was no correlation to the nucleosome height when compared to the position on the DNA, this includes the end binding which can be seen at the 0 on the X-axis.

translocation of the nucleosomes away from the DNA ends. The yield analysis was also completed for the CENP-A_{nuc}; the results were 70%, 67%, and 71% for control, 1 to 1, and 1 to 2, respectively.

5.4 Discussion

5.4.1 Implications of transcription limitation in the centromere

Our major findings are summarized in Figure 41. According to the graph in Figure 41, NF-κB unravels canonical H3 nucleosomes, removing more than 20 bp DNA out of 147 bp total DNA wrapped around the nucleosome core. The unraveling of nucleosomes by NF-κB was reported in our recent publication.[76] However, nucleosomes were assembled on the highly specific 601 sequence in that publication, and a lower unwrapping effect was observed. Elevated stability of the nucleosome assembled by the specific 601 DNA sequence can explain this effect.[142] Still, we need to consider the difference in the interaction of NF-κB with both DNA templates. The 601 motif contained only one κB binding site for NF-κB.[76] However, analysis of the NF-κB binding data did not reveal a preference for NF-κB binding at that site.[76] In contrast, the α-sat DNA substrate used in this work reveals a specific binding pattern of NF-

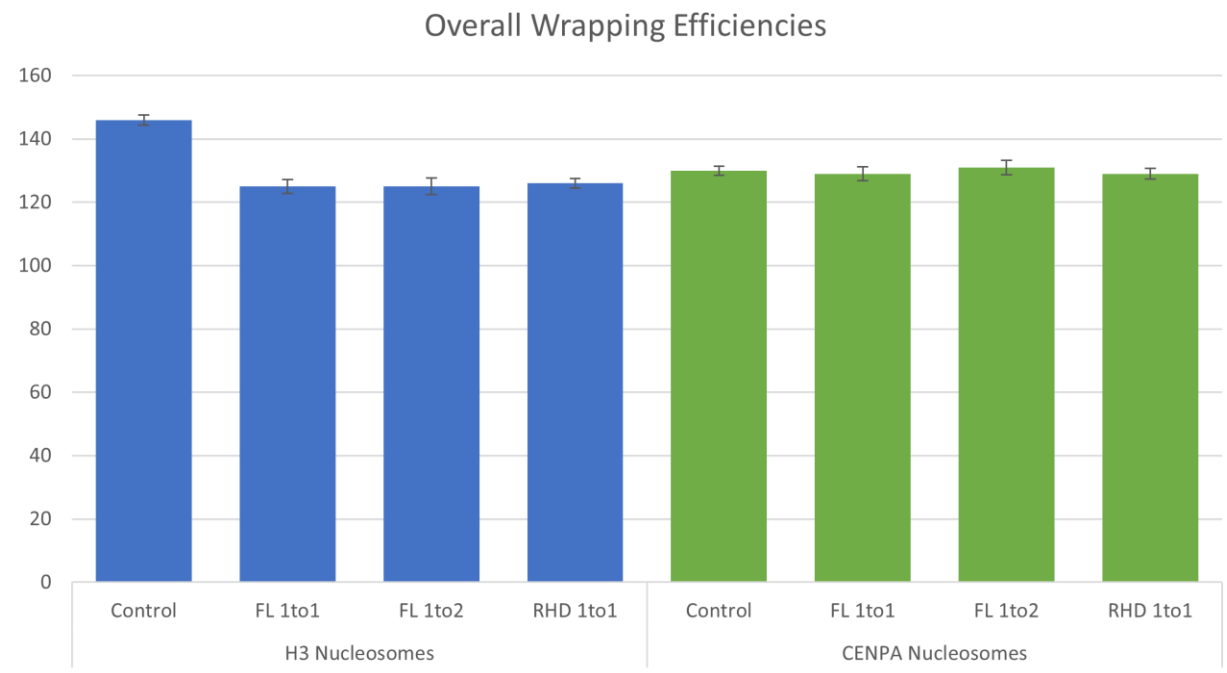

Figure 41- Effect of NF-κB on nucleosome wrapping efficiency.

The $H3_{nuc}$ control had the highest wrapping efficiency at 146 ± 1.6 (SEM) bp, whereas the H3nuc with NF-$κB_{FL}$ 1 to 1, NF-$κB_{FL}$ 1 to 2, and NF-$κB_{RHD}$ 1 to 1 had a lower wrapping at 125 ± 2.2 (SEM) bp, 125 ± 2.2 (SEM) bp, and 126 ± (SEM) 1.5 bp, respectively. The CENP-Anuc results were very different from the $H3_{nuc,}$ with the NF-κB not affecting the wrapping efficiency: the CENP-A_{nuc} control (130 ± 1.4 [SEM] bp), with 1 to 1 NF-$κB_{FL}$(129 ± 2.2 [SEM] bp), with 1 to 2 NF-κBFL(131 ± 2.3 [SEM] bp), and with 1 to 1 NF-$κB_{RHD}$ (129 ± 1.6 [SEM] bp). FL and RHD stand for the full-length and truncated variant NF-κB, respectively. The blue bars represent the $H3_{nuc}$ wrapping, the green bars represent the CENP-A_{nuc} wrapping, and the error bars show the SEM.

κB (Figure 25). Importantly, the protein showed higher affinity for the DNA ends as well as for a cluster of half κB sites near the middle of the sequence. The affinity of NF-κB to the DNA ends can explain the decrease in the population of the end-bound nucleosomes in the presence of NF-κB by 1.5 times (Figure 38A-C). These observations suggest that binding of NF-κB to specific sites on DNA weakens nucleosome interactions, resulting in their displacement and/or dissociation.

Similar results of unraveling nucleosomes by NF-κB were obtained for the truncated variant NF-$κB_{RHD}$ (Figure 30), suggesting that the RelA C-terminal TAD does not define the unwrapping property of NF-κB. Given that the full-length NF-κB and its truncated variant NF-$κB_{RHD}$ have similar DNA binding

patterns (Figure 26), we hypothesize that the DNA binding affinity of NF-κB is the factor defining the nucleosome unraveling property of NF-κB. We hypothesize that NF-κB binds to transiently dissociated DNA segments formed during the breathing of the nucleosome, stabilizing such an open state of the nucleosome and shifting the location of the nucleosome, explaining the repositioning of the population of the end-bound nucleosomes in the presence of NF-κB.

To look at the effect of the wrapping vs. the height of the nucleosomes both with and without NF-κB, we plotted them in Figure 42 and Figure 43. The trend can be seen that typically, a lower height is indicative of lower wrapping. The interaction of NF-κB with CENP-A nucleosomes is entirely different. As seen in Figure 28,Figure 29, Figure 32, and Figure 34, there is no change in the nucleosome wrapping, suggesting that regardless of the same affinity of NF-κB to DNA, the protein cannot unravel the CENP-A nucleosome. If breathing of nucleosomes is the pathway by which NF-κB unwraps the nucleosome, the NF-κB will bind to the transiently dissociated DNA segments. In that case, these data indicate that CENP-A nucleosomes are more stable than canonical H3 nucleosomes. According to the graph in Figure 36B and C, there are no changes in the CENP-A nucleosome, suggesting that NF-κB does not bind the CENP-A nucleosome, which can be explained by the elevated stability of CENP-A nucleosomes compared with canonical ones.[100] The ability of CENP-A nucleosomes to resist the binding of the high affinity of NF-κB to DNA can be a factor contributing to findings that in vitro CENP-A chromatin was predominantly nonpermissive for transcription compared to H3 chromatin.[190] This finding is in line with previous results, which showed a 200-300 fold lower transcriptional activity, including that of NF-κB, of centromeric chromatin with euchromatin.[184]

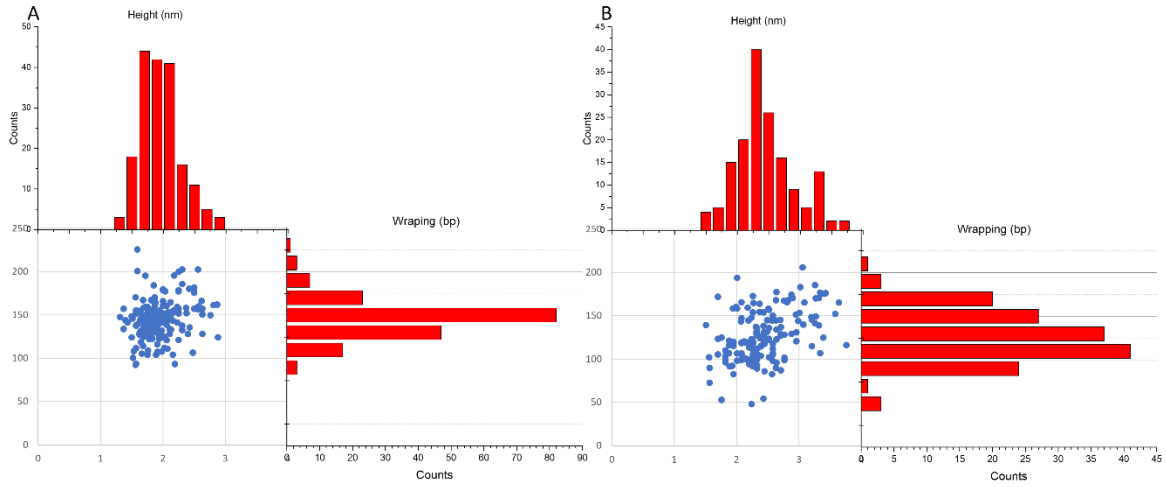

Figure 42- Height vs Wrapping analysis for $H3_{nuc}$.

Overall populational analysis of the height and wrapping efficiency of the $H3_{nuc}$ samples. In frame A, the $H3_{nuc}$ control sample had a mean wrapping of 146 ± 1.6 bp (SEM) and a mean height of 1.9 ± 0.02 nm (SEM). In frame B, the $H3_{nuc}$ with NF-κB_{FL} had a mean wrapping of 125 ± 2.2 bp (SEM) and a mean height of 2.3 ± 0.04 nm (SEM). The X-axis is the height of each population, and the Y-axis is the wrapping efficiency of the nucleosomes.

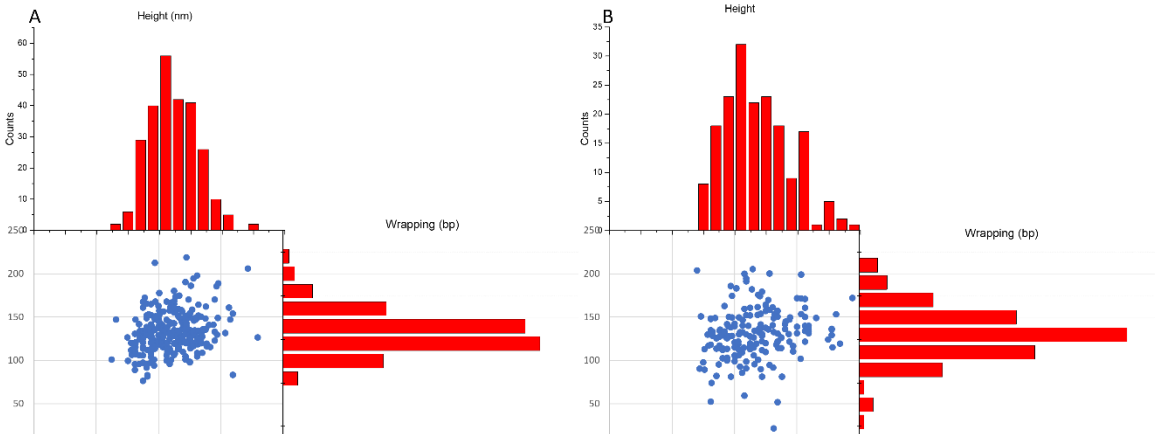

Figure 43- Height vs Wrapping analysis for CENP-A_{nuc}.

Overall populational analysis of the height and wrapping efficiency of the CENP-A_{nuc} samples. In frame A, the CENP-A_{nuc} control sample had a mean wrapping of 130 ± 1.4 bp (SEM) and a mean height of 2.2 ± 0.02 nm (SEM). In frame B, the CENP-A_{nuc} with NF-κB_{FL} had a mean wrapping of 129 ± 2.2 bp (SEM) and a mean height of 2.2 ± 0.04 nm (SEM). The X-axis is the height of each population, and the Y-axis is the wrapping efficiency of the nucleosomes.

5.5 Conclusion

We found that NF-κB has tremendous effects on H3 nucleosomes because it is a pioneer transcription factor, which results in the binding of NF-κB directly to the nucleosome core, proven through height and volume measurements. But nucleosomes must be displaced for transcription to occur, which is facilitated in the H3 nucleosomes through the unwrapping of ~20 bp of DNA. This unwrapping was not discovered in the CENP-A nucleosomes nor the binding to the core of the nucleosome. These results indicate that these nucleosomes, which are only found in the centromere, do not allow for transcription factors to displace them and, therefore, actively blocking transcription from occurring in the centromere. These results might be a bit surprising considering H3 nucleosomes have 75% identical histone homology, and the CENP-A and H3 histone share 50% homology. Such a minor modification to the nucleosome core could disallow NF-κB from binding was an exciting finding. However, this inability to bind to the CENP-A nucleosomes likely plays a biological role in the centromere to prevent unwanted transcription and disruption to the centromere region of the chromosome, ultimately providing stability to the whole chromosome.

Chapter 6. Overall Conclusions

6.1 Nucleosomal Dynamics

6.1.1 Nucleosome Stability

Our study revealed that the balance between energies of internucleosomal interaction and the affinity of the nucleosome core to the DNA sequence influences the formation of tight contacts between nucleosomes. The lower yield of dinucleosome complexes for CENP-A_{nuc} may be due to the repulsion generated by the CENP-A tail. The DNA sequence is the primary factor defining nucleosome positioning in the chromatin. The binding affinity of CENP-A_{nuc} to the DNA ends is also higher than for $H3_{nuc}$.

Time-lapse HS-AFM studies revealed different stabilities of H3 and CENP-A nucleosomes under scanning conditions. CENP-A_{nuc} appeared more stable than $H3_{nuc}$, with 38% of mono$H3_{nuc}$ lasting longer than 20 frames, while 52% of monoCENP-A_{nuc} lasted longer than 20 frames. This increase in dwell time is counterintuitive as the wrapping efficiency of CENP-A_{nuc} is less than $H3_{nuc}$. Similarly, the di$H3_{nuc}$ has a dwell time of more than 20 frames only 48% of the time compared to diCENP-A_{nuc} at 66%, a dramatic increase of 18%. These increased dwell times for CENP-A_{nuc} indicate that these nucleosomes are more stable than their $H3_{nuc}$ counterparts.

6.1.2 Asymetric Unwrapping

Interestingly, we found that nucleosomes undergo a step-wise asymmetrical unwrapping, which was also recently discovered by another group of investigators.[162] The unwrapping process for the CENP-A_{nuc} was asymmetrical but did not result in the loss of histones. The step-wise unwrapping of H3 nucleosomes is directly correlated to the loss of histones, where one step in the unwrapping process is the loss of an H2A/H2B histone, resulting in a hexasome, with the next step being the loss of another H2A/H2B histone resulting in a stable tetrasome. These intermediate steps in unwrapping likely play a biological role whereby the DNA becomes more accessible to transcription factors (like NF-κB).

Conversely, the CENP-A_{nuc} had a much lower occurrence of the histones vacating the octameric core, indicating an intrinsic difference between the DNA and nucleosome interactions. Despite the lower wrapping efficiency of CENP-A_{nuc} compared with $H3_{nuc}$, they not only have longer dwell times on the DNA, but their octameric structural integrity is greater than that of $H3_{nuc}$.

In conclusion, CENP-A nucleosomes are more stable than canonical nucleosomes. The unwrapping process is highly asymmetric, and HS-AFM revealed higher CENP-A nucleosome stability than H3 nucleosomes. This feature of CENP-A nucleosomes can be important for centromere dynamics during mitosis and chromatin replication and for protecting the centromere from unwanted interactions.

6.2 Effect NF-κB on Nucleosomes

Our study revealed that NF-κB, a pioneer transcription factor, significantly affects H3 nucleosomes, removing more than 20 bp of DNA from the DNA wrapped around the nucleosome core. The binding affinity of NF-κB to specific sites on DNA weakened nucleosome interactions, resulting in their displacement or dissociation. Similar results were obtained for the truncated variant NF-κB$_{RHD}$, suggesting that the DNA binding affinity of NF-κB does not exist in the Rel Homology Domain portion of the protein. The interaction of NF-κB with CENP-A nucleosomes was drastically different, with no change in the nucleosome wrapping. This suggests that CENP-A nucleosomes are more stable than canonical H3 nucleosomes, and NF-κB does not bind to them. This inability to bind to CENP-A nucleosomes may play a biological role in the centromere to prevent unwanted transcription and disruption to the centromere region of the chromosome.[178,191]

References

1. Watson JD, Crick FHC. THE STRUCTURE OF DNA. *Cold Spring Harb Symp Quant Biol*. 1953;18(0):123-131. doi:10.1101/SQB.1953.018.01.020

2. Bebenek K, Kunkel TA. Functions of DNA Polymerases. In: *Advances in Protein Chemistry*. Vol 69. Elsevier; 2004:137-165. doi:10.1016/S0065-3233(04)69005-X

3. Dong Y, Sun F, Ping Z, Ouyang Q, Qian L. DNA storage: research landscape and future prospects. *Natl Sci Rev*. 2020;7(6):1092-1107. doi:10.1093/nsr/nwaa007

4. Bancroft C, Bowler T, Bloom B, Clelland CT. Long-Term Storage of Information in DNA. *Science*. 2001;293(5536):1763-1765. doi:10.1126/science.293.5536.1763c

5. Bram S. The function of the structure of DNA in chromosomes. *Biochimie*. 1972;54(8):1005-1011. doi:10.1016/S0300-9084(72)80051-8

6. Travers A, Muskhelishvili G. DNA structure and function. *FEBS J*. 2015;282(12):2279-2295. doi:10.1111/febs.13307

7. Nirenberg MW, Jones OW, Leder P, Clark BFC, Sly WS, Pestka S. On the Coding of Genetic Information. *Cold Spring Harb Symp Quant Biol*. 1963;28(0):549-557. doi:10.1101/SQB.1963.028.01.074

8. Case-Green SC, Mir KU, Pritchard CE, Southern EM. Analysing genetic information with DNA arrays. *Curr Opin Chem Biol*. 1998;2(3):404-410. doi:10.1016/S1367-5931(98)80016-1

9. Morrow JF, Cohen SN, Chang ACY, Boyer HW, Goodman HM, Helling RB. Replication and Transcription of Eukaryotic DNA in *Esherichia coli*. *Proc Natl Acad Sci*. 1974;71(5):1743-1747. doi:10.1073/pnas.71.5.1743

10. Von Hippel PH. On the Molecular Bases of the Specificity of Interaction of Transcriptional Proteins with Genome DNA. In: Goldberger RF, ed. *Biological Regulation and Development*. Springer US; 1979:279-347. doi:10.1007/978-1-4684-3417-0_8

11. McCarthy BJ, Bolton ET. Interaction of complementary RNA and DNA. *J Mol Biol*. 1964;8(2):184-200. doi:10.1016/S0022-2836(64)80128-5

12. Milman G, Langridge R, Chamberlin MJ. The structure of a DNA-RNA hybrid. *Proc Natl Acad Sci*. 1967;57(6):1804-1810. doi:10.1073/pnas.57.6.1804

13. Cassiday LA. Having it both ways: transcription factors that bind DNA and RNA. *Nucleic Acids Res*. 2002;30(19):4118-4126. doi:10.1093/nar/gkf512

14. Estévez-Torres A, Baigl D. DNA compaction: fundamentals and applications. *Soft Matter*. 2011;7(15):6746. doi:10.1039/c1sm05373f

15. Strick TR, Kawaguchi T, Hirano T. Real-Time Detection of Single-Molecule DNA Compaction by Condensin I. *Curr Biol*. 2004;14(10):874-880. doi:10.1016/j.cub.2004.04.038

16. Zinchenko AA, Chen N. Compaction of DNA on nanoscale three-dimensional templates. *J Phys Condens Matter*. 2006;18(28):R453-R480. doi:10.1088/0953-8984/18/28/R01

17. Lindman B, Dias R. *DNA Interactions with Polymers and Surfactants*. Wiley-Interscience; 2011.

18. Berman H, Campbell S, Clore M, et al. *Protein-Nucleic Acid Interactions: Structural Biology*. Royal Society of Chemistry; 2008.

19. Sanbonmatsu KY. Large-scale simulations of nucleoprotein complexes: ribosomes, nucleosomes, chromatin, chromosomes and CRISPR. *Curr Opin Struct Biol*. 2019;55:104-113. doi:10.1016/j.sbi.2019.03.004

20. Fransz P, De Jong H. From nucleosome to chromosome: a dynamic organization of genetic information. *Plant J*. 2011;66(1):4-17. doi:10.1111/j.1365-313X.2011.04526.x

21. Luger K. Structure and dynamic behavior of nucleosomes. *Curr Opin Genet Dev*. 2003;13(2):127-135. doi:10.1016/S0959-437X(03)00026-1

22. McGinty RK, Tan S. Nucleosome Structure and Function. *Chem Rev*. 2015;115(6):2255-2273. doi:10.1021/cr500373h

23. Jevtić P, Edens LJ, Vuković LD, Levy DL. Sizing and shaping the nucleus: mechanisms and significance. *Curr Opin Cell Biol*. 2014;28:16-27. doi:10.1016/j.ceb.2014.01.003

24. Luger K, Hansen JC. Nucleosome and chromatin fiber dynamics. *Curr Opin Struct Biol*. 2005;15(2):188-196. doi:10.1016/j.sbi.2005.03.006

25. Mueller-Planitz F, Klinker H, Becker PB. Nucleosome sliding mechanisms: new twists in a looped history. *Nat Struct Mol Biol*. 2013;20(9):1026-1032. doi:10.1038/nsmb.2648

26. Bassett A, Cooper S, Wu C, Travers A. The folding and unfolding of eukaryotic chromatin. *Curr Opin Genet Dev*. 2009;19(2):159-165. doi:10.1016/j.gde.2009.02.010

27. Parmar JJ, Padinhateeri R. Nucleosome positioning and chromatin organization. *Curr Opin Struct Biol*. 2020;64:111-118. doi:10.1016/j.sbi.2020.06.021

28. Luger K. Dynamic nucleosomes. *Chromosome Res*. 2006;14(1):5-16. doi:10.1007/s10577-005-1026-1

29. Eslami-Mossallam B, Schiessel H, Van Noort J. Nucleosome dynamics: Sequence matters. *Adv Colloid Interface Sci*. 2016;232:101-113. doi:10.1016/j.cis.2016.01.007

30. Forties RA, North JA, Javaid S, et al. A quantitative model of nucleosome dynamics. *Nucleic Acids Res*. 2011;39(19):8306-8313. doi:10.1093/nar/gkr422

31. Adkins NL, Niu H, Sung P, Peterson CL. Nucleosome dynamics regulates DNA processing. *Nat Struct Mol Biol*. 2013;20(7):836-842. doi:10.1038/nsmb.2585

32. McKinley KL, Sekulic N, Guo LY, Tsinman T, Black BE, Cheeseman IM. The CENP-L-N Complex Forms a Critical Node in an Integrated Meshwork of Interactions at the Centromere-Kinetochore Interface. *Mol Cell*. 2015;60(6):886-898. doi:10.1016/j.molcel.2015.10.027

33. Talbert PB, Henikoff S. What makes a centromere? *Exp Cell Res*. 2020;389(2). doi:10.1016/j.yexcr.2020.111895

34. Pluta AF, Mackay AM, Ainsztein AM, Goldberg IG, Earnshaw WC. The Centromere: Hub of Chromosomal Activities. *Science*. 1995;270(5242):1591-1594. doi:10.1126/science.270.5242.1591

35. McIntosh JR, Hering GE. Spindle Fiber Action and Chromosome Movement. *Annu Rev Cell Biol*. 1991;7(1):403-426. doi:10.1146/annurev.cb.07.110191.002155

36. Bloom K, Costanzo V. Centromere Structure and Function. In: Black BE, ed. *Centromeres and Kinetochores*. Vol 56. Progress in Molecular and Subcellular Biology. Springer International Publishing; 2017:515-539. doi:10.1007/978-3-319-58592-5_21

37. Battaglia E. Chromosome Morphology and Terminology: (with 12 figures). *Caryologia*. 1955;8(1):179-187. doi:10.1080/00087114.1955.10797556

38. Madian N, Jayanthi KB. Analysis of human chromosome classification using centromere position. *Measurement*. 2014;47:287-295. doi:10.1016/j.measurement.2013.08.033

39. Lončarek J, Kisurina-Evgenieva O, Vinogradova T, et al. The centromere geometry essential for keeping mitosis error free is controlled by spindle forces. *Nature*. 2007;450(7170):745-749. doi:10.1038/nature06344

40. Draviam VM, Xie S, Sorger PK. Chromosome segregation and genomic stability. *Curr Opin Genet Dev*. 2004;14(2):120-125. doi:10.1016/j.gde.2004.02.007

41. Potapova T, Gorbsky G. The Consequences of Chromosome Segregation Errors in Mitosis and Meiosis. *Biology*. 2017;6(4):12. doi:10.3390/biology6010012

42. Gisselsson D. Classification of chromosome segregation errors in cancer. *Chromosoma*. 2008;117(6):511-519. doi:10.1007/s00412-008-0169-1

43. Tachiwana H, Kurumizaka H. Structure of the CENP-A nucleosome and its implications for centromeric chromatin architecture. *Genes Genet Syst*. 2011;86(6):357-364. doi:10.1266/ggs.86.357

44. Tachiwana H, Kagawa W, Shiga T, et al. Crystal structure of the human centromeric nucleosome containing CENP-A. *Nature*. 2011;476(7359):232-235. doi:10.1038/nature10258

45. Stellfox ME, Bailey AO, Foltz DR. Putting CENP-A in its place. *Cell Mol Life Sci*. 2013;70(3):387-406. doi:10.1007/s00018-012-1048-8

46. Ariyoshi M, Makino F, Watanabe R, et al. Cryo-EM structure of the CENP-A nucleosome in complex with phosphorylated CENP-C. *EMBO J*. 2021;40(5). doi:10.15252/embj.2020105671

47. Quénet D, Dalal Y. The CENP-A nucleosome: a dynamic structure and role at the centromere. *Chromosome Res*. 2012;20(5):465-479. doi:10.1007/s10577-012-9301-4

48. Sekulic N, Bassett EA, Rogers DJ, Black BE. The structure of (CENP-A-H4) 2 reveals physical features that mark centromeres. *Nature*. 2010;467(7313):347-351. doi:10.1038/nature09323

49. Li Y, Wang J, Chen X, Czajkowsky DM, Shao Z. Quantitative Super-Resolution Microscopy Reveals the Relationship between CENP-A Stoichiometry and Centromere Physical Size. *Int J Mol Sci*. 2023;24(21):15871. doi:10.3390/ijms242115871

50. Mahlke MA, Nechemia-Arbely Y. Guarding the Genome: CENP-A-Chromatin in Health and Cancer. *Genes*. 2020;11(7):810. doi:10.3390/genes11070810

51. Mitra S, Srinivasan B, Jansen LET. Stable inheritance of CENP-A chromatin: Inner strength versus dynamic control. *J Cell Biol*. 2020;219(10):e202005099. doi:10.1083/jcb.202005099

52. Woodcock CL, Ghosh RP. Chromatin Higher-order Structure and Dynamics. *Cold Spring Harb Perspect Biol*. 2010;2(5):a000596-a000596. doi:10.1101/cshperspect.a000596

53. Li G, Reinberg D. Chromatin higher-order structures and gene regulation. *Curr Opin Genet Dev*. 2011;21(2):175-186. doi:10.1016/j.gde.2011.01.022

54. Chen P, Li G. Dynamics of the higher-order structure of chromatin. *Protein Cell*. 2010;1(11):967-971. doi:10.1007/s13238-010-0130-y

55. Grewal SIS, Elgin SCR. Transcription and RNA interference in the formation of heterochromatin. *Nature*. 2007;447(7143):399-406. doi:10.1038/nature05914

56. Grewal SIS, Moazed D. Heterochromatin and Epigenetic Control of Gene Expression. *Science*. 2003;301(5634):798-802. doi:10.1126/science.1086887

57. Allshire RC, Madhani HD. Ten principles of heterochromatin formation and function. *Nat Rev Mol Cell Biol*. 2018;19(4):229-244. doi:10.1038/nrm.2017.119

58. Morrison J, Koeman JM, Johnson BK, et al. Evaluation of whole-genome DNA methylation sequencing library preparation protocols. *Epigenetics Chromatin*. 2021;14(1):28. doi:10.1186/s13072-021-00401-y

59. Babu A, Verma RS. Chromosome Structure: Euchromatin and Heterochromatin. In: *International Review of Cytology*. Vol 108. Elsevier; 1987:1-60. doi:10.1016/S0074-7696(08)61435-7

60. Bascom G, Schlick T. Linking Chromatin Fibers to Gene Folding by Hierarchical Looping. *Biophys J*. 2017;112(3):434-445. doi:10.1016/j.bpj.2017.01.003

61. Razin SV, Gavrilov AA. Chromatin without the 30-nm fiber: Constrained disorder instead of hierarchical folding. *Epigenetics*. 2014;9(5):653-657. doi:10.4161/epi.28297

62. Ricci MA, Manzo C, García-Parajo MF, Lakadamyali M, Cosma MP. Chromatin Fibers Are Formed by Heterogeneous Groups of Nucleosomes In Vivo. *Cell*. 2015;160(6):1145-1158. doi:10.1016/j.cell.2015.01.054

63. Luger K, Dechassa ML, Tremethick DJ. New insights into nucleosome and chromatin structure: an ordered state or a disordered affair? *Nat Rev Mol Cell Biol*. 2012;13(7):436-447. doi:10.1038/nrm3382

64. Lambert M, Jambon S, Depauw S, David-Cordonnier MH. Targeting Transcription Factors for Cancer Treatment. *Molecules*. 2018;23(6):1479. doi:10.3390/molecules23061479

65. Biswas R, Bagchi A. NFkB pathway and inhibition: an overview. *Comput Mol Biol*. Published online 2016. doi:10.5376/cmb.2016.06.0001

66. Siebenlist U, Franzoso G, Brown K. Structure, Regulation and Function of NF-kappaB. *Annu Rev Cell Biol*. 1994;10(1):405-455. doi:10.1146/annurev.cb.10.110194.002201

67. Gilmore TD. The Rel / NF- k B signal transduction pathway : introduction. Published online 1999:6842-6844.

68. Nishikori M. Classical and Alternative NF-.KAPPA.B Activation Pathways and Their Roles in Lymphoid Malignancies. *J Clin Exp Hematop*. 2005;45(1):15-24. doi:10.3960/jslrt.45.15

69. Zandi E, Rothwarf DM, Delhase M, Hayakawa M, Karin M. The I?B Kinase Complex (IKK) Contains Two Kinase Subunits, IKK ⎵ and IKK␋, Necessary for I?B Phosphorylation and NF-?B Activation.

70. Israel A. The IKK Complex, a Central Regulator of NF- B Activation. *Cold Spring Harb Perspect Biol*. 2010;2(3):a000158-a000158. doi:10.1101/cshperspect.a000158

71. Israël A. The IKK complex: an integrator of all signals that activate NF-κB? *Trends Cell Biol*. 2000;10(4):129-133. doi:10.1016/S0962-8924(00)01729-3

72. Karin M. How NF-κB is activated: the role of the IκB kinase (IKK) complex. *Oncogene*. 1999;18(49):6867-6874. doi:10.1038/sj.onc.1203219

73. Leung TH, Hoffmann A, Baltimore D. One Nucleotide in a κB Site Can Determine Cofactor Specificity for NF-κB Dimers. *Cell*. 2004;118(4):453-464. doi:10.1016/j.cell.2004.08.007

74. Martone R, Euskirchen G, Bertone P, et al. Distribution of NF-κB-binding sites across human chromosome 22. *Proc Natl Acad Sci*. 2003;100(21):12247-12252. doi:10.1073/pnas.2135255100

75. Chen FE, Ghosh G. Regulation of DNA binding by Rel/NF-κB transcription factors: Structural views. *Oncogene*. 1999;18(49):6845-6852. doi:10.1038/sj.onc.1203224

76. Stormberg T, Filliaux S, Baughman HER, Komives EA, Lyubchenko YL. Transcription factor NF-κB unravels nucleosomes. *Biochim Biophys Acta - Gen Subj*. 2021;1865(9):129934. doi:10.1016/j.bbagen.2021.129934

77. Kearns JD, Basak S, Werner SL, Huang CS, Hoffmann A. IκBε provides negative feedback to control NF-κB oscillations, signaling dynamics, and inflammatory gene expression. *J Cell Biol*. 2006;173(5):659-664. doi:10.1083/jcb.200510155

78. Renner F, Schmitz ML. Autoregulatory feedback loops terminating the NF-κB response. *Trends Biochem Sci*. 2009;34(3):128-135. doi:10.1016/j.tibs.2008.12.003

79. Niederberger E, Geisslinger G. The IKK-NF-κB pathway: a source for novel molecular drug targets in pain therapy? *FASEB J*. 2008;22(10):3432-3442. doi:10.1096/fj.08-109355

80. Muriel P. NF- *κ* B in liver diseases: a target for drug therapy. *J Appl Toxicol*. 2009;29(2):91-100. doi:10.1002/jat.1393

81. Freitas RHCN, Fraga CAM. NF-κB-IKKβ Pathway as a Target for Drug Development: Realities, Challenges and Perspectives. *Curr Drug Targets*. 2018;19(16):1933-1942. doi:10.2174/1389450119666180219120534

82. Haefner B. The Transcription Factor NF-κB as Drug Target. In: *Progress in Medicinal Chemistry*. Vol 43. Elsevier; 2005:137-188. doi:10.1016/S0079-6468(05)43005-2

83. Labbozzetta M, Notarbartolo M, Poma P. Can NF-κB Be Considered a Valid Drug Target in Neoplastic Diseases? Our Point of View. *Int J Mol Sci*. 2020;21(9):3070. doi:10.3390/ijms21093070

84. Xia L, Tan S, Zhou Y, et al. Role of the NFκB-signaling pathway in cancer. *OncoTargets Ther*. 2018;Volume 11:2063-2073. doi:10.2147/OTT.S161109

85. Lone IN, Shukla MS, Charles Richard JL, Peshev ZY, Dimitrov S, Angelov D. Binding of NF-κB to Nucleosomes: Effect of Translational Positioning, Nucleosome Remodeling and Linker Histone H1. Schübeler D, ed. *PLoS Genet*. 2013;9(9):e1003830. doi:10.1371/journal.pgen.1003830

86. Anest V, Hanson JL, Cogswell PC, Steinbrecher KA, Strahl BD, Baldwin AS. A nucleosomal function for IκB kinase-α in NF-κB-dependent gene expression. *Nature*. 2003;423(6940):659-663. doi:10.1038/nature01648

87. Park YJ, Luger K. Structure and function of nucleosome assembly proteinsThis paper is one of a selection of papers published in this Special Issue, entitled 27th International West Coast Chromatin and Chromosome Conference, and has undergone the Journal's usual peer review process. *Biochem Cell Biol*. 2006;84(4):549-549. doi:10.1139/o06-088

88. Battistini F, Hunter CA, Gardiner EJ, Packer MJ. Structural mechanics of DNA wrapping in the nucleosome. *J Mol Biol*. 2010;396(2):264-279. doi:10.1016/j.jmb.2009.11.040

89. Mariño-Ramírez L, Kann MG, Shoemaker BA, Landsman D. Histone structure and nucleosome stability. *Expert Rev Proteomics*. 2005;2(5):719-729. doi:10.1586/14789450.2.5.719

90. Henikoff S. Nucleosome destabilization in the epigenetic regulation of gene expression. *Nat Rev Genet*. 2008;9(1):15-26. doi:10.1038/nrg2206

91. Lai WKM, Pugh BF. Understanding nucleosome dynamics and their links to gene expression and DNA replication. *Nat Rev Mol Cell Biol*. 2017;18(9):548-562. doi:10.1038/nrm.2017.47

92. Svaren J, Hörz W. Regulation of gene expression by nucleosomes. *Curr Opin Genet Dev*. 1996;6(2):164-170. doi:10.1016/S0959-437X(96)80046-3

93. Zhu F, Farnung L, Kaasinen E, et al. The interaction landscape between transcription factors and the nucleosome. *Nature*. 2018;562(7725):76-81. doi:10.1038/s41586-018-0549-5

94. Perea-Resa C, Blower MD. Centromere Biology: Transcription Goes on Stage. *Mol Cell Biol*. 2018;38(18):e00263-18. doi:10.1128/MCB.00263-18

95. Shlyakhtenko LS, Rekesh D, Lindsay SM, et al. Structure of three-way dna junctions: 1. non-planar dna geometry. *J Biomol Struct Dyn*. 1994;11(6):1175-1189. doi:10.1080/07391102.1994.10508062

96. Shlyakhtenko LS, Appella E, Harrington RE, Kutyavin I, Lyubchenko YL. Structure of three-way dna junctions. 2. effects of extra bases and mismatches. *J Biomol Struct Dyn*. 1994;12(1):131-143. doi:10.1080/07391102.1994.10508092

97. Lowary PT, Widom J. *New DNA Sequence Rules for High Affinity Binding to Histone Octamer and Sequence-Directed Nucleosome Positioning*.

98. Stormberg T, Vemulapalli S, Filliaux S, Lyubchenko YL. Effect of histone H4 tail on nucleosome stability and internucleosomal interactions. *Sci Rep*. 2021;11(1). doi:10.1038/s41598-021-03561-9

99. Vemulapalli S, Hashemi M, Lyubchenko YL. Site-search process for synaptic protein-dna complexes. *Int J Mol Sci*. 2022;23(1). doi:10.3390/ijms23010212

100. Stumme-Diers MP, Banerjee S, Hashemi M, Sun Z, Lyubchenko YL. Nanoscale dynamics of centromere nucleosomes and the critical roles of CENP-A. *Nucleic Acids Res*. 2018;46(1):94-103. doi:10.1093/nar/gkx933

101. Stumme-Diers MP, Sun Z, Lyubchenko YL. Probing the Structure and Dynamics of Nucleosomes Using AFM Imaging. Published online 2020.

102. Sue SC, Cervantes C, Komives EA, Dyson HJ. Transfer of Flexibility between Ankyrin Repeats in IκBα upon Formation of the NF-κB Complex. *J Mol Biol*. 2008;380(5):917-931. doi:10.1016/j.jmb.2008.05.048

103. Miyagi A, Ando T, Lyubchenko YL. Dynamics of nucleosomes assessed with time-lapse high-speed atomic force microscopy. *Biochemistry*. 2011;50(37):7901-7908. doi:10.1021/bi200946z

104. Lyubchenko YL. Atomic Force Microscopy Methods for DNA Analysis. In: Meyers RA, ed. *Encyclopedia of Analytical Chemistry*. 1st ed. Wiley; 2019:1-31. doi:10.1002/9780470027318.a9258.pub2

105. Neish CS, Martin IL, Henderson RM, Edwardson JM. Direct visualization of ligand-protein interactions using atomic force microscopy. *Br J Pharmacol*. 2002;135(8):1943-1950. doi:10.1038/sj.bjp.0704660

106. Niemeyer C. Self-assembly of DNA-streptavidin nanostructures and their use as reagents in immuno-PCR. *Nucleic Acids Res*. 1999;27(23):4553-4561. doi:10.1093/nar/27.23.4553

107. Seong GH, Yanagida Y, Aizawa M, Kobatake E. *Atomic Force Microscopy Identification of Transcription Factor NFjB Bound to Streptavidin-Pin-Holding DNA Probe ANALYTICAL BIOCHEMISTRY*. Vol 309.; 2002:241-247. www.academicpress.com

108. Buzio R, Repetto L, Giacopelli F, Ravazzolo R, Valbusa U. Label-free, atomic force microscopy-based mapping of DNA intrinsic curvature for the nanoscale comparative analysis of bent duplexes. *Nucleic Acids Res*. 2012;40(11):e84-e84. doi:10.1093/nar/gks210

109. Meir A, Helppolainen SH, Podoly E, et al. Crystal Structure of Rhizavidin: Insights into the Enigmatic High-Affinity Interaction of an Innate Biotin-Binding Protein Dimer. *J Mol Biol*. 2009;386(2):379-390. doi:10.1016/j.jmb.2008.11.061

110. Helppolainen SH, Nurminen KP, Määttä JAE, et al. Rhizavidin from *Rhizobium etli* : the first natural dimer in the avidin protein family. *Biochem J*. 2007;405(3):397-405. doi:10.1042/BJ20070076

111. Editor JK. *Electron Microscopy Methods and Protocols Third Edition Methods in Molecular Biology 1117*. http://www.springer.com/series/7651

112. Shlyakhtenko LS, Lushnikov AJ, Li M, Harris RS, Lyubchenko YL. Interaction of APOBEC3A with DNA assessed by atomic force microscopy. *PLoS ONE*. 2014;9(6). doi:10.1371/journal.pone.0099354

113. Shlyakhtenko LS, Lushnikov AY, Miyagi A, Lyubchenko YL. Specificity of Binding of Single-Stranded DNA-Binding Protein to Its Target. *Biochemistry*. 2012;51(7):1500-1509. doi:10.1021/bi201863z

114. Hart D. The salt dependence of DNA recognition by NF-kappaB p50: a detailed kinetic analysis of the effects on affinityand specificity. *Nucleic Acids Res*. 1999;27(4):1063-1069. doi:10.1093/nar/27.4.1063

115. Sharp KA, Honig B. Salt effects on nucleic acids. *Curr Opin Struct Biol*. 1995;5(3):323-328. doi:10.1016/0959-440X(95)80093-X

116. Jensen J. Calculating pH and Salt Dependence of Protein-Protein Binding. *Curr Pharm Biotechnol*. 2008;9(2):96-102. doi:10.2174/138920108783955146

117. Waldron TT, Schrift GL, Murphy KP. The Salt-dependence of a Protein–Ligand Interaction: Ion–Protein Binding Energetics. *J Mol Biol*. 2005;346(3):895-905. doi:10.1016/j.jmb.2004.12.018

118. Yager TD, Van Holde KE. Dynamics and equilibria of nucleosomes at elevated ionic strength. *J Biol Chem*. 1984;259(7):4212-4222. doi:10.1016/S0021-9258(17)43032-8

119. Ballestar E, Boix-Chornet M, Franco L. Conformational Changes in the Nucleosome Followed by the Selective Accessibility of Histone Glutamines in the Transglutaminase Reaction: Effects of Ionic Strength. *Biochemistry*. 2001;40(7):1922-1929. doi:10.1021/bi001575b

120. Bednar J, Horowitz RA, Dubochet J, Woodcock CL. Chromatin conformation and salt-induced compaction: three-dimensional structural information from cryoelectron microscopy. *J Cell Biol*. 1995;131(6):1365-1376. doi:10.1083/jcb.131.6.1365

121. Allahverdi A, Chen Q, Korolev N, Nordenskiöld L. Chromatin compaction under mixed salt conditions: Opposite effects of sodium and potassium ions on nucleosome array folding. *Sci Rep*. 2015;5(1):8512. doi:10.1038/srep08512

122. Billingsley DJ, Crampton N, Kirkham J, Thomson NH, Bonass WA. Single-stranded loops as end-label polarity markers for double-stranded linear DNA templates in atomic force microscopy. *Nucleic Acids Res*. 2012;40(13):e99-e99. doi:10.1093/nar/gks276

123. Chammas O, Billingsley DJ, Bonass WA, Thomson NH. Single-stranded DNA loops as fiducial markers for exploring DNA-protein interactions in single molecule imaging. *Methods*. 2013;60(2):122-130. doi:10.1016/j.ymeth.2013.03.002

124. Rybenkov VV, Cozzarelli NR, Vologodskii AV. Probability of DNA knotting and the effective diameter of the DNA double helix. *Proc Natl Acad Sci*. 1993;90(11):5307-5311. doi:10.1073/pnas.90.11.5307

125. Lyubchenko YL, Shlyakhtenko LS. AFM for analysis of structure and dynamics of DNA and protein–DNA complexes. *Methods*. 2009;47(3):206-213. doi:10.1016/j.ymeth.2008.09.002

126. Shlyakhtenko LS. Structure and dynamics of three-way DNA junctions: atomic force microscopy studies. *Nucleic Acids Res*. 2000;28(18):3472-3477. doi:10.1093/nar/28.18.3472

127. Oussatcheva EA, Shlyakhtenko LS, Glass R, Sinden RR, Lyubchenko YL, Potaman VN. Structure of branched DNA molecules: gel retardation and atomic force microscopy studies 1 1Edited by I. Tinoco. *J Mol Biol*. 1999;292(1):75-86. doi:10.1006/jmbi.1999.3043

128. Yamamoto D, Nagura N, Omote S, Taniguchi M, Ando T. Streptavidin 2D crystal substrates for visualizing biomolecular processes by atomic force microscopy. *Biophys J*. 2009;97(8):2358-2367. doi:10.1016/j.bpj.2009.07.046

129. Woolley AT, Cheung CL, Hafner JH, Lieber CM. *Structural Biology with Carbon Nanotube AFM Probes*.

130. Ando T, Uchihashi T, Kodera N. High-speed AFM and applications to biomolecular systems. *Annu Rev Biophys*. 2013;42(1):393-414. doi:10.1146/annurev-biophys-083012-130324

131. Zhang Y, Hashemi M, Lv Z, et al. High-speed atomic force microscopy reveals structural dynamics of α -synuclein monomers and dimers. *J Chem Phys*. 2018;148(12). doi:10.1063/1.5008874

132. Lyubchenko YL. Direct AFM visualization of the nanoscale dynamics of biomolecular complexes. *J Phys Appl Phys*. 2018;51(40):403001. doi:10.1088/1361-6463/aad898

133. Onufriev AV, Schiessel H. The nucleosome: from structure to function through physics. *Curr Opin Struct Biol*. 2019;56:119-130. doi:10.1016/j.sbi.2018.11.003

134. Zhou K, Gaullier G, Luger K. Nucleosome structure and dynamics are coming of age. *Nat Struct Mol Biol*. 2019;26(1):3-13. doi:10.1038/s41594-018-0166-x

135. Pan YG, Banerjee S, Zagorski K, Shlyakhtenko LS, Kolomeisky AB, Lyubchenko YL. *A Molecular Model of the Surface-Assisted Protein Aggregation Process*. Biophysics; 2018. doi:10.1101/415703

136. Clapier CR, Cairns BR. The Biology of Chromatin Remodeling Complexes. *Annu Rev Biochem*. 2009;78(1):273-304. doi:10.1146/annurev.biochem.77.062706.153223

137. Becker PB, Workman JL. Nucleosome Remodeling and Epigenetics. *Cold Spring Harb Perspect Biol*. 2013;5(9):a017905-a017905. doi:10.1101/cshperspect.a017905

138. Forties RA, North JA, Javaid S, et al. A quantitative model of nucleosome dynamics. *Nucleic Acids Res*. 2011;39(19):8306-8313. doi:10.1093/nar/gkr422

139. Stormberg T, Stumme-Diers M, Lyubchenko YL. Sequence-dependent nucleosome nanoscale structure characterized by atomic force microscopy. *FASEB J*. 2019;33(10):10916-10923. doi:10.1096/fj.201901094R

140. Stormberg T, Lyubchenko YL. The Sequence Dependent Nanoscale Structure of CENP-A Nucleosomes. *Int J Mol Sci*. 2022;23(19):11385. doi:10.3390/ijms231911385

141. Sun Z, Stormberg T, Filliaux S, Lyubchenko YL. Three-Way DNA Junction as an End Label for DNA in Atomic Force Microscopy Studies. *Int J Mol Sci*. 2022;23(19):11404. doi:10.3390/ijms231911404

142. Wang Y, Stormberg T, Hashemi M, Kolomeisky AB, Lyubchenko YL. Beyond Sequence: Internucleosomal Interactions Dominate Array Assembly. *J Phys Chem B*. 2022;126(51):10813-10821. doi:10.1021/acs.jpcb.2c05321

143. Lancrey A, Joubert A, Duvernois-Berthet E, et al. Nucleosome Positioning on Large Tandem DNA Repeats of the '601' Sequence Engineered in Saccharomyces cerevisiae. *J Mol Biol*. 2022;434(7):167497. doi:10.1016/j.jmb.2022.167497

144. Cutter AR, Hayes JJ. A brief review of nucleosome structure. *FEBS Lett*. 2015;589(20PartA):2914-2922. doi:10.1016/j.febslet.2015.05.016

145. McGhee JD, Felsenfeld G. Nucleosome Structure.

146. Zhou BR, Yadav KNS, Borgnia M, et al. Atomic resolution cryo-EM structure of a native-like CENP-A nucleosome aided by an antibody fragment. *Nat Commun*. 2019;10(1):2301. doi:10.1038/s41467-019-10247-4

147. Ohtomo H, Kurita J ichi, Sakuraba S, et al. The N-terminal Tails of Histones H2A and H2B Adopt Two Distinct Conformations in the Nucleosome with Contact and Reduced Contact to DNA. *J Mol Biol*. 2021;433(15):167110. doi:10.1016/j.jmb.2021.167110

148. Luger K. Crystal structure of the nucleosome core particle at 2.8 A˚resolution. 1997;389.

149. Park PJ. ChIP-seq: Advantages and challenges of a maturing technology. *Nat Rev Genet*. 2009;10(10):669-680. doi:10.1038/nrg2641

150. Poirier MG, Oh E, Tims HS, Widom J. Dynamics and function of compact nucleosome arrays. *Nat Struct Mol Biol*. 2009;16(9):938-944. doi:10.1038/nsmb.1650

151. Szerlong HJ, Hansen JC. Nucleosome distribution and linker DNA: connecting nuclear function to dynamic chromatin structureThis paper is one of a selection of papers published in a Special Issue entitled 31st Annual International Asilomar Chromatin and Chromosomes Conference, and has undergone the Journal's usual peer review process. *Biochem Cell Biol*. 2011;89(1):24-34. doi:10.1139/O10-139

152. McKinley KL, Cheeseman IM. The molecular basis for centromere identity and function. *Nat Rev Mol Cell Biol*. 2016;17(1):16-29. doi:10.1038/nrm.2015.5

153. Pidoux AL, Allshire RC. The role of heterochromatin in centromere function. In: *Philosophical Transactions of the Royal Society B: Biological Sciences*. Vol 360. Royal Society; 2005:569-579. doi:10.1098/rstb.2004.1611

154. Boopathi R, Danev R, Khoshouei M, et al. Phase-plate cryo-EM structure of the Widom 601 CENP-A nucleosome core particle reveals differential flexibility of the DNA ends. *Nucleic Acids Res*. 2020;48(10):5735-5748. doi:10.1093/nar/gkaa246

155. Stumme-Diers MP, Banerjee S, Sun Z, Lyubchenko YL. Assembly of Centromere Chromatin for Characterization by High-Speed Time-Lapse Atomic Force Microscopy. In: Lyubchenko YL, ed. *Nanoscale Imaging*. Vol 1814. Methods in Molecular Biology. Springer New York; 2018:225-242. doi:10.1007/978-1-4939-8591-3_14

156. Lowary PT, Widom J. *Nucleosome Packaging and Nucleosome Positioning of Genomic DNA (Chromatingene Regulationtranscriptional Activation)*. Vol 94.; 1997:1183-1188. www.pnas.org.

157. Widom J. Role of DNA sequence in nucleosome stability and dynamics. *Q Rev Biophys*. 2001;34(3):269-324. doi:10.1017/S0033583501003699

158. Menshikova I, Menshikov E, Filenko N, Lyubchenko and YL. *Nucleosomes Structure and Dynamics: Effect of CHAPS*. www.ijbmb.org

159. Lyubchenko YL, Shlyakhtenko LS. Chromatin Imaging with Time-Lapse Atomic Force Microscopy. In: Chellappan SP, ed. *Chromatin Protocols*. Vol 1288. Methods in Molecular Biology. Springer New York; 2015:27-42. doi:10.1007/978-1-4939-2474-5_3

160. Lyubchenko YL. Nanoscale nucleosome dynamics assessed with time-lapse AFM. *Biophys Rev*. 2014;6(2):181-190. doi:10.1007/s12551-013-0121-3

161. Lyubchenko YL, Shlyakhtenko LS, Ando T. Imaging of nucleic acids with atomic force microscopy. *Methods*. 2011;54(2):274-283. doi:10.1016/j.ymeth.2011.02.001

162. Onoa B, Díaz-Celis C, Cañari-Chumpitaz C, Lee A, Bustamante C. Real-Time Multistep Asymmetrical Disassembly of Nucleosomes and Chromatosomes Visualized by High-Speed Atomic Force Microscopy. *ACS Cent Sci*. 2024;10(1):122-137. doi:10.1021/acscentsci.3c00735

163. Chua EYD, Vasudevan D, Davey GE, Wu B, Davey CA. The mechanics behind DNA sequence-dependent properties of the nucleosome. *Nucleic Acids Res*. 2012;40(13):6338-6352. doi:10.1093/nar/gks261

164. Kixmoeller K, Allu PK, Black BE. The centromere comes into focus: from CENP-A nucleosomes to kinetochore connections with the spindle. *Open Biol*. 2020;10(6):200051. doi:10.1098/rsob.200051

165. Ngo TTM, Ha T. Nucleosomes undergo slow spontaneous gaping. *Nucleic Acids Res*. 2015;43(8):3964-3971. doi:10.1093/nar/gkv276

166. Chen Y, Tokuda JM, Topping T, et al. Asymmetric unwrapping of nucleosomal DNA propagates asymmetric opening and dissociation of the histone core. *Proc Natl Acad Sci*. 2017;114(2):334-339. doi:10.1073/pnas.1611118114

167. Zhang B, Zheng W, Papoian GA, Wolynes PG. Exploring the Free Energy Landscape of Nucleosomes. *J Am Chem Soc*. 2016;138(26):8126-8133. doi:10.1021/jacs.6b02893

168. Crick F. Central Dogma of Molecular Biology. *Nature*. 1970;227(5258):561-563. doi:10.1038/227561a0

169. North JA, Shimko JC, Javaid S, et al. Regulation of the nucleosome unwrapping rate controls DNA accessibility. *Nucleic Acids Res*. 2012;40(20):10215-10227. doi:10.1093/nar/gks747

170. Wang X, Bai L, Bryant GO, Ptashne M. Nucleosomes and the accessibility problem. *Trends Genet*. 2011;27(12):487-492. doi:10.1016/j.tig.2011.09.001

171. McAinsh AD, Meraldi P. The CCAN complex: Linking centromere specification to control of kinetochore-microtubule dynamics. *Semin Cell Dev Biol*. 2011;22(9):946-952. doi:10.1016/j.semcdb.2011.09.016

172. Gambogi CW, Black BE. The nucleosomes that mark centromere location on chromosomes old and new. Gilbert N, Allan J, eds. *Essays Biochem*. 2019;63(1):15-27. doi:10.1042/EBC20180060

173. Alexandrov I, Kazakov A, Tumeneva I, Shepelev V, Yurov Y. Alpha-satellite DNA of primates: old and new families. *Chromosoma*. 2001;110(4):253-266. doi:10.1007/s004120100146

174. McNulty SM, Sullivan BA. Alpha satellite DNA biology: finding function in the recesses of the genome. *Chromosome Res*. 2018;26(3):115-138. doi:10.1007/s10577-018-9582-3

175. Willard HF. *Chromosome-Specific Organization of Human Alpha Satellite DNA 524 ALPHA SATELLITE DNA*. Vol 37.; 1985:524-532.

176. Aldrup-MacDonald ME, Kuo ME, Sullivan LL, Chew K, Sullivan BA. Genomic variation within alpha satellite DNA influences centromere location on human chromosomes with metastable epialleles. *Genome Res*. 2016;26(10):1301-1311. doi:10.1101/gr.206706.116

177. Rosandić M, Paar V, Basar I, Glunčić M, Pavin N, Pilaš I. CENP-B box and pJα sequence distribution in human alpha satellite higher-order repeats (HOR). *Chromosome Res*. 2006;14(7):735-753. doi:10.1007/s10577-006-1078-x

178. Smurova K, De Wulf P. Centromere and Pericentromere Transcription: Roles and Regulation … in Sickness and in Health. *Front Genet*. 2018;9:674. doi:10.3389/fgene.2018.00674

179. Mcghee 1980.

180. Arunkumar G, Melters DP. Centromeric Transcription: A Conserved Swiss-Army Knife. *Genes*. 2020;11(8):911. doi:10.3390/genes11080911

181. Black BE, Foltz DR, Chakravarthy S, Luger K, Woods VL, Cleveland DW. Structural determinants for generating centromeric chromatin. *Nature*. 2004;430(6999):578-582. doi:10.1038/nature02766

182. McNulty SM, Sullivan LL, Sullivan BA. Human Centromeres Produce Chromosome-Specific and Array-Specific Alpha Satellite Transcripts that Are Complexed with CENP-A and CENP-C. *Dev Cell*. 2017;42(3):226-240.e6. doi:10.1016/j.devcel.2017.07.001

183. Quénet D, Dalal Y. A long non-coding RNA is required for targeting centromeric protein A to the human centromere. *eLife*. 2014;3:e26016. doi:10.7554/eLife.03254

184. Bergmann JH, Jakubsche JN, Martins NM, et al. Epigenetic engineering: histone H3K9 acetylation is compatible with kinetochore structure and function. *J Cell Sci*. 2012;125(2):411-421. doi:10.1242/jcs.090639

185. Gilmore TD. Introduction to NF-κB: players, pathways, perspectives. *Oncogene*. 2006;25(51):6680-6684. doi:10.1038/sj.onc.1209954

186. Hunter CJ, De Plaen IG. Inflammatory signaling in NEC: Role of NF-κB, cytokines and other inflammatory mediators. *Pathophysiology*. 2014;21(1):55-65. doi:10.1016/j.pathophys.2013.11.010

187. Mulero MC, Wang VYF, Huxford T, Ghosh G. Genome reading by the NF-κB transcription factors. *Nucleic Acids Res*. 2019;47(19):9967-9989. doi:10.1093/nar/gkz739

188. Siggers T, Chang AB, Teixeira A, et al. Principles of dimer-specific gene regulation revealed by a comprehensive characterization of NF-κB family DNA binding. *Nat Immunol*. 2012;13(1):95-102. doi:10.1038/ni.2151

189. Konrad SF, Vanderlinden W, Frederickx W, et al. High-throughput AFM analysis reveals unwrapping pathways of H3 and CENP-A nucleosomes. *Nanoscale*. 2021;13(10):5435-5447. doi:10.1039/D0NR08564B

190. Sharma AB, Dimitrov S, Hamiche A, Van Dyck E. Centromeric and ectopic assembly of CENP-A chromatin in health and cancer: old marks and new tracks. *Nucleic Acids Res*. 2019;47(3):1051-1069. doi:10.1093/nar/gky1298

191. Zhu J, Guo Q, Choi M, Liang Z, Yuen KWY. Centromeric and pericentric transcription and transcripts: their intricate relationships, regulation, and functions. *Chromosoma*. 2023;132(3):211-230. doi:10.1007/s00412-023-00801-x